Erosion Characteristics of Cohesive Sediment Bed and Bank, and Their Effects on River Morphology

By

Puji Harsanto

2012

Abstract

Cohesive and non-cohesive materials are often coexists in rivers whether on bank or bed. The presence or absence both of them affect on river morphology due to different characteristics on erosion process. However, this effect is simplified by many scientists especially the effect of cohesive material. Many numerical analysis and experimental studies have developed to study the evolution of channel. Most of them use non-cohesive material and ignore the presence of cohesive material. In case cohesive material is a part of bank material in channels, a recent study using numerical analysis to compare the bank line migration with bank composed of both cohesive and non-cohesive material. The results show that, the rate of the bank line migrations is quite different among of banks that is composed of non-cohesive only or cohesive only or both of them. Therefore, the experimental studies use cohesive material and non cohesive material is needed to get better understanding on channel evolution modeling. In case cohesive material as cohesive sediment bed, the erosion characteristics also have studied by many researchers. They clarify the erosion behavior by considering the physicochemical parameters such as salinity, temperature, water content and bulk density. However, most of them use clear water as eroding media. Therefore, study the erosion characteristics of cohesive sediment bed using water contain bed-load transport is a new knowledge.

This research involving field study, experimental study and numerical study to clarify the erosion characteristics of cohesive material both on the bank and bed of channel. This report is divided mainly into six chapters. Chapter 1 explains the background, original research and objective of this research. The effects of cohesive material on bank erosion process are explained in the Chapter 2. In Chapter 3, the erosion characteristics of cohesive sediment bed are presented. Chapter 4 consists of field study and numerical simulation on bank line retreat and countermeasure of bank erosion problem in real rivers. The river in this chapter has a similar bank characteristic which is studied in Chapter 2. Chapter 5 is numerical simulation in a river which has a similar phenomenon with Chapter 3. The conclusions and recommendations from this research are presented in Chapter 6.

The experiments of bank erosion characteristic using cohesive and non-cohesive layers were conducted. Three types of bank are used in this research. First type is the bank that composed of non-cohesive material layer. Second type is the bank that composed of cohesive and non-cohesive material layer. Third type is the bank that composed of cohesive material layer. For all cases, the channel bed used same non-cohesive material. In case the bank composed only non-cohesive material, the shape of bank line is a smooth curve and tends to form large radius of bend. In case the bank composed of cohesive material on the upper layer and non-cohesive at the bottom layer the shape of bank line at the end experiment is not a smooth curve. The radius of bend is smaller than in case the bank composed of non-cohesive material only. The bank which composed only cohesive material is not eroded. There is no lateral migration line in this case. The flow is not enough to erode the cohesive bank. The overhang and mass failure mechanism occurs in case bank composed cohesive layer on the top and non-cohesive layer at the bottom. Some of the failed blocks shelter near the bank toe. This material changes or disturbs the flow in the channel. The local scouring occurs at around the failed block and a part of them remain for a long time on the bed near the bank toe. This phenomenon is very important because most of scientists ignore this phenomenon in numerical calculation and it assumed flush away with flow.

The presence of cohesive material suppresses the erosion process in the bank. In the other hand, it forces erosion process on the channel bed that composed only non-cohesive material. In case the bank composed cohesive and non-cohesive layer, the bed near the bank toe was eroded well and the bank line retreat is a small magnitude. In case the bank composed only non-cohesive layer, the bed near the bank toe was not eroded well and the bank line retreat is a large magnitude. The cohesive characteristics and the high surface slope of the upper layer cause the difference. This result indicates that the cohesive characteristics of the material in banks must be considered, when the bank erosion process is reproduced by mathematical models. The bed degradations also play the rule whether the bank will collapse or not. It has strong relation to the flow condition. So, controlling the flow in the channel becomes one of solutions to counteract the bank erosion problem. Using numerical simulation, this method is applied in Sesayap River East Kalimantan Indonesia. The results show that the controlling of flow pattern can reduce the bed degradation. It will keep the bank in

stable condition. However, the installing construction to prevent bank erosion such as revetment may produce high flow velocity that lead to the bank erosion.

The erosion characteristic of cohesive sediment bed is investigated by experimental study. These experiments studied the erosion characteristics of cohesive sediment bed by flowing water that containing bed-load transport material. The fine and coarse material for sediment feeding are used. The sediment feeding discharge is widely distributed from 0 (0%) to 1.5 (150%) times as the potential equilibrium sediment transport rate, q_b. The general results show that the erosion of bed will increase by increasing the volume of bed-load transport. However, after achieving in a certain volume of bed-load transport, the erosion will decrease even the deposition occurs. In cases using fine and coarse material for sediment feeding, the maximum erosion is larger than without sediment feeding. The maximum erosion occurs when the bed-load transport volume is less than equilibrium transport rate. In case using fine material for sediment feeding, the starting of deposition process occurs at 35% q_b but in case using coarse material occur at 150% q_b. This indicates that supplied fine sediment is trapped so much by cohesive bed. The cohesive sediment bed suppresses the degradation process when the bed-load material is fine material. This phenomenon is applied in natural rivers that the bed material is composed cohesive sediment or fine material. Tonle Sap River in Cambodia is chosen as case study. This river has a confluence with Mekong River in Chacktomuk Cambodia. The bed material in Mekon River is coarse material. During dry season, the bed material in Tonle Sap River is fine material and in Mekong River is coarse material. During flood season, the coarse material from Mekong River flows on the fine material in Tonle Sap River. During the flood season, the bed material in the Tonle Sap River becomes coarse because of the inverse flow from the Mekong River. The numerical simulations show that due to the cohesiveness, the coarse bed-load transport from Mekong River deposited in Tonle Sap River. These results are agreed with the experimental study. Some of the bed-load transport material trapped on the surface of cohesive layer and then suppresses the erosion process.

Keywords: *cohesive material, non-cohesive material, erosion characteristics, experimental and numerical study, river bed and bank*

Acknowledgements

I would like to express my sincere gratitude and appreciation to many people who made this thesis. Also, I would like to thank a number of people for their assistance during I was study in Kyoto University Japan.

I have been indebted in the preparation of this thesis to my supervisor, Prof. Masaharu Fujita, Disaster Prevention Research Institute of Kyoto University, whose patience and kindness, as well as his academic experience, have been invaluable to me. And also who has give opportunity to study in Kyoto University and for recommendation to get scholarship provided by Monbukagakusho under Kyoto University-International Doctoral Program, which funded my study in Kyoto University.

I am extremely grateful to Prof. Hajime Nakagawa and Prof. Tetsuya Sumi, Disaster Prevention Research Institute of Kyoto University, who have given their valuable comments and suggestions for refining this thesis.

Herein, I would like to express my sincere appreciation to Dr. Hiroshi Takebayashi, for his invaluable guidance, suggestions, encouragement, kindness, idea and patience during my study. I also would like to express my gratitude to Dr. Daizo Tsutsumi, for his inspiring guidance and kind hospitality during field observation in Hodaka Sedimentation Observatory. My gratitude is also for Dr. Shusuke Miyata for kind support, help and fruitful discussion. I thank all the professors and friends in the Research Center for Fluvial and Coastal Disaster, Disaster Prevention Research Institute of Kyoto University, who have made my academic experience rich and memorable. The help of the staff of Kyoto University and also Mrs. Junko Amano have also been most helpful.

The informal support and encouragement of many friends have been indispensable, and I would like particularly to acknowledge the contribution of Mr. Jazaul Ikhsan, Mr. Hiroaki Izumiyama, Ms. Kyuka Tomoko, and also all laboratory members, which have a friendly relationship (Mukai Akie, Takebe Masaki, Suzuki Yuichiro, Oshio Seitaro, Toan Nguyen MM, Hironao Kobayashi, Tamaki Tetsuya, Samoto Yoshiaki, Kamito Ryosuke, Ikkanda Satoshi, Nagano Kai, Yamanoi Kazuki, Kajihara, Ahmed Alaeidin, Chen Chen Yu and Chichi), also other members of Ujigawa Open Laboratory for their encouragement, cooperation, and unforgettable friendship.

I would like to express my special thanks to Prof. Djoko Legono, Gadjah Mada University, for giving the recommendation to study at Kyoto University. Also I would like to express my thanks for Prof. Bambang Triatmodjo, the head of Civil and Environmental Engineering Dept., and Dr. Adam Pamudji R., Gadjah Mada University. Special thanks to Dr. Muhammad Sulaiman, Dr. Adhi Kurniawan and Dr. Faisal Fathani, for their kind support and help. I also would like to say my special thanks to Mr. Suyitno and Mr Ade for supporting time and effort during field investigation in Sesayap River, Malinau, East Kalimantan Indonesia. I gratefully acknowledge to the Indonesian Government and Wijayakusuma University Purwokerto for having given me the opportunity and supports for continuing my study, and to the Japanese Government through Monbukagakusho for providing me the scholarship during my study.

My parent and my family have been a constant source for supporting emotional and moral during my doctoral years, and this thesis would certainly not have existed without them.

Special thank for my small family, my love wife Siti Uma Farida, my daughter Alifia Husnadhiya and my son Huda Ikhtiari. I am so sorry during three years, I couldn't bring all of you to enjoy the Japan's Culture. I wish, it will happen in the future.

Thank you all.

Kyoto, August 2012

Table Content

Chapter 1

Introduction

1.1 Background

Schumm (1971) has classified rivers into two major groups depending on their freedom to adjust their channel geometry. The first group is bedrock controlled channels, which are confined between outcrops of rock that material forming their bed and banks determines the morphology of the channel. The second group is alluvial channels, which are free to adjust their dimension, shape, pattern, and gradient in response to changes of hydraulic conditions. Alluvial channels have bed and banks composed of material that transported by the river. The bed and banks of alluvial rivers have high susceptibility on the lateral migration (Hooke, 1979; Hagerty, *et al.*, 1985; Schumm, 1985). Which means that the occurrence of the bank erosion more active in the alluvial rivers than other kinds of rivers.

Bank erosion is an important geomorphology phenomenon affecting changes in channel geometry. The bank erosion has a close relation or direct impact to human living and planning the countermeasure of it becomes one of challenges in erosion hazard in many countries. Bank erosion is not a massive disaster such as tsunami, earthquake or others. However, it can result in serious economic losses of private and public lands, infrastructure of transportations, agricultural and environmental sectors, and so on.

In a case of bank erosion, there are three fundamentals factors that are directly involved in its processes. These factors can be classified as geological, geomorphic and hydraulic factors. There are mutual relations among them. Thus bank erosion is close linked to other processes such as sediment transport and deposition. According to the interrelated processes, it should be note that of bank erosion problem cannot be solved by considering only one factor. Hence, integrated and spatial analyses are necessary to

apply on a countermeasure of bank erosion problem. And also the ecosystem in and around rivers and cost of countermeasures also should be considered.

The lack of understanding the mechanism of bank erosion process may lead to an inappropriate construction and only waste the budget. For a small and simple case as an example, Photo 1.1 shows the revetment wall used as a bank protection in Kuning River Yogyakarta, Indonesia. A part of the protection works was collapsed as shown in Photo 1.1 (b). It is may be due to the bed degradation at concave bend. And also the type of construction may not the well chosen, because if the bed degradation occurs, the weight of the construction becomes a sediment movement force as a bank failure. This case shows that the interaction among the geometry, bed material, flow and the method to protect the bank is not well understood by engineers. For example, the engineers which have successful experience to prevent bank erosions, they apply the same method at another place, which have different characteristics.

(a) (b)

Photo 1.1 Failed structure at outer bank. (Photo courtesy: Djoko Legono)

The geological factor, especially in the characteristics of the bank material, Schumm (1963) found that sinuous channels are characterized by a high percentage of silt and clay in the bank. In straight channels, the silt and clay contents tend to be smaller than in sinuous channels. This indicates that the type of bank material has a significant contribution on the result of bank erosion activity.

The bank materials can be classified as two types; cohesive and non-cohesive materials. The bank that composed of only non-cohesive material is not common in natural rivers. Hooke (1979) studied seven rivers in Great Britain. The results indicate that more than 50% the bank material is cohesive. Simon, *et al.* (2000) and Thorne,

(1991) have studied the Mississippi River, USA. The results show that the riverbank composed of cohesive material at the upper layer and non-cohesive material at the bottom layer. The Arno River in Central Italy also has riverbank stratification the same as in that Goodwin Creek (Dapporto, *et al.*, 2003). Photo 1.2 shows an example of a bank composed of both cohesive and non-cohesive layer in Sesayap River, East Kalimantan Indonesia.

Photo 1.2 The alluvial bank in Sesayap River showing non-cohesive sediment layer under the cohesive sediment layer

Photo 1.3 The failure block in Sesayap River that still covers a part area of the bank surface

The bank erosion process in such kind of riverbank which composed of cohesive material is mass failure process. Photo 1.3 shows the fallen block of cohesive material in Sesayap River still remain and cover a part of the bank surface. General processes in planar erosion of the alluvial bank are explained in analytical concept by Osman and Thorne (1988) and Thorne and Osman (1988). Figure 1.1(a) shows the initial bank

geometry. In this concept, the processes of bank failure are mainly triggered by bed degradation near the bank. As shown Figure 1.1(b), the bed degradation, Δz, increases the relative bank height or over steepening and increases the potential for destabilization of the bank with respect to mass failure. In this method, the basal point (see Figure 1.1(b) at point K) is assumed as an initial of the failure plane, which makes an angle with horizontal, and ending at the surface of the bank or the crack point. This concept was modified by Darby and Thorne (1996) with exchange of the initial point of the plane failure is not at the basal (see Figure 1.2 at point A). However, the bed degradation still as a factor on triggering bank erosion. Recently, many researchers also use bed degradation near the bank toe as the main factor on triggering bank failure (ex. Duan, 2005). The failure concept from those researchers indicates that the analysis of bed degradation near the bank toe is one of the important for countermeasures on bank erosion problem. In the other words, the bed degradation can be a indictor the possibility of bank erosion.

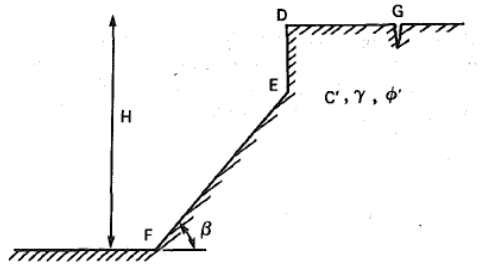

(a) Bank geometry at initial condition

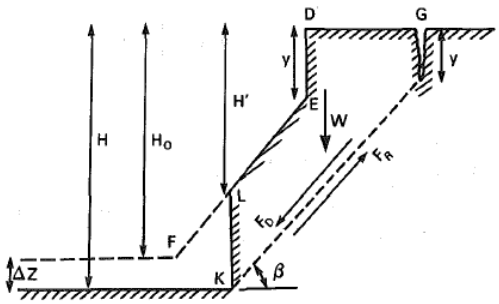

(b) Bank geometry at the beginning of failure

Figure 1.1 The type of bank geometry before and at beginning of failure that proposed by Osman and Thorne (1988)

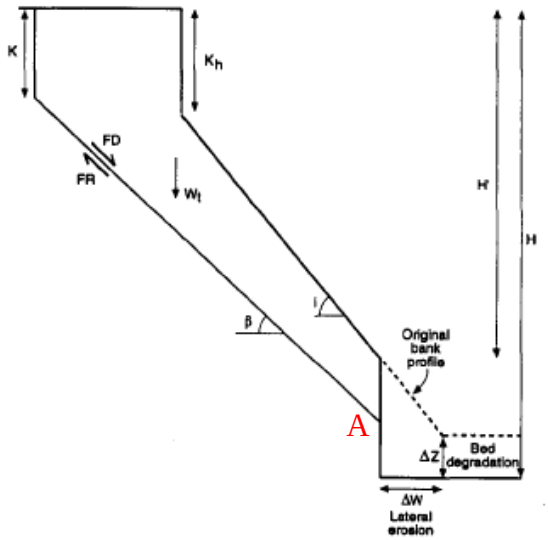

Figure 1.2 The type of bank geometry at beginning of failure that proposed by Darby and Thorne (1996)

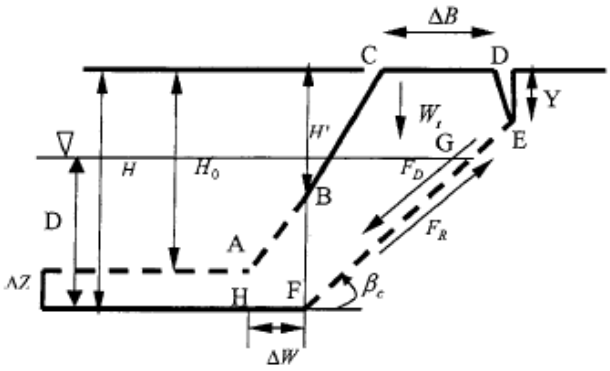

Figure 1.3 The concept of bank failure by Duan (2005)

In a geomorphic factor, the sand bar development has a significant contribution on the bank erosion problem. The relationship between bars and bank erosion has been shown implicitly by researchers from more than 50 years ago. As described by Leopold and Wolman (1957), Hooke (1986), Bridge and Gabel (1992) and Ashworth (1996). The mechanism of mid-channel bar is described in this research. The first stage in the development of the mid-channel bar is deposition of a layer of coarse material. Gradually, the bar extends in the downstream direction and with some increase in height by addition of gravel size material as well as more cobbles. Finer sediment accumulates particularly at the downstream end of bars. The end of the sand bar formation is usually indicated by covering of vegetation on the surface of bar. The bar splits the flow into two parts and the velocity concentrate at around the downstream end of the sand bar. The channel width continues to increase as long as the sand bar continues to grow. This

can be easily understood that the bank erosion occurs more strong during the bar growth. Figure 1.4 shows the bar that covered by vegetation and split the flow into two parts.

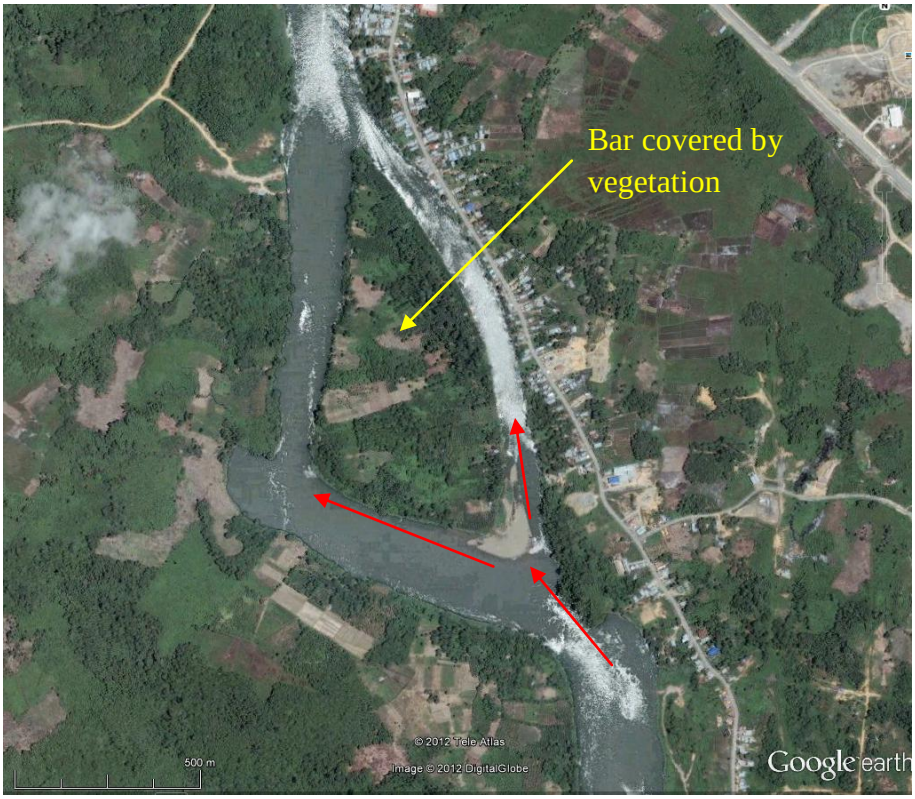

Figure 1.4 Aerial image of Sesayap River in Malinau reach showing the bar which covered by vegetation and split the flow into two parts

Another phenomenon that is close to bank erosion processes is the sediment transport, especially bed-load transport. The influence of coarse material sediment moving on the bed has been investigated by researchers, such as Kamphuis (1990), Thompson and Amos (2004) and many others. The results of these investigations show that the presence of bed-load transport can increase or decrease the shear stress magnitude on the bed surface. In natural rivers, the increase of bed shear stress can produce more erosion of the bed and promote the bank failure.

The relationship between bed-load transport and bank erosion can be noticed in volcanic rivers. Usually after an eruption, the concentration of sediment in volcanic rivers increases significantly due to the sediment supply from the erupted material. In a simple understanding, the material from eruptions can increase the volume of sediment because sediment supply is too much. However, in fact the riverbank erosion occurs

more strong. Furthermore, in particular reach the bed deggradation occurs too much and produce bank failure or other erosion hazards. For example, Putih River, which located in Central Java, Indonesia is one of the rivers that the origin is located at Mt. Merapi. After the eruption in 2010, the bank erosions have been occurred very intensively. Photo 1.4 shows the bank erosions taken place at a reach that caused land loss of paddy area. Photo 1.5 (a) shows the Srowol bridge (on Putih River). The bridge was collapsed just after the eruption of Mt. Merapi. Photo 1.5 (b) shows embankment after flowing out the bridge construction during flood. The structure of the bridge was collapsed due to the intensive degradation of the river bed. These facts give knowledge that the coarse material, which flowing in water as bed-load, can increase the degradation rate significantly.

The bed-load transport consumes a portion of energy of flow and causes an increase or a decrease of the flow velocity (Carbonneau and Bergeron, 2000). Most of scientists have been studied well on erosion due to the flow but the eroding media use clear water only and still few researchers consider the bed-load transport on erosion processes. Study the effect of bed-load transport on the dynamic shear stress is one challenge to improve the knowledge of erosion process on cohesive sediment bed.

(a) (b)

Photo 1.4 The bank erosion is very active after the eruption of Mt. Merapi, Indonesia on November 2010. Location is at the downstream end of Putih River before the merge to the Progo River

(a) (b)

Photo 1.5 The bed erosion is very active after Mt. Merapi eruption November 2010 (source: http://sekilasberita.blogspot.jp/2010/12/jembatan-srowol-jalur-alternatif.html)

1.2 Problem Statement

Regarding the riverbank erosion problem, it is shown that the relationship among the geological, geomorphic and hydraulic factors is not well understood. Many engineers, after having success with a particular protection technique, apply this single method to all situations, regardless of the site conditions. Due to the difficulties of the analysis of a river system in one model calculation, most of the calculations are done separately. Usually the flow and bank erosion are not done in one modeling system. This is not a problem if the integrated analysis always be done by engineers. The integrated investigations for flow and bank erosion are necessary for achieving the successful project works, because the selection of an appropriate countermeasure for a specific bank erosion problem depends on many factors such as the erosion mechanism, stream characteristics, construction and maintenance requirements, and costs. Determination of the dominant factors is a basic step in the countermeasure of bank erosion problem.

In an analytical theory for calculating the bank failure, the bed deformation is an important parameter on triggering the bank erosion, so the calculation accurately on this magnitude will determine the quality of the results. In most of bank stability analysis, the calculations of bed deformation are simplified and they also ignore the effect of flow

characteristics. The calculation become inaccurate if the bed deformation is strongly influenced by flow characteristics.

In restoration projects, the structures of bank protection are applied generally as a countermeasure of the bank erosion problem. The structures, such as groynes, revetments and so on, will success to protect the riverbank locally. Usually the structures will change the cross-sectional geometry, which lead to change the flow pattern or others hydraulic parameters. In other words, the structure will produce another bank erosion problem in other places, especially in the case that the flow and bed morphology are a dominant factor for triggering the bank erosion problem. It is necessary to evaluate the negative effect of such countermeasures. A reach of the Sesayap River, in Indonesia, is studied in order to examine the interaction of channel geometry, water flow, sediment transport and deposition associated with countermeasures of bank erosion problem in this research. Field surveys to get primary data such as topography, flow velocity, bed material, bank material, and river stages were conducted.

The most common stratification of riverbank is cohesive sediment layer overlaying on the non-cohesive sediment layer. The presence of cohesive material in riverbank has an important effect on the bank line migration. As explained in the background, the bed deformation of non-cohesive material is the dominant processes on triggering the bank erosion on the bank, which has high cohesive content. However, the most experimental or numerical study in river morphology used only non-cohesive material as an eroded bank. Studying the effect of cohesive material on bank erosion processes may give advance in river morphology modeling.

It is widely known that the presence of sediment transport can increase the occurrence of bank erosion. Many great experimental studies have been conducted on the erosion processes, but most of them used clear water as an eroding media, and few studies consider on the presence of bed-load transport on erosion phenomenon. Therefore, it is essential to develop an experimental study for the erosion process considering bed-load transport. This is important to improve the knowledge in the erosion mechanism on the river bed morphology. The presence of bed-load transport has a close relationship to the process of deformation on the bed as already mentioned that the deformation of the river bed is mainly related to the process of bank erosion.

The bed deformation has been studied in experimental laboratory by many researchers, however only using clear water as eroding media. And also, they used the non-cohesive material on the bed. However, the bed material in many rivers all over the world is composed cohesive sediment or fine material, (ex. Tonle Sap River in Cambodia). The influence of bed-load transport on cohesive sediment bed should be studied to understand the formative mechanism of bed morphology.

1.3 Objectives of the Research

This research addresses the fundamental issues related to the interaction of fluvial and geotechnical factors affecting erosion processes. Especially, the effect of the presence of the cohesive material in river channels both as a bank and sediment bed. The objectives of this study can be described as follows:

(1) Based on field analysis, this study figures out the processes and the mechanism of bank erosion problem in such as alluvial river with the bank composed of both cohesive and non-cohesive material. This research will figure out the erosion process in river which bank composed of both cohesive and non-cohesive material and the bed material is non-cohesive.

(2) Based on numerical analysis, this study seeks to apply simulation model in Sesayap River in order to understand the causes of bank erosion problem. Field analysis was conducted to identify dominant mechanisms of bank failure along the Sesayap River and apply methods in countermeasure of bank erosion problem and identify the characteristic impact on it. In addition, one of the objectives is to develop a method to counteract the bank erosion problem in such alluvial river for the banks which have cohesive and non-cohesive materials.

(3) By using experimental test, this research investigates the erosion characteristics of cohesive sediment bed. The water and bed-load transport are used as eroding media. The results from the experiments are applied in a natural river to study the effect of the horizontal distribution of cohesive material on bed deformation characteristics.

1.4 Thesis Outline

The thesis is composed of six chapters. The framework of this research and its correspondence of each chapter is shown in Figure 1.5. The synopsis of each chapter is described as follows:

In Chapter 1, the main factors that involved on bank erosion processes are described. The effect of cohesive and non-cohesive sediment and the important relations among them in erosion processes of alluvial river are presented. The problem statement and objectives of the research are also described.

In Chapter 2, the problems related to the bank erosion are presented in general view. The experiments using cohesive and non-cohesive materials were performed. The purpose from this experiment is to get better understanding of the processes of bank erosion on bank which is composed of non-cohesive and cohesive materials. The model of bank erosion and the effect of flow magnitude on bank line retreat are discussed.

In Chapter 3, the effects of bed-load transport on erosion rate of the fine materials were conducted experimentally. The purpose of these experiments is to investigate the effect of bed-load transport on erosion rate of cohesive sediment bed.

In Chapter 4, the field investigation data in study site are presented. The hydro-climatology data of Sesayap River basin are collected. The topography of floodplain and the bathymetry of river channel are investigated. And also the river bank characteristic is investigated by soil test procedure. The main purpose in this chapter is to determine the dominant factor that triggers bank erosion. Numerical analysis for countermeasure of the bank erosion problems is performed. The finite difference and MacCormack scheme is used to solve the equation in curvilinear non-orthogonal grid. The calculation of sediment transport and morphologic evolution on the river bed is considered along with the size distribution of bed material. A sediment transport multilayer model is used to reproduce the bed deformation process. The effects of mid channel bar in associate to the bank erosion are discussed. A countermeasure by removing the bar and a construction of bank protection are presented in Chapter 4. The effects of countermeasures on the bed morphology and flow pattern are investigated, spatially.

In chapter 5, the numerical analysis on relationship between the erosion characteristics of cohesive sediment and transport process of non-cohesive sediment in the natural river is presented. The Tonle Sap River in Cambodia was chosen as study site. A unique hydraulic condition in this river gives a natural example on interaction between cohesive and non-cohesive material in the river. The hydraulic conditions in this river are strongly affected by Tonle Sap Lake and Mekong River. The non-cohesive bed-load transport flows on the cohesive sediment bed during flood season. The bed deformation characteristics of cohesive sediment bed are discussed.

In Chapter 6, the conclusions and the future perspectives of researches are stated.

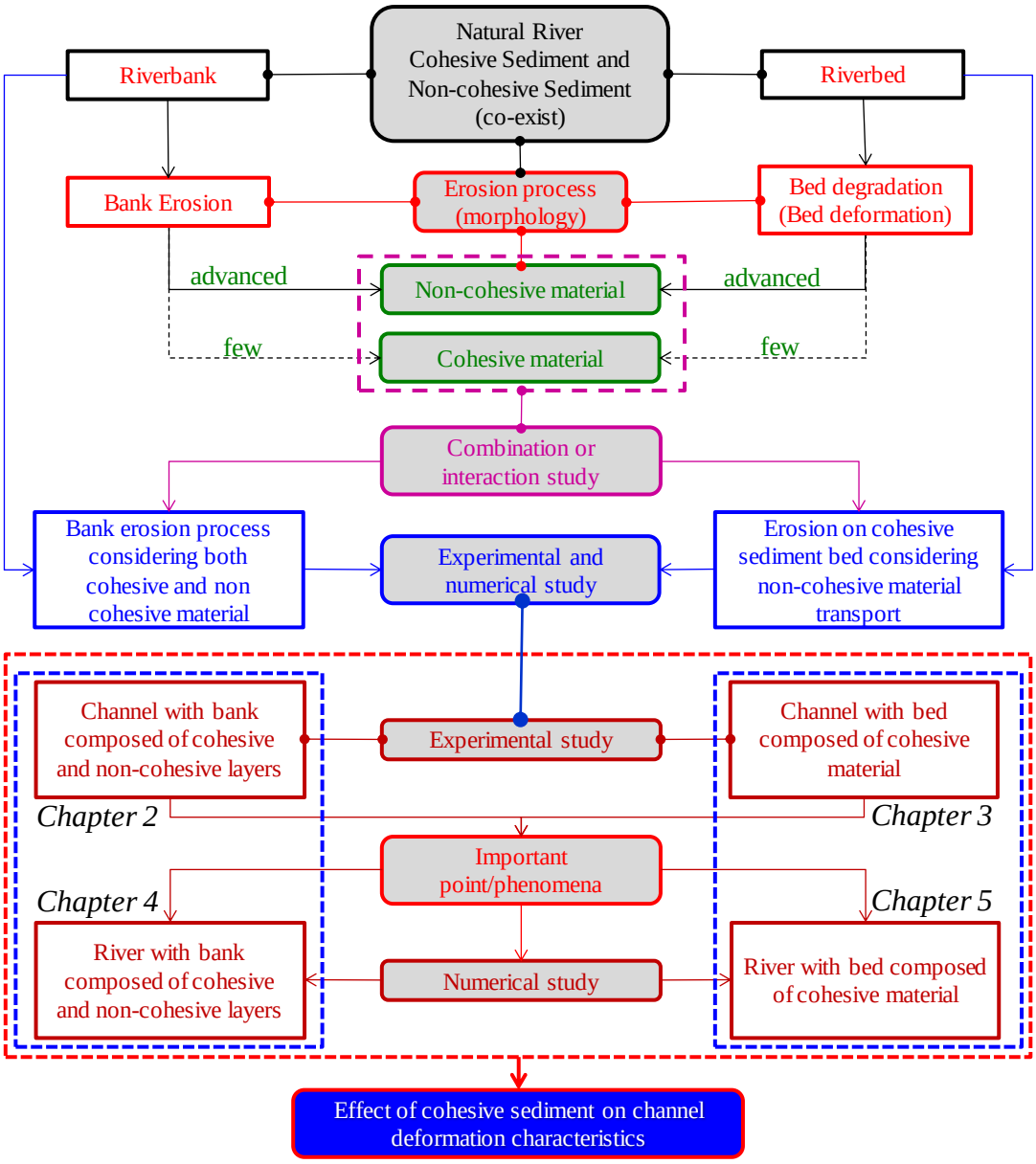

Figure 1.5 The framework of research and its correspondence of each chapter

References

Ashworth, P.J.: Mid-channel bar growth and its relationship to local flow strenght and direction, *Earth Surface Processes and Landforms*, Vol. 21, pp. 103-123, 1996.

Bridge, J.S., and Gabel, S.L.: Flow and sediment dynamics in a low sinuosity, braided river: Calamus River, Nebraska Sandhills, *Sedimentology*, Vol. 39, pp. 125-142, 1992.

Carbonneau, P.E., and Bergeron, N.E.: The effect of bed-load transport on mean and turbulent flow properties, *Geomorphology*, Vol. 35, pp. 267-278, 2000.

Dapporto, S., Rinaldi, M., Casagli, N., and Vannocci, P.: Mechanisms of riverbank failure along the Arno river, central Italy, *Earth Surf. Process. Landforms*, Vol. 28, pp. 1303–1323, 2003.

Darby, S.E., and Thorne, C.R.: Development and testing of riverbank stability analysis, *Journal of Hydraulic Engineering*, ASCE, Vol. 122, No. 8, pp. 443-454, 1996.

Duan, J.G.: Analytical approach to calculate rate of bank erosion, *Journal of Hydraulic Engineering*, ASCE, Vol. 131, pp. 980-990, 2005.

Hagerty, D.J., Spoor, M.F., and Unrich, C.R.: Bank failure and erosion on the Ohio River, *Engineering Geology*, Vol. 17, pp. 141–158, 1981.

Hooke, J.M.: An analysis of the processes of river bank erosion, *Journal of Hydrology*, Vol. 42, pp. 39-62, 1979.

Hooke, J.M.: The sinificance of mid-channel bars in an active meandering river, *Sedimentology*, Vol. 33, pp. 839-850, 1986.

Kamphuis, J.W.: Influence of sand or gravel on the erosion of cohesive sediment, *J. of Hyd. Research*, Vol. 28, No. 1, pp. 43-53, 1990.

Legono, D.: Flood Phenomena in Yogyakarta, Indonesia, *Discussion Handout*, Gadjah Mada University, 2008. http://djokolegono.staff.tsipil.ugm.ac.id/files/2008/06/fenomena-banjir-diy.pdf

Leopold, L.B. and Wolman, M.G.: River channel patterns: braided, meandering, and straight, *U.S. Geological Survey Prof.* Paper 282-B, pp 283-300, 1957.

Osman, A.M., and Thorne, C.R.: Riverbank stability analysis I: Theory, *Journal of Hydraulic Engineering*, Vol. 114, No. 2, pp. 134-150, 1988.

Schumm, S.A.: Sinuosity of Alluvial Rivers on the Great Plains, *Geological Society of America Bulletin*, Vol. 74, No. 9, pp. 1089-1099, 1963.

Schumm, S.A.:Fluvial geomorphology in river mechanics, *Water Resources Publication*, Fort Collins, Co., pp. 365-395, 1971.

Schumm, S.A.: Patterns of alluvial rivers, *Ann. Rev. Earth Planet. Sci.*, Vol. 13, pp. 5-27, 1985.

Simon, A., Curini, A., Darby, S.E., Langendoen, E.J.: Bank and near-bank processes in an incised channel, *Geomorphology*, Vol. 35, pp. 193-217, 2000.

Thompson, C.E.L., and Amos, C.L.: Effect of sand movement on a cohesive substrate, *Journal of Hydraulic Engineering*, ASCE, Vol. 130, No. 11, pp. 1123-1125, 2004.

Thorne, C.R.: Bank erosion and meander migration of th red and Mississippi River, USA, *IAHS, Proceed. of the Vienna Symp.*, No. 201, pp. 301-313, 1991.

Thorne, C.R., and Osman, A.M.: Riverbank stability analysis II: Application, *Journal of Hydraulic Engineering*, Vol. 114, No. 2, pp. 151-172, 1988.

Chapter 2

Experimental Study on Erosion Process of Banks with Composed of Both Cohesive and Non-cohesive Layers

2.1 Introduction

Composite river bank formation is quite common in large alluvial rivers and very high bank erosion rate is commonly reported in this type of formation. As one of the bank composition, usually cohesive layers are sandwiched by non-cohesive layers. For example, the top sediment layer of banks in the Sesayap River at Malinau reach, East Kalimantan Province, Indonesia has cohesive characteristics. On the other hand, the bottom layer of the bank is composed of coarser material and does not have cohesive characteristics. Both of cohesive and non-cohesive materials are the most important component of the river that plays rule in the bank erosion process. Due to the differences of the mechanical properties of cohesive and non-cohesive materials, the standard characteristic of bank erosion that is composed of only non-cohesive or cohesive or both of them have different mechanism. Many researchers have studied the bank erosion processes in natural rivers (Hooke, 1979; Lawler 1995, Couper and Maddock 2001; etc.). The results give basic knowledge on the processing of the removal of bank material.

Hooke (1979) concluded the removing of bank material into two main processes, i.e. fluvial erosion and bank failure process. In recent studies, the process has been added with the sub-aerial process (Lawler 1995, Couper and Maddock 2001). Subaerial process is a process that contributes to bank retreat and as usually a preparatory process weakens the bank face prior to fluvial erosion (Couper and Maddock 2001) and also acting on the upper part of the bank (Lawler 1995).

The fluvial erosion is a common process at the lower part of the bank and riverbed and directly controlled by river flow condition (Hooke, 1979). Fluvial erosion is the direct removal of particles from the bed or bank by hydraulic forces associated with

flow velocity (ASCE Task Committee, 1998; Prosser *et al*., 2000; Couper and Maddock, 2001). As water flows in a channel, the shear stresses developed on the bed and banks. If the shear stress on the bed or bank is more than the critical shear stress, erosion will occur, and deposition will occur elsewhere.

Bank failure, which includes bank collapse and slumping, occurs when large pieces of material or complete sections of the bank become unstable and dislodge from the rest of the bank. This process is controlled by gravitational process, moisture and mechanical properties of the bank and also can act only on upper part or all part of the bank.

In natural rivers which have a composite structure of non-cohesive overlaid by cohesive silt (or clay), the fluvial erosion occurs at the lower bank with higher rate than at the upper layer that leads to undermining then produces cantilevers of cohesive material. The upper layer eroded by the failure of these cantilevers (Thorne, 1981; Simon, *et al.*, 2000). This gives the knowledge that the composition of bank material is determines the rate and type of bank erosion process. This is very important on channel evolution model.

Numerical model is a familiar analysis to predict the future condition. Many scientists have developed numerical analysis on channel evolution model. Most of numerical in bank erosion model using non-cohesive material (Nagata *et al.*, 2000; Duan and Julien, 2005; Duan and Julien, 2010; etc). However, for natural rivers, the practical applications of analyses for non-cohesive banks are limited by the fact that most alluvial bank materials exhibit some cohesion (Thorne, 1991). Takebayashi (2010) has developed a numerical analysis to compare the bank line migration with bank composed of both cohesive and non-cohesive material. The rate of the bank line migrations is quite different among of banks that is composed of non-cohesive only or cohesive only or both of them. However, few researchers studied the processes of such kind of the bank in an experimental laboratory.

The objective of this experiment is to study the effect of cohesive material on the bank erosion process. The effect of cohesive sediment is divided into three categories, i.e. bank without cohesive material, bank with half cohesive and with full cohesive material. The rate and characteristics of bank line migration will be investigated.

2.2 Experimental Setup

The objective of this experiment is to study the erosion process and mechanism of bank failure for one side of flood plain bank. The experiments are conducted in flume test which has 10 m long, which is divided into two parts. Upstream channel that has 0.15 m wide and 8 m long is channel for providing the sediment continuously from the upstream end of channel. The 8 m long is to provide sediment transport in equilibrium. Downstream channel that has 0.4 m wide and 2 m long is an observation channel. The walls have 0.25 m high, which are made from wood (left side) and acrylic (right side). The flume test has a tilting machine to adjust the slope of the channel. Figure 2.1 shows the schematic of experiment setup from the top and right side view.

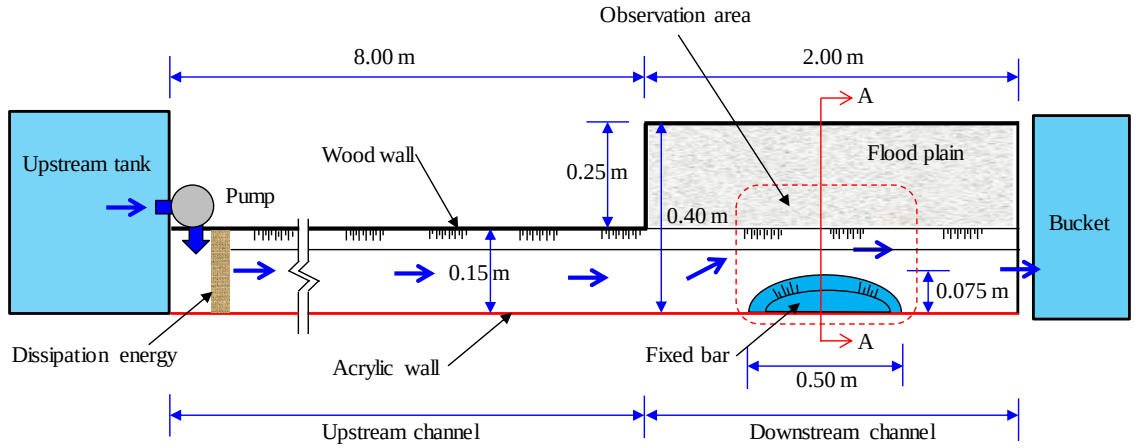

(a)

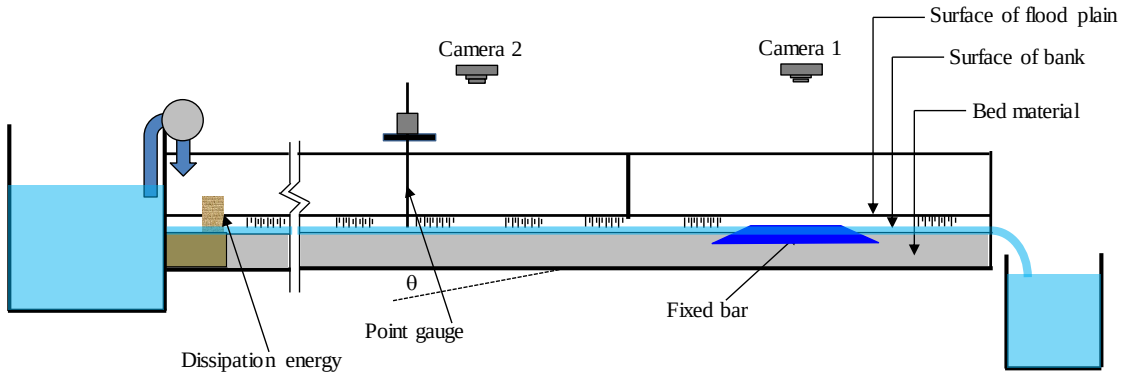

(b)

Figure 2.1 Schematic of the experiment setup, (a) top view and (b) right side view

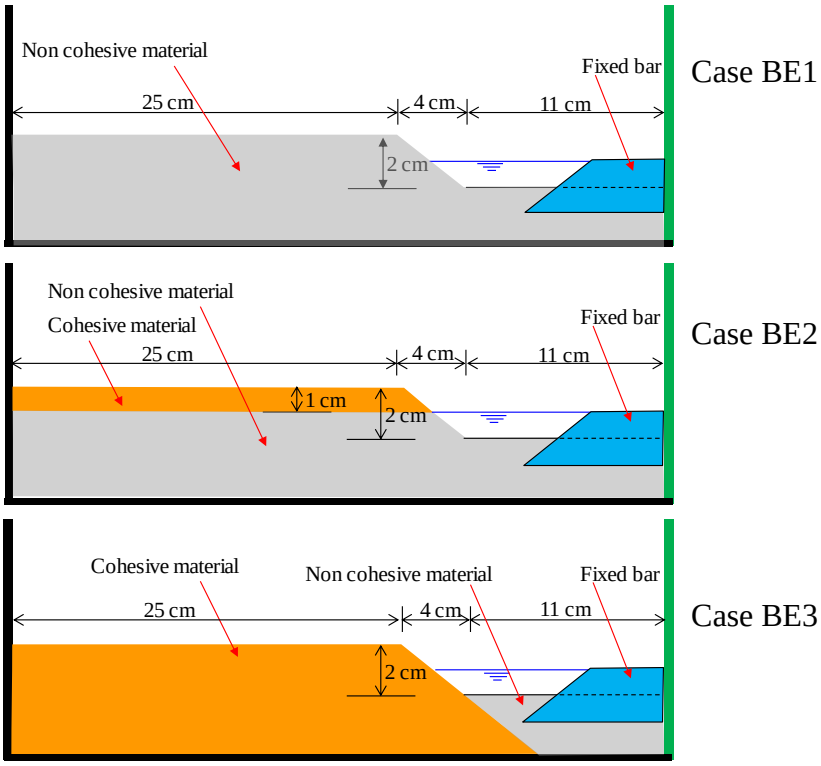

Figure 2.2 Cross section A-A for each case

2.3 Experiment Cases and Properties of Materials

To accelerate the bank erosion process, a fixed point bar was set around at the middle of the observation channel (see Figure 2.1 and Figure 2.2). This bar will divert the flow from upstream channel and attack the bank surface in the observation area. This experiment was run under three cases (Case BE1, Case BE2 and Case BE3), which have different bank properties on the floodplain. The properties of bank for each case are explained as follow:

(1) Case BE1: the bank has non-cohesive material only.

(2) Case BE2: the bank has two layers material. Top layer is composed of cohesive material and lower layer is composed of non-cohesive material.

(3) Case BE3: the bank has cohesive material only.

Figure 2.2 shows the cross sectional view and dimension of the bank for all experiments.

The eroded material from the riverbank is considered as one of sediment sources to the channel, so the geometries of the banks for all cases are designed with the same dimension. This is to make sure that there are no differences in the resources volume of sediment from the bank. In the natural river, there is some difference in shape and slope of bank between the cohesive sediment and non-cohesive sediment bank. The surface bank slope is about 31 degree with horizontal, which is considered to equal the repose angle of the non-cohesive material in dry condition. The processes of bank erosion depend on many factors. Some simplifications of these experiments are conducted, such as:

– The water content of cohesive materials is designed in the same condition.

– The effect of the vegetations on the bank failure processes is neglected.

– The influence of water pressure from the bank is neglected.

The non-cohesive material has 0.88 mm for D_{50} and 1.66 mm for D_{90}. The specific weight is 2.65. The cohesive material is the industrially white kaolin, which has 4.616 μmm for D_{50}. The size distributions of non-cohesive and cohesive materials are shown in Figure 2.3.

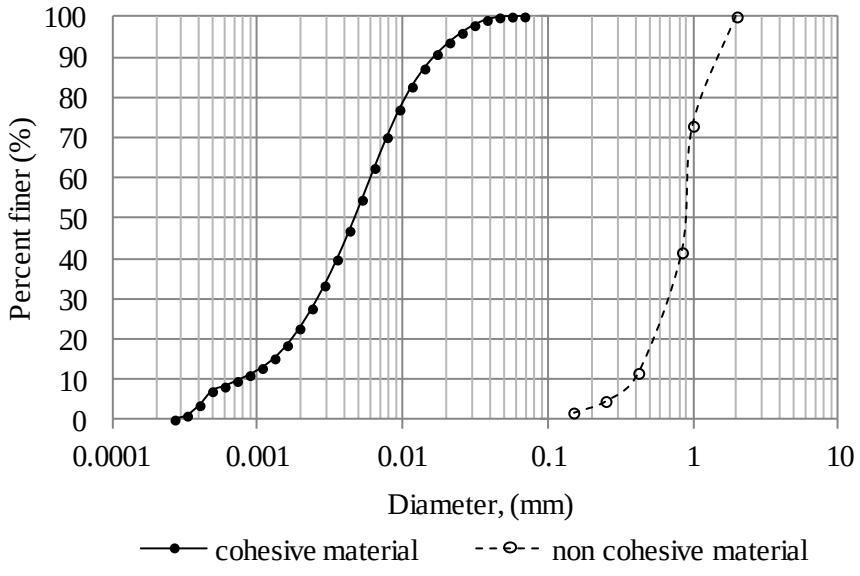

Figure 2.3 Size distributions of cohesive and non-cohesive materials

2.4 Experiment Methods

This experiment is to study the effect of cohesive material on erosion process and the mechanism of the bank erosion. According to the objective, the cases are designed under the same condition except for the bank properties. Two kinds of observation are conducted, i.e., first is observation of lateral migration of the bank line and second is observation of cross section profile of the bank.

Lateral migrations are observed by a fixed camera to capture the shift of the bank line in floodplain area. The camera was put on the above of the downstream channel and take pictures during experiment with a certain time interval. In this experiment, the time interval is 10 second. The position of the camera is shown in Figure 2.1 (b) and indicates by name Camera 1.

The cross section at initial and the final stages of experiment are measured using point gauge, which has accuracy 0.1 mm. The location of the cross section is at the maximum erosion for each case and two cross section at around 10 cm upstream and downstream sides. Additional measurements are also conducted, i.e. flow depth and velocity for initial condition. These measurements were conducted to calibrate between the designed hydraulic condition and the real hydraulic condition. The location for these measurements is at the middle of the upstream channel as shown in Figure 2.1 (b). The bed and the water level are observed to calculate the flow depth for initial hydraulic condition. The velocity on the surface flow is observed by tracking of the floating material. Using the fixed high speed camera, which is put on the above the channel. The vertical distribution of the flow is assumed as depth average velocity. The measurement of the water discharge is conducted by collecting the volume of water at the downstream end of the channel during a certain time.

2.5 Hydraulic Conditions

Bed shear stress is an important parameter for bed deformation processes, whether aggradation or degradation process. If the bed shear stress does not exceed the critical value, no bed load transport takes place, but maybe the deposition will occur. This experiment is addressed on bank erosion processes, which has strong relation to bed

deformation. So, the hydraulic conditions are designed in order to produce the bed shear stress, τ^*, exceed the critical value. The critical value is the critical shear stress of the bed material, τ_c^*. The mean diameter for the non-cohesive material in these experiments is 0.88 mm, so the critical shear stress is 0.34 (Iwagaki, 1956).

Hydraulic conditions for Case BE1, Case BE2, and Case BE3 are under the same condition. The slope of the flume is 0.01. The water discharge and depth are 0.45 l/s and 1.2 cm, respectively. The discharge flowing in the flume was controlled by a pump. The water discharge was measured with collecting water at the downstream end by bucket within a certain time. Before the main experiment, the preliminary experiment is conducted to calibrate the roughness of the channel. This magnitude is used to calculate volume bed-load transport then predict the maximum duration for experiment As explained in Sub-chapter 2.2 that the upstream channel is performed to produce the bed-load transport continuously. So, according to the non-cohesive material properties and hydraulic condition, the maximum experiment time is predicted within 27 minutes long. The hydraulic conditions for all cases are shown in Table 2.1.

Table 2.1 Hydraulic conditions for Case BE1, Case BE2 and Case BE3

Parameters	Case BE1	Case BE2	Case BE3
Discharge (l/s)	0.455904	0.450095	0.449549
Slope, I	0.01	0.01	0.01
Water depth, Ho (m)	0.012	0.012	0.012
Width average, B (m)	0.115	0.115	0.115
Aspect ratio, B/Ho	9.58	9.66	9.66
Hydrailic radius, R (m)	0.0099	0.0098	0.0098
ρ_w (kg/m^3)	1000	1000	1000
ρ_s (kg/m^3)	2650	2650	2650
g (m/s^2)	9.81	9.81	9.81
Flow velocity (m/s)	0.3317	0.3300	0.3298
D_{50} of the bed material (mm)	0.88	0.88	0.88
τ_c*	0.034	0.034	0.034
τ*	0.0677	0.0682	0.0677
qb (m^3/s)	1.82044E-07	1.73758E-07	1.72987E-07
Froude number, F	0.969	0.967	0.967
$BI^{0.2}/Ho$	3.830	3.860	3.863

The hydraulic condition is also designed to produce the uniform flow. In this condition, the flow in experiment should not produce the bar formation on the channel bed. The regime criteria on bar by Kuroki and Kishi (1984) is used to design the flow

depth and the width of channel. Figure 2.4 show the hydraulic condition of the experiment in the graph of regime criteria on bar. From this figure indicate that the flow does not produce bar on the bed. The bed form is also checked by using *R/d* parameter. Figure 2.5 show that the flow regime of the experiment in transition regime. The hydraulic condition of the experiment, as shown in Figure 2.4 and Figure 2.5, indicates that the flow can produce a uniform flow.

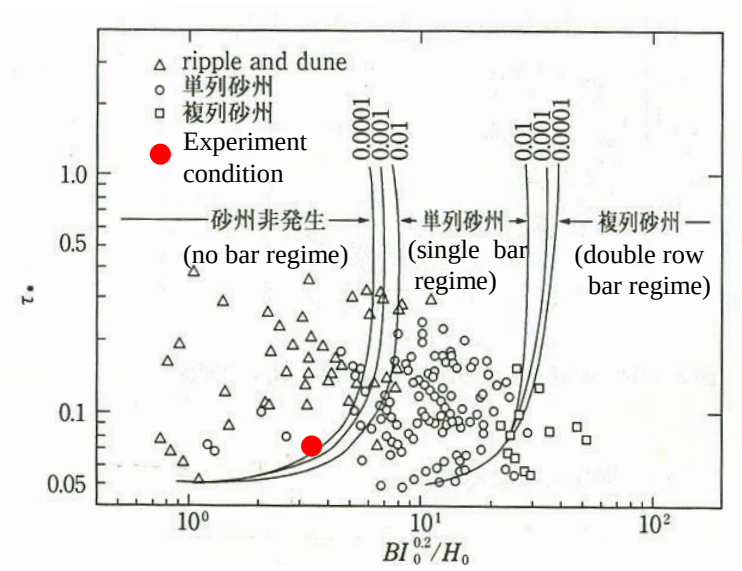

Figure 2.4 Hydraulic condition in regime criteria on bar (Kuroki and Kishi, 1984)

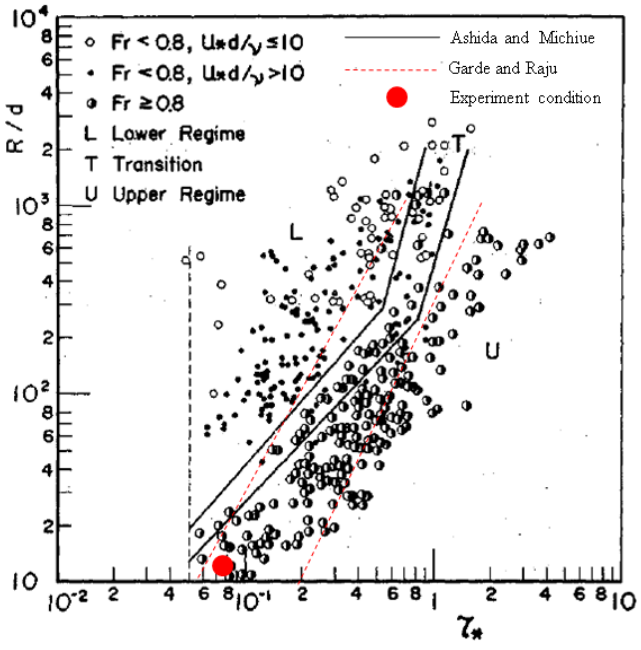

Figure 2.5 The flow regime condition of the experiment

2.6 Characteristics of Erosion Rate of Bank

2.6.1. Initial Condition of Bank

These experiments consist of three main cases. For all experiment, the bed is composed of non-cohesive material. First case is a bank erosion experiment which bank composed non-cohesive material only (Case BE1). Photo 2.1 and Photo 2.2 show the condition of the channel in Case BE1. The bank and bed material have same characteristics. Second case is a bank erosion experiment which bank composed cohesive and non-cohesive material (Case BE2). Photo 2.3 and Photo 2.4 show the condition of the channel in Case BE2. The bottom layer material of the bank and bed material have same characteristics. Photo 2.5 and Photo 2.6 show the condition of the channel in Case BE3. The bank material is totally composed of cohesive material.

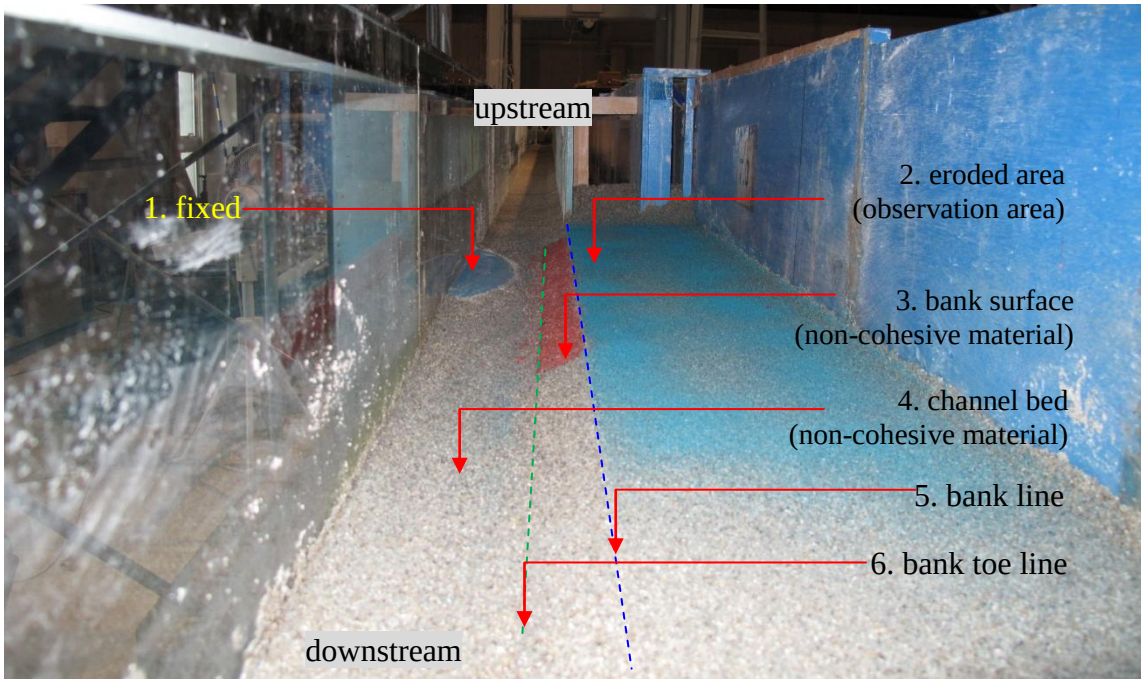

Photo 2.1 The initial condition of channel and bank in Case BE1 (perspective view)

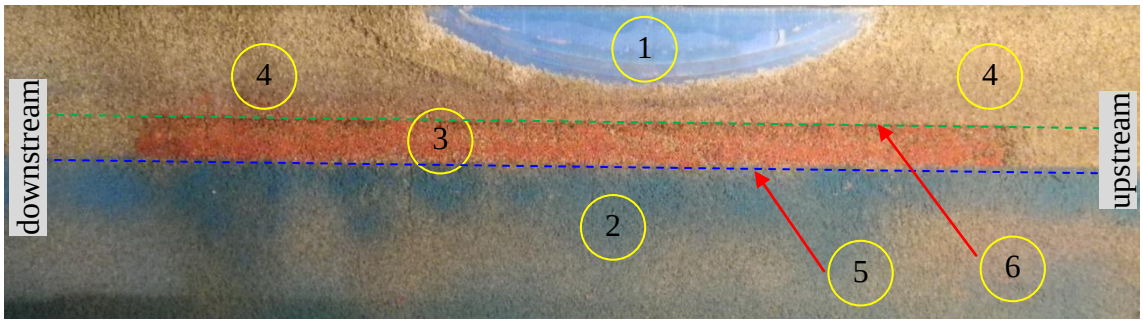

Photo 2.2 The initial condition of channel and bank in Case BE1 (top view)

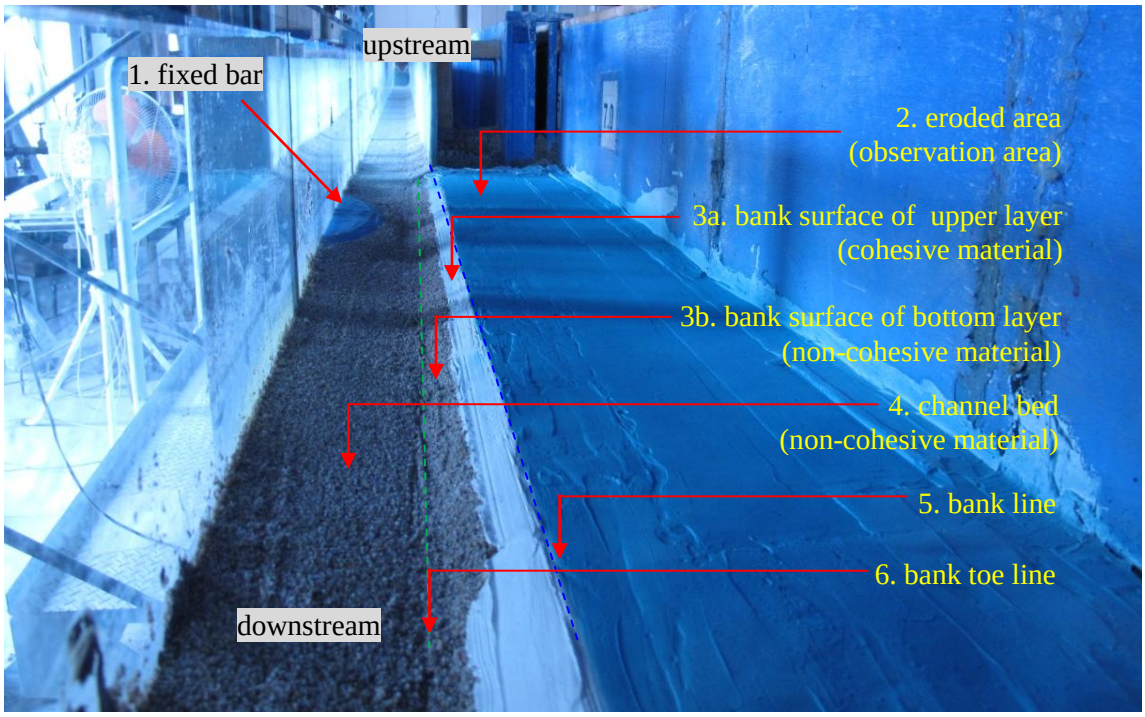

Photo 2.3 The initial condition of channel and bank in Case BE2 (perspective view)

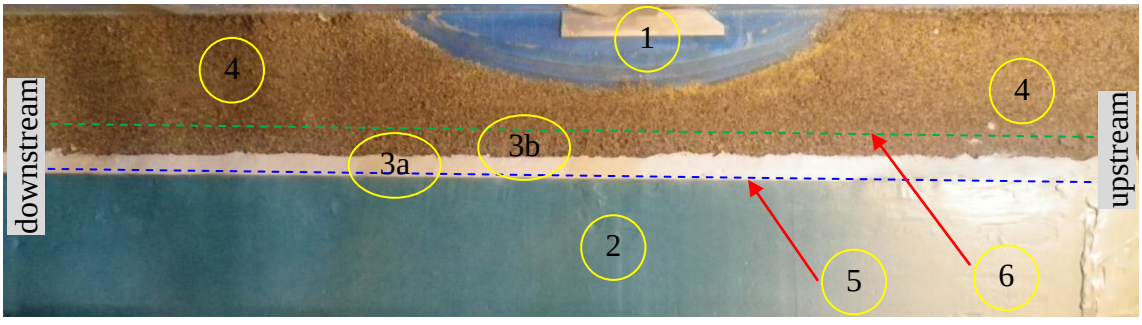

Photo 2.4 The initial condition of channel and bank in Case BE2 (top view)

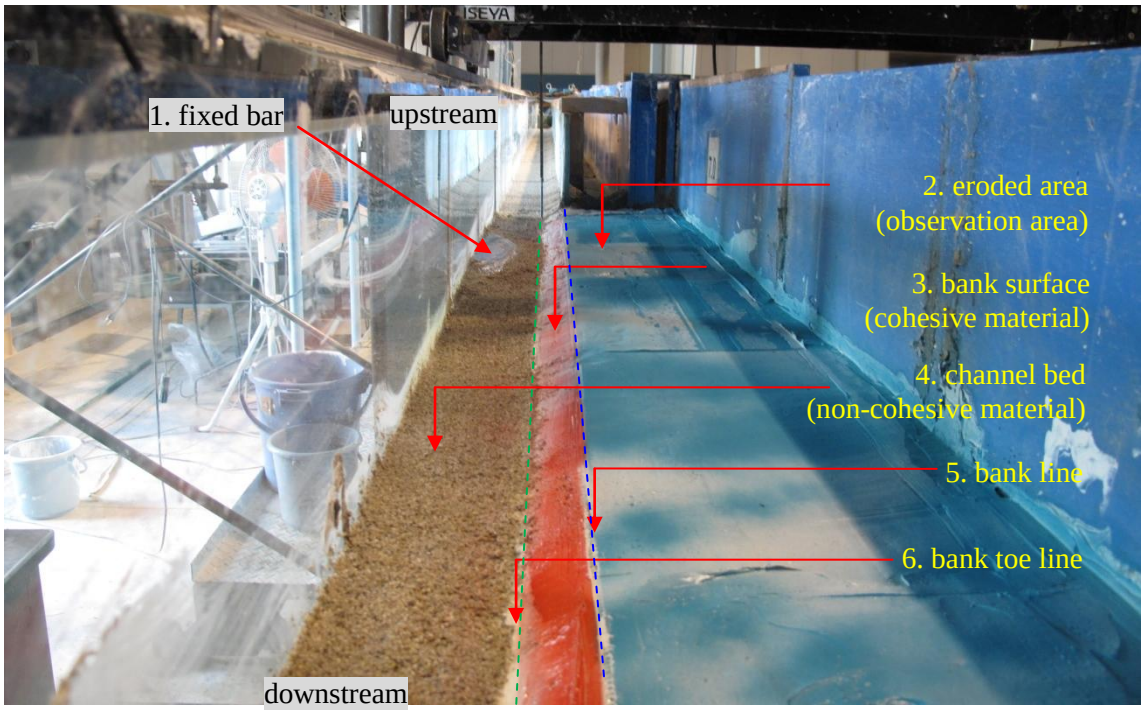

Photo 2.5 The initial condition of channel and bank in Case BE3 (perspective view)

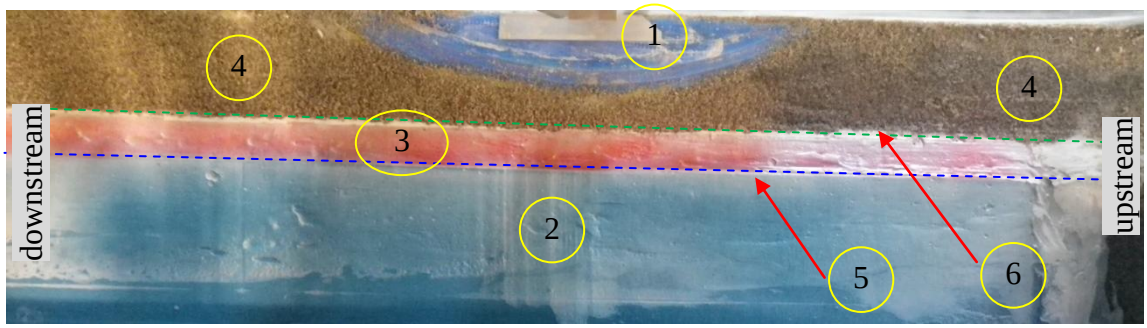

Photo 2.6 The initial condition of channel and bank in Case BE3 (top view)

2.6.2. Erosion Characteristics

The condition of bank migration was investigated under all experiments. If the bank line is not altered, the experiment will be stopped or experiment will be stopped at around 27 minutes. Photo 2.7, Photo 2.8 and Photo 2.9 show the top view at the beginning of the experiment in Case BE1, Case BE2 and Case BE3, respectively. With visual observation during experiment, at the beginning of the experiment, the flow initiates the fluvial erosion of the bed material. This occurred in all cases. The fluvial

erosion rate on the bank at the lower part in Case BE1 and Case BE2 is faster than that Case BE3. The fluvial erosion may cause the bed degradation at the bank toe area in Case BE1 and Case BE2. However, in Case BE3 erosion rate is very slow, because the bank is composed of cohesive material. The flow condition is not enough to erode large volume of the cohesive layer bank. The erosion process occurs in the cohesive layer with very small value so that it cannot be recognized by the photo.

The bank toe erosion is the important parameter for triggering mass failure processes of bank (Darby and Thorne, 1996; ASCE Task Committee, 1998; Simon *et al.*, 2000; etc.). The erosion on the bank toe in Case BE1 is followed by mass failure of the upper layer. The upper layer in Case BE1 is non-cohesive layer (the same with the bottom layer) so the mass failure only depends on the repose angle. If the bank angle exceeds the repose angle, the bank will fail into the channel and entrainment by the flow. The duration for achieving the critical repose angle is relatively short. And it is indicated by the mass failure of the upper part of the bank. Bank failure in Case BE1 failure occurred earlier compared to another cases. As shown in Photo 2.7 (b) (indicated by red arrow), the bank line is clearly visible retreated.

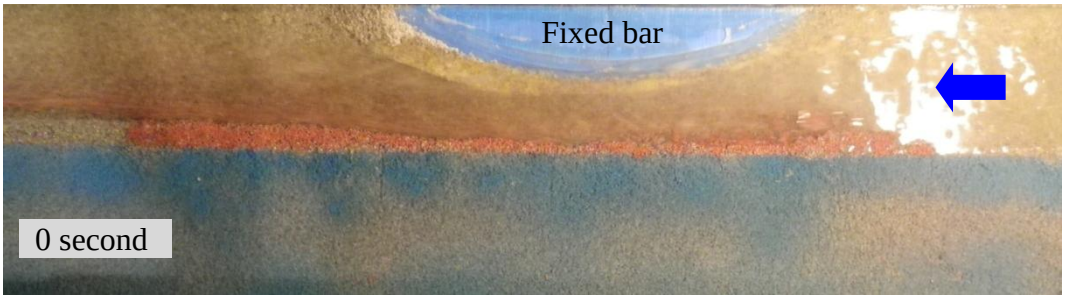

(a)

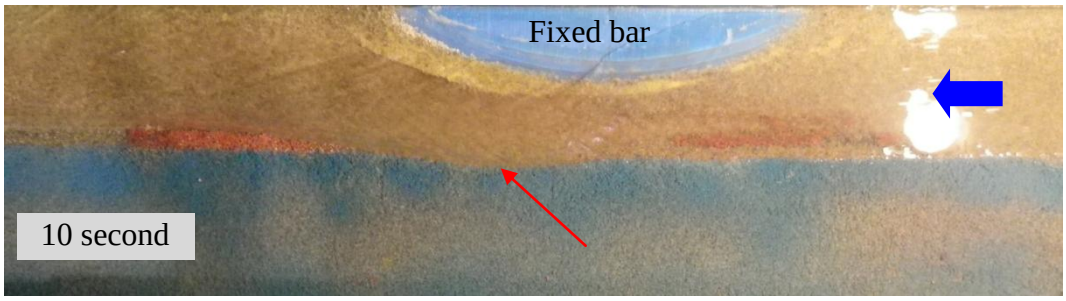

(b)

Photo 2.7 Temporal changes of channel geometry in Case BE1 at the beginning of flow. The flow direction is from right to left side

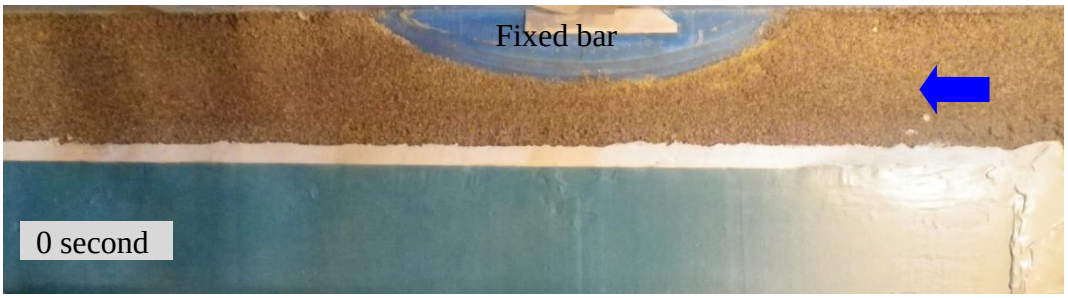

(a)

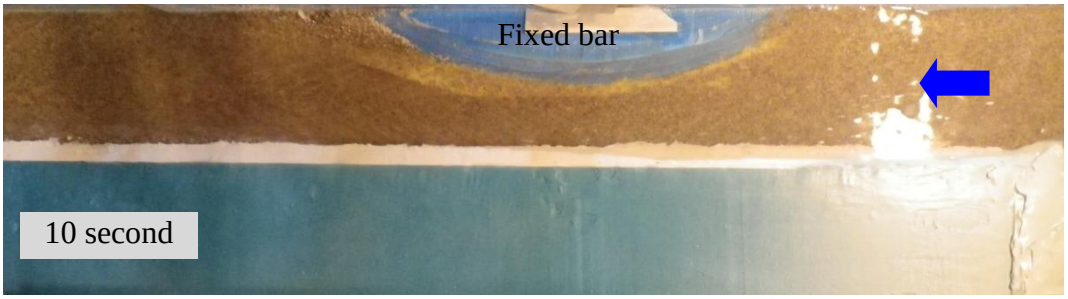

(b)

Photo 2.8 Temporal changes of channel geometry on Case BE2 at the beginning of flow. The flow direction is from right to left side

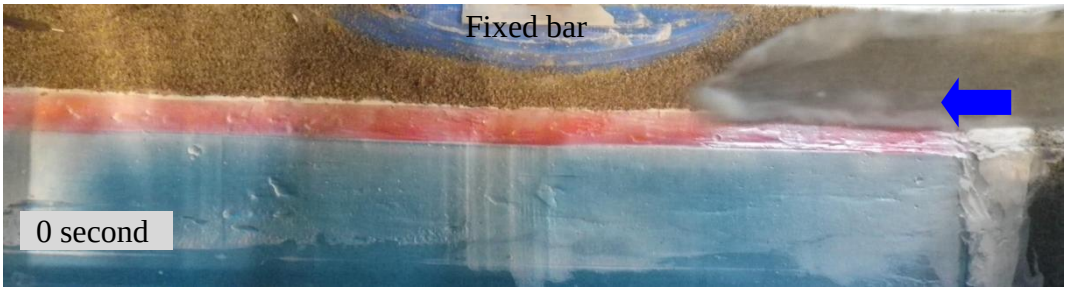

(a)

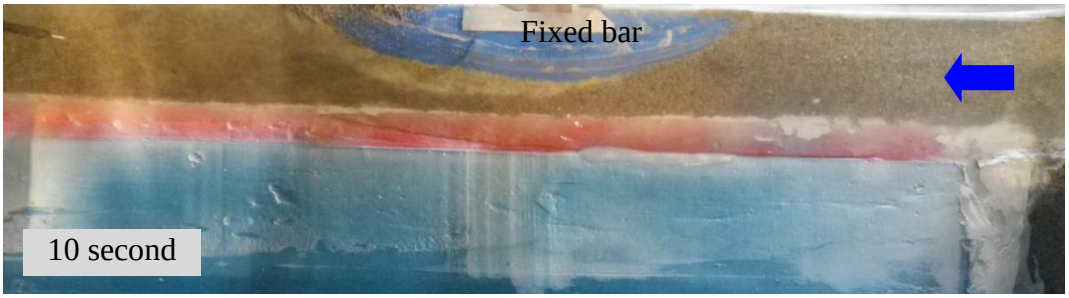

(b)

Photo 2.9 Temporal changes of channel geometry under Case BE3 at the beginning of experiment. The flow direction is from right to left side

The erosion processes of the bank toe in Case BE2 is also followed by mass failure process. However, the process of mass failure has different mechanism. In Case BE2 the mass failure of the upper part of the bank need longer time compared to the Case BE1. The upper layer in Case BE2 is cohesive layer, so the mass failure strongly depends on the cohesiveness strength. The erosion at the bank toe will produce the overhang of the upper layer. If the weight of the overhang part exceeded the sum of the friction stress and the cohesive stress, mass failure will occur. The time from starting erosion of the bank toe until achieving the critical condition to occur the overhang mass failure needs longer time than that required for achieving repose angle in Case BE1. This can be indicated by visual observation at the beginning of experiment. In the beginning of flow, the mass failure from upper part of the bank was not occurred in Case BE2 as shown in Photo 2.8. The mass failure of the upper layer start in 40 to 50 second at the beginning of experiment as shown in Photo 2.10 (a) and (b) . The location of mass failure is indicated by dashed red circle. However, mass failure still occurs at the surface of the lower bank and the bank line migration still not occurs yet and it occurs at 270 second as shown in Photo 2.10 (c). The tension crack also occurs under this condition as shown in Photo 2.10 (c) indicated by arrow. After 270 second, the mass failure was occurred. Some of the fallen block deposited around the toe of bank (Photo 2.11 (a)). Furthermore, the fallen block split into small parts by flow then part of them will enter to the channel (Photo 2.11 (b)).

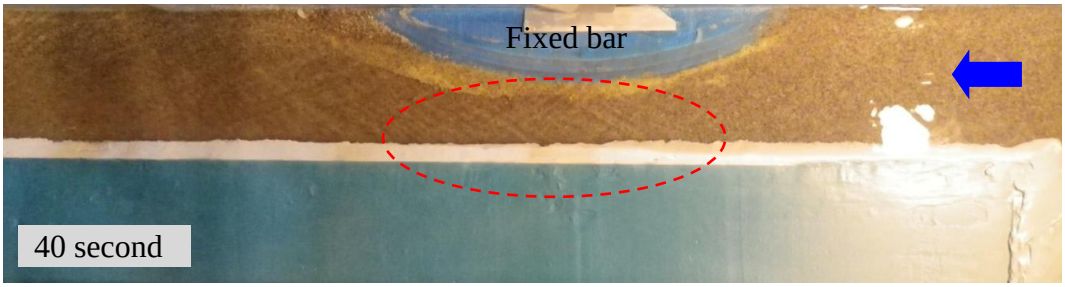

(a)

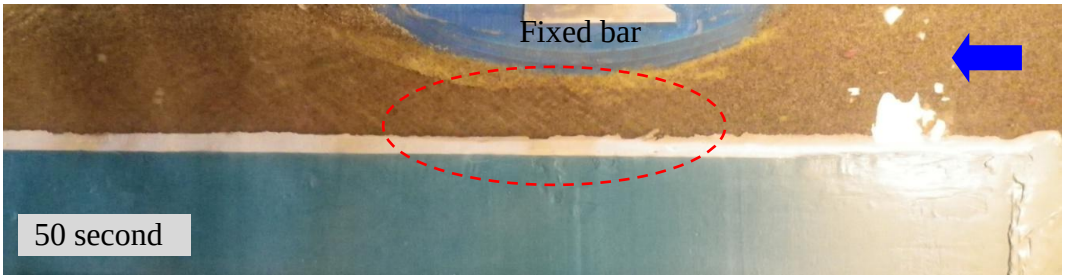

(b)

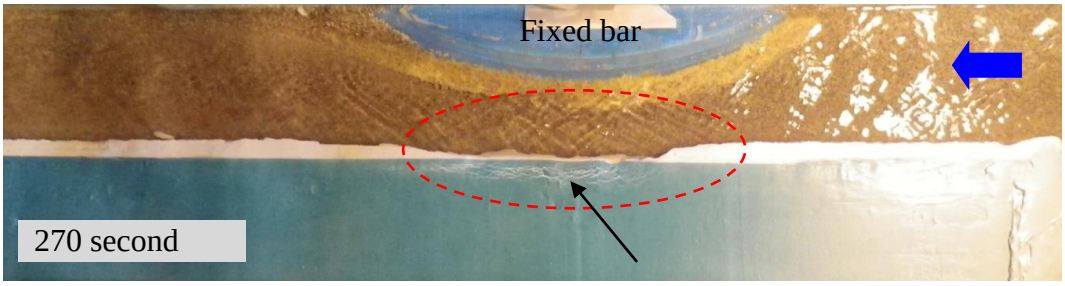

(c)

Photo 2.10 The initial mass failure process in Case BE2, a) mass failure at 40 second, b) the mass failure at 50 second and c) the mass failure at 270 second. Flow direction is from right to left side

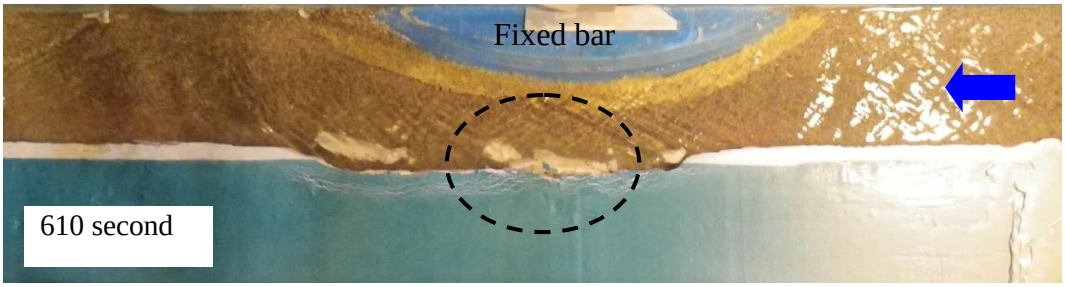

(a)

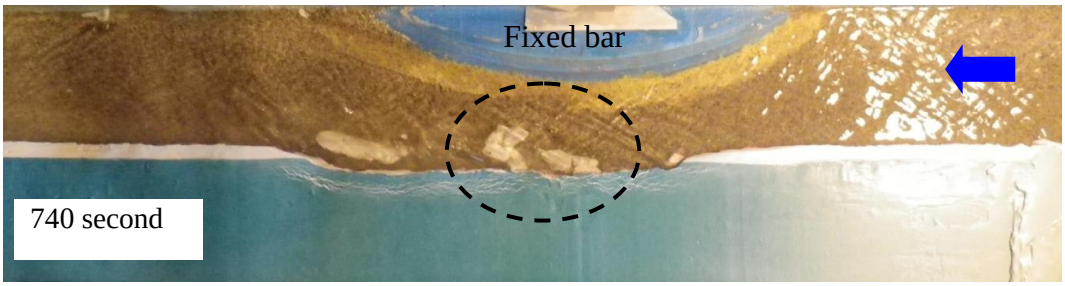

(b)

Photo 2.11 The fallen block deposited around the toe of bank. The failed block split into small parts by flow then part of them will entrance to the channel. Flow direction is from right to left side

2.7 Erosion Processes of Bank

There are two main types of bank erosion process, namely hydraulic action (also referred to as fluvial entrainment or corrosion) and mass failure (Brierley and Fryirs, 2005). Hydraulic action refers to grain by grain detachment and entrainment. It is typically associated with bank comprising non-cohesive material. Removal of bank material by hydraulic action is closely related to the magnitude of hydraulic stress. Usually, this process occurs at the lower bank or at the bank toe. Mass failure process is erosion that dominated by the gravitational force. It is including the planar and rotational failure. Primarily the process occurred in cohesive bank. The failed of individual grain is also including in this process. The susceptibility of bank to mass failure depends on their geometry, structure and material properties.

To produce both of the two processes, the discharge in this experiment was designed on low flow condition and the water level is at around a half of the bank height. The submerged or lower layer is addressed to produce the hydraulic action process and upper layer is addressed to produce the mass failure process. The bed shear stress at initial condition was larger than the critical shear stress of the bed material. The trapezoidal cross section was chosen for all experiments. The bed-load transport zone associated to the hydraulics condition is shown in Figure 2.6 (ASCE Task Committee, 1998). This concept is also explained by Fujita (1979).

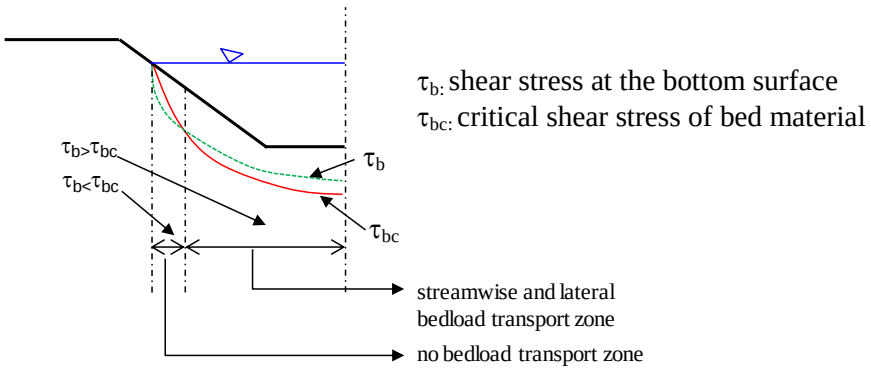

Figure 2.6 Bed-load transport zone in initially trapezoidal cross section (ASCE Task Committee, 1998)

The erosion of the bank and near the bank toe can be explained through the following steps:

Step 1 is the bed and bank material eroded by flow (hydraulic action). After flowing water for certain time, the profile in bed-load transport zone will change due to bed and bank erosion by flow (area “a” in Figure 2.7 (a)). The fixed bar will give the bottle neck effect, so the flow velocity is more than that in upstream channel and also the shear stress. The erosion material from the bed and the bank is more than sediment supply from upstream channel. Furthermore, bed degradation occurs. The condition of cross section profile is shown in Figure 2.7 (a).

Step 2 is the mass failure of the bank material. The slope of the bank surface becomes steeper than the initial condition. This condition gives the possibility of the mass failure of the upper layer (area “b” in Figure 2.7 (a)). The non-cohesive materials usually are failed by avalanching with very slightly curved slip surfaces (ASCE Task Committee, 1998). In Case BE1, this process is depended by the repose angle. However, in Case BE2, the overhang phenomenon occurs and the failure process is determined by the cohesiveness and the weight of the overhang material of the upper layer. After the erosion of area “b”, the cross section has new condition and also water surface elevation as shown in Figure 2.7 (b). In Case BE1, the sediment transport near the bank toe becomes surplus due to the sediment supply from channel and eroded bank. The additional sediment is deposited on the bed near the bank toe. In case BE2, some of the failed block (from area “b”) was sheltered near the bank toe.

Step 3 is the erosion of the deposited sediment and bank material. In Case BE1, the “a” area in Figure 2.7 (c) will be eroded by flow then the bank surface is steepen, which triggers the mass failure process of the bank. The processes in step 2 and step 3 shown in Figure 2.7 (b) and (c) will be repeated until achieving the equilibrium condition of sediment transport near the bank. In Case BE2, the failed block will make a temporary protection for the bank. The sediment supply from the bank is equal to zero and cause the bed degradation. These bank erosion processes will be applied in a real river (Chapter 4) to discuss the effect of cohesive material on bank line retreat.

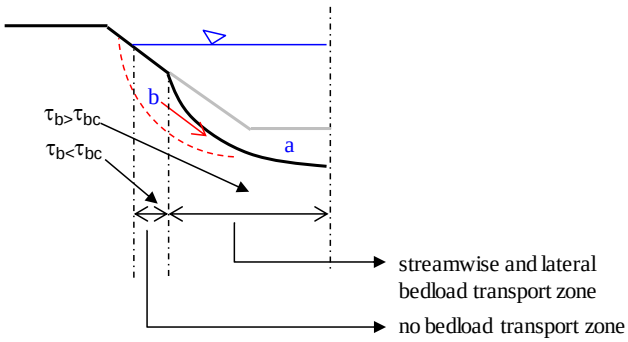

(a)

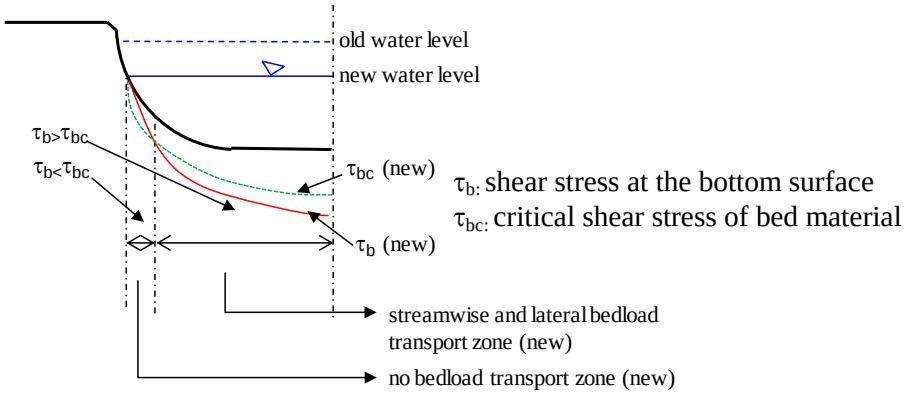

(b)

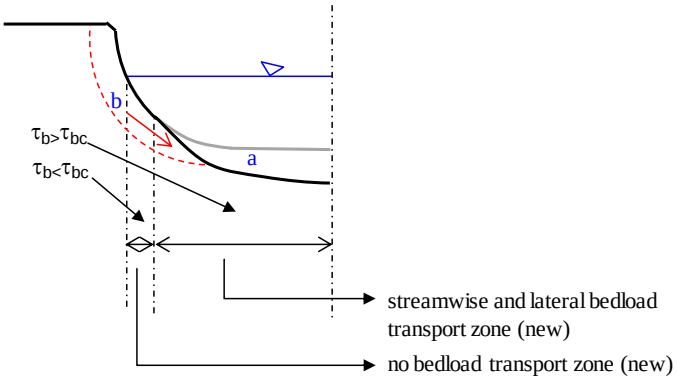

(c)

Figure 2.7 Erosion process on the bank and near the bank toe

2.8 Bank Line Migration Processes

Photo 2.12 shows the bank line retreat until 300 second in Case BE1. Photo 2.13 shows the bank retreat at 14 minute and 27 minute 15 second. The shape of bank line at the final stage of experiment is a smooth curve. Photo 2.14 shows the bank line retreat in Case BE2 until 300 second. This shows the different phenomenon compared to the Case BE1. In Case BE1, until 300 second the bank line already retreated. However, in Case BE2, the bank line starts to retreat. Photo 2.15 shows the bank retreat at 14 minute and 27 minute 15 second. The shape of the bank line is not a smooth curve as in Case BE1. Photo 2.16 shows the top view in Case BE3 until 300 second. In this case, the bank erosion is not occurs significantly. It is not enough to recognize the erosion of the bank from the photo. The cohesiveness of the bank is too strong comparing to the shear stress of the flow. The erosion only occurs on the bed of channel (indicated by red arrow). As information, the changes of the color on the bank and floodplain become white (indicated by dashed circle) in 40, 200 and 300 second because of the removing of the dye by flow and don’t have relation to the experiment result.

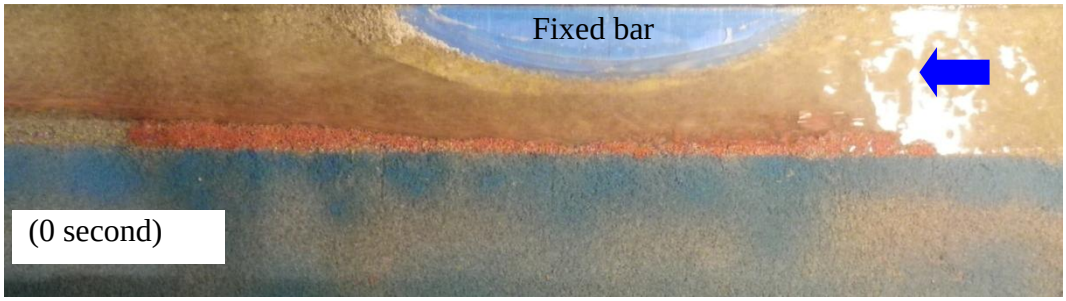

(a)

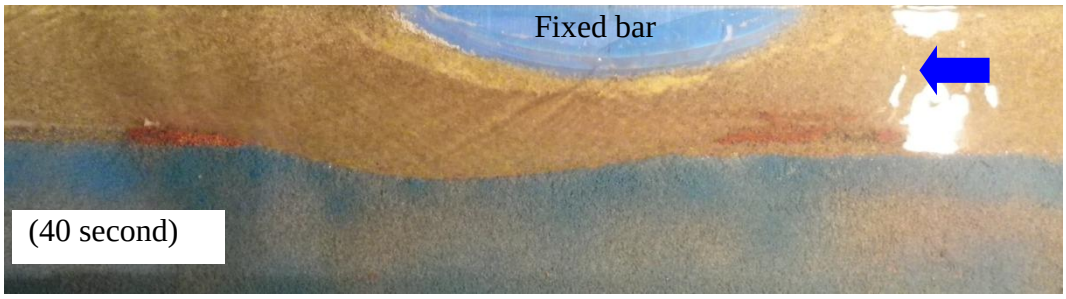

(b)

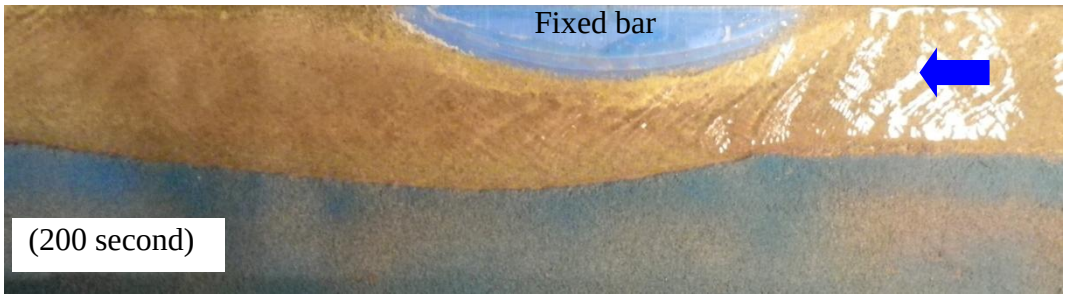

(c)

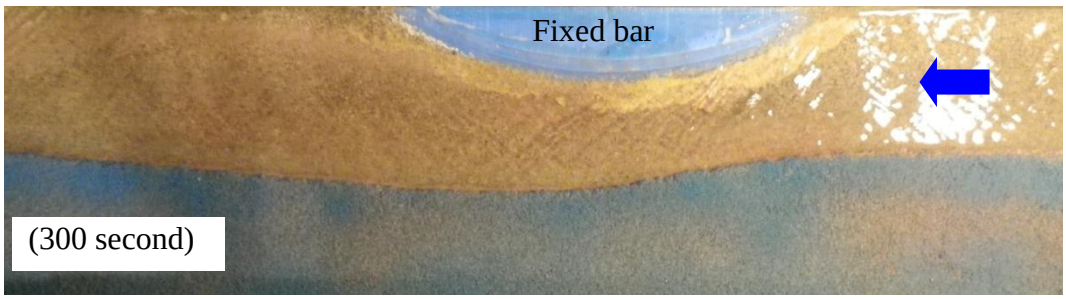

(d)

Photo 2.12 Temporal changes of channel geometry on Case BE1. The flow direction is from right side to left side

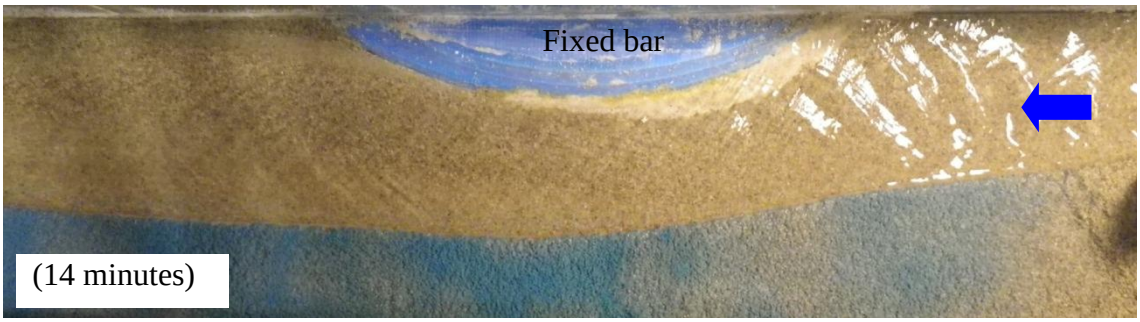

(a)

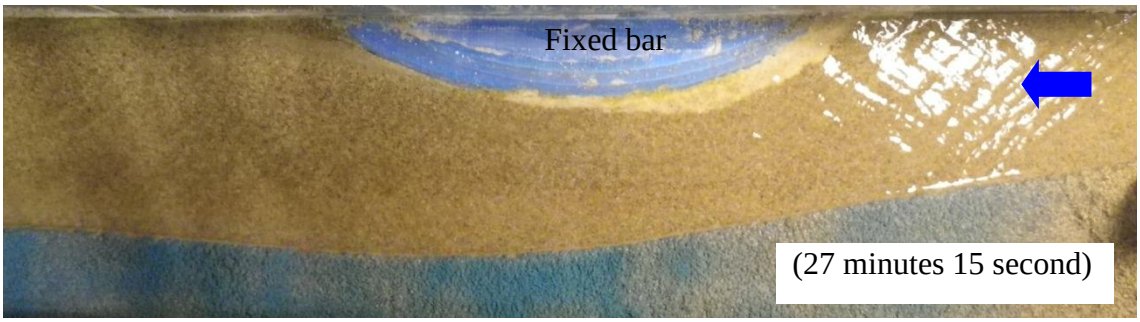

(b)

Photo 2.13 Temporal changes of channel geometry on Case BE1, at 14 minutes and 27 minutes 15 second. The flow direction is from right side to left side

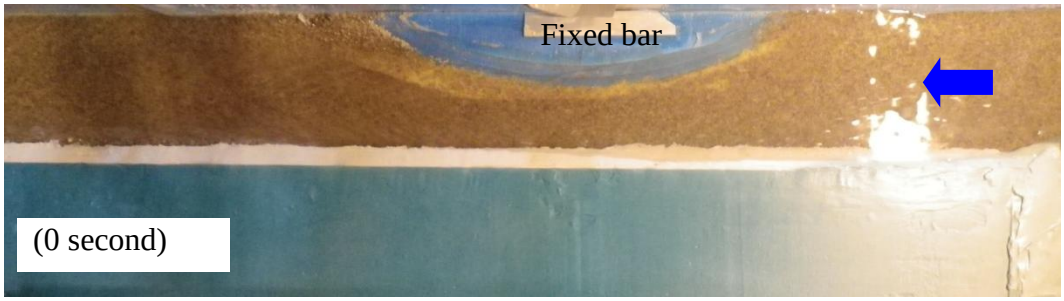

(a)

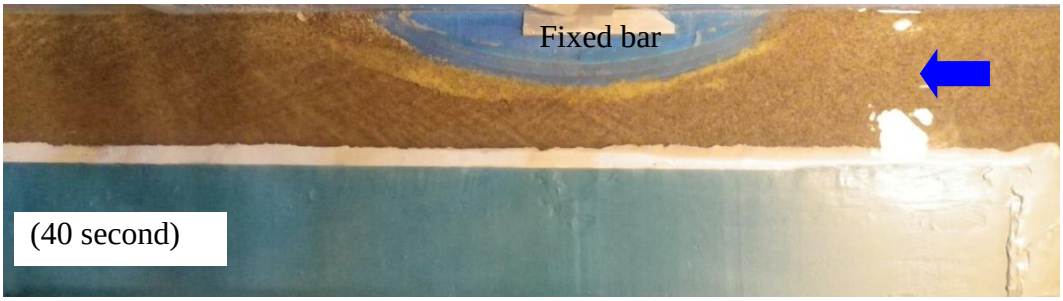

(b)

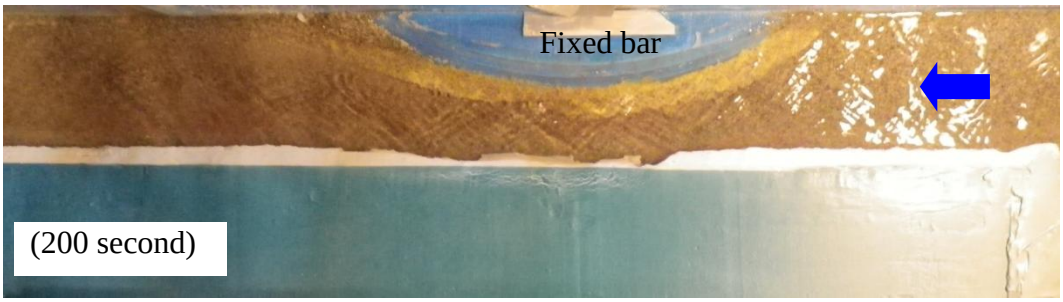

(c)

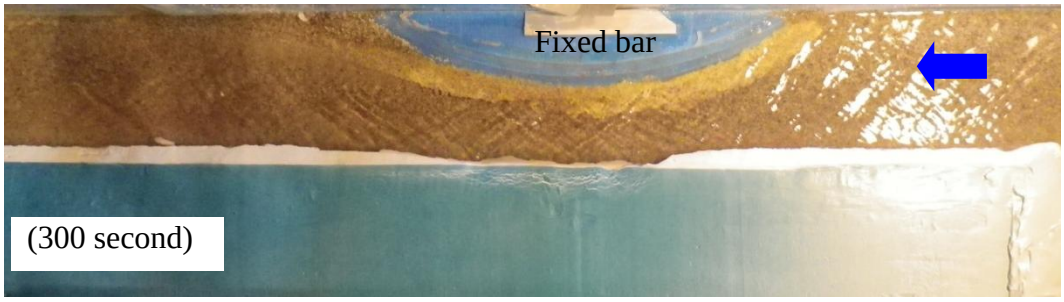

(d)

Photo 2.14 Temporal changes of channel geometry on Case BE2 until 300 second. The flow direction is from right side to left side

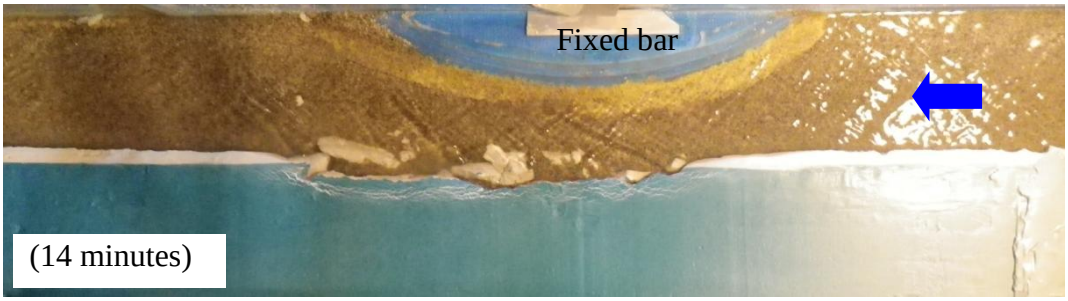

(a)

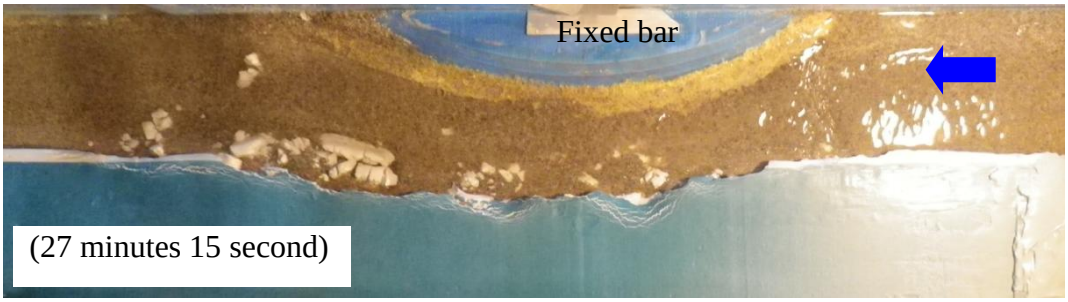

(b)

Photo 2.15 Temporal changes of channel geometry on Case BE2, at 14 minutes and 27 minutes 15 second. The flow direction is from right side to left side

(a)

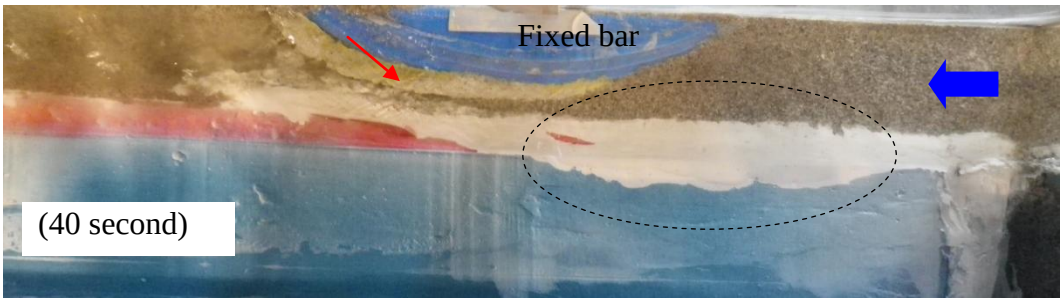

(b)

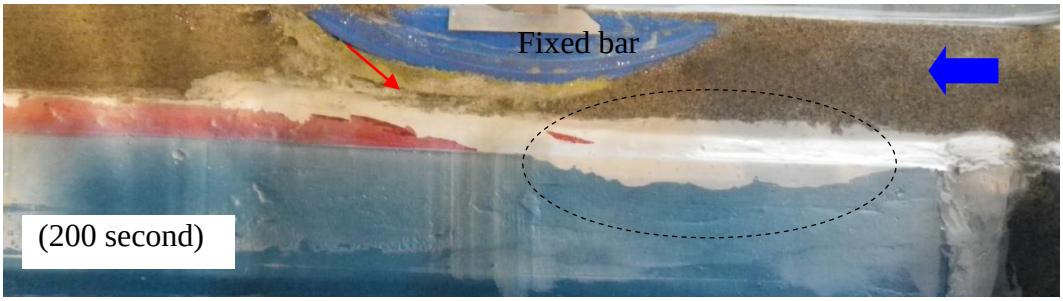

(c)

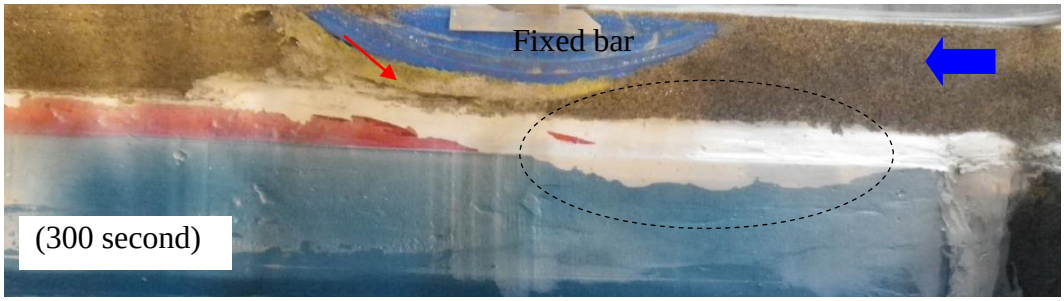

(d)

Photo 2.16 Temporal changes of channel geometry on Case BE3. The flow direction is from right side to left side

To investigate the total bank line migration, three cross section are measured in Case BE1, Case BE2 and Case BE3. In Case BE1, the maximum bank line migration

profile was measured. And also two cross sections at 10 cm upstream and downstream of the cross-section at maximum bank line migration side. The upstream side cross section namely cross section I-I, the maximum bank line migration namely cross section II-II and the downstream side namely cross section III-III. Figure 2.8, Figure 2.9 and Figure 2.10 show the location of those cross sections.

In Case BE2 and Case BE3, three cross sections are also measured at the same place in Case BE1. The maximum bank line migration in Case BE2 and Case BE3 are also measured. However, in Case BE3, there is no maximum bank line migration because the bank line is not eroded well by flow.

Figure 2.11 shows the three of cross section profiles at initial condition and final condition in Case BE1. The total bank line migration is about 10.5 cm during 27 minutes 15 second. The shape of bank is slightly curved. Photo 2.17 shows the typical bank surface at initial and final condition (indicate by dashed line). In this case, the dominant process is the bank line retreat.

Figure 2.12 shows the three cross section profiles at initial condition and final condition in Case BE2. Figure 2.14 shows the maximum bank line migration profiles at initial condition and final condition. The total bank line migration is about 6.5 cm during 27 minutes 15 second. Photo 2.18 shows the typical bank surface at initial and final condition (indicate by dash line). The shape of the bank is characterized by overhang of upper layer. In this case, the dominant processes are the bank line retreat, the overhang and the bed degradation.

Figure 2.15 shows the three of cross section profiles at initial condition and final condition in Case BE3. In Case BE3, the total bank line migration is not occurred. The dominant process is the bed degradation as show in Photo 2.19 (indicate by red arrow).

From the results of the cross sections show that the cohesive material in the bank suppresses the erosion of the bank and trigger the large bed degradation on the channel bed.

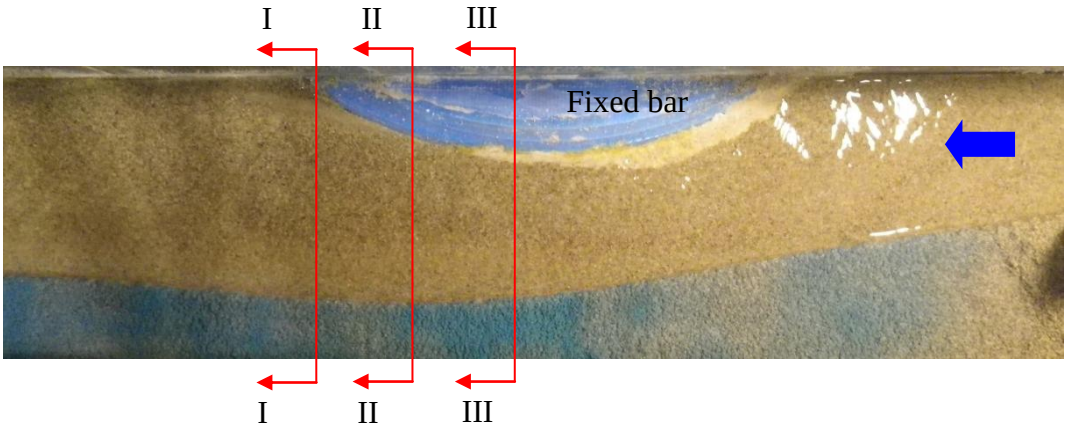

Figure 2.8 Location of the cross section in Case BE1

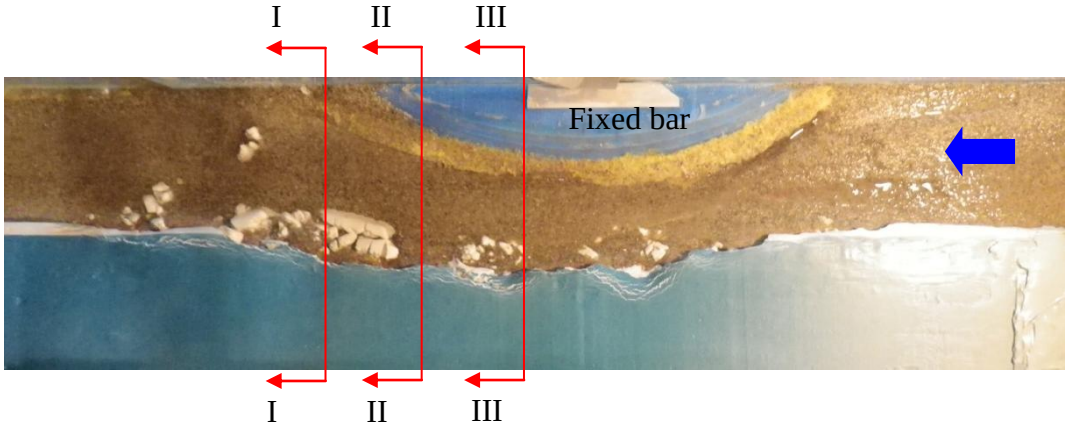

Figure 2.9 Location of the cross section in Case BE2

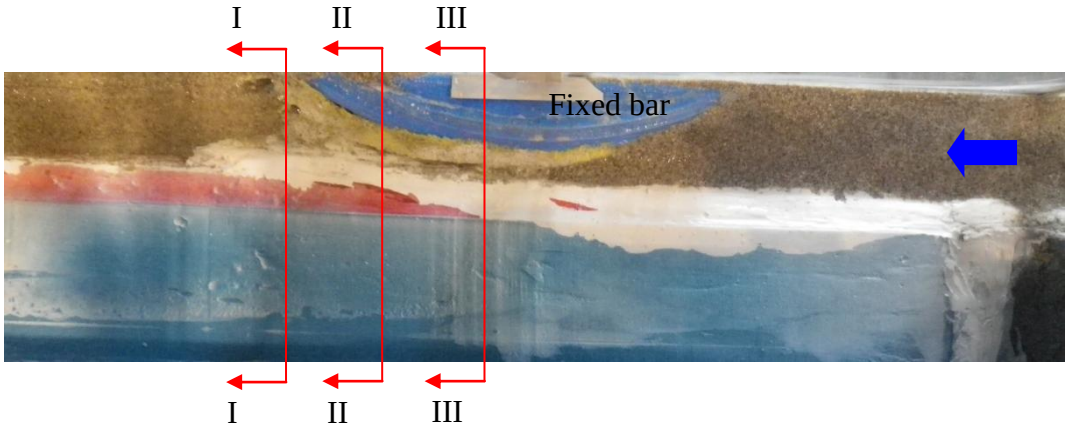

Figure 2.10 Location of the cross section in Case BE3

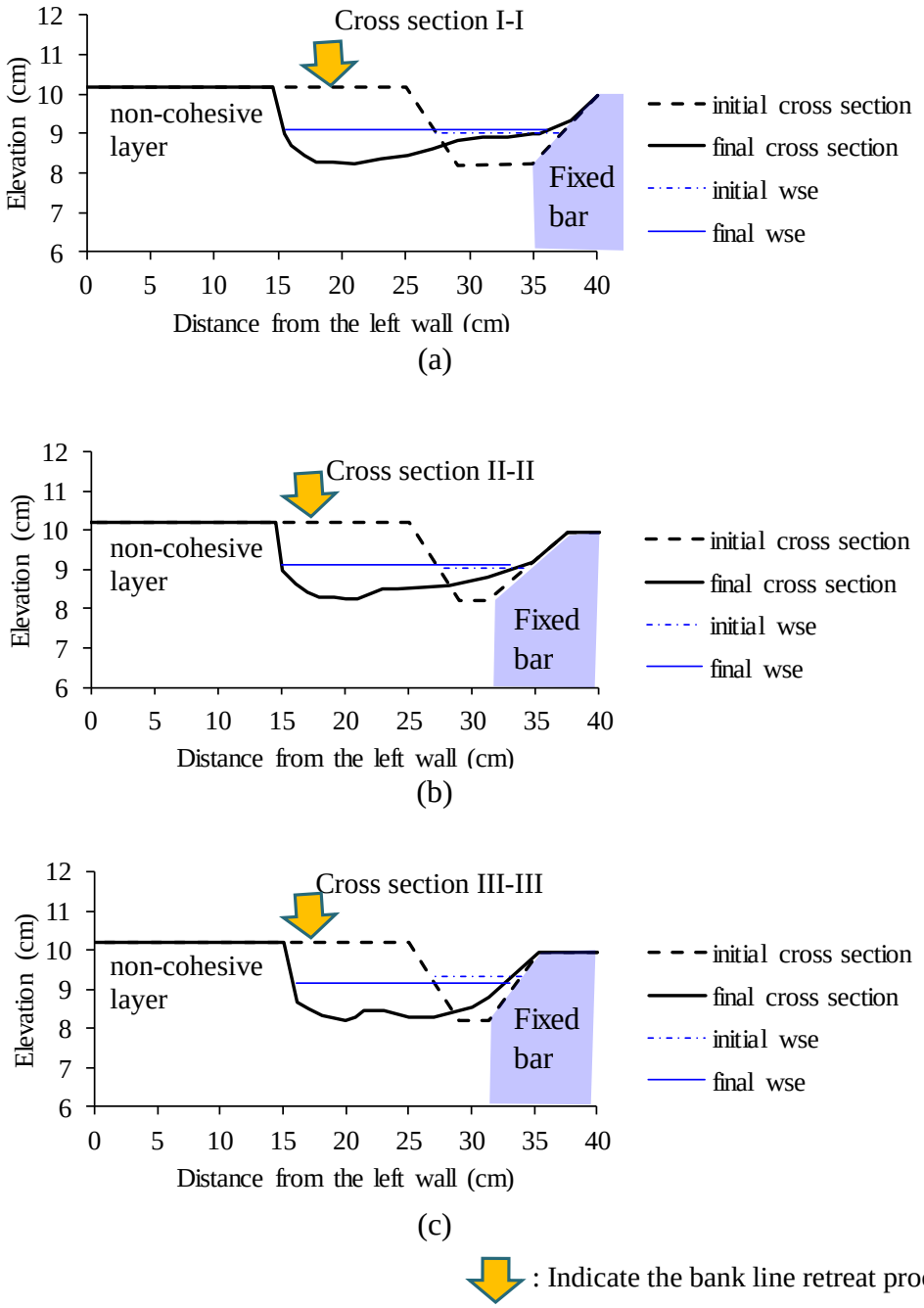

Figure 2.11 Water surface elevation (wse) and profiles of cross section I-I, II-II and III-III on the initial and final condition in Case BE1

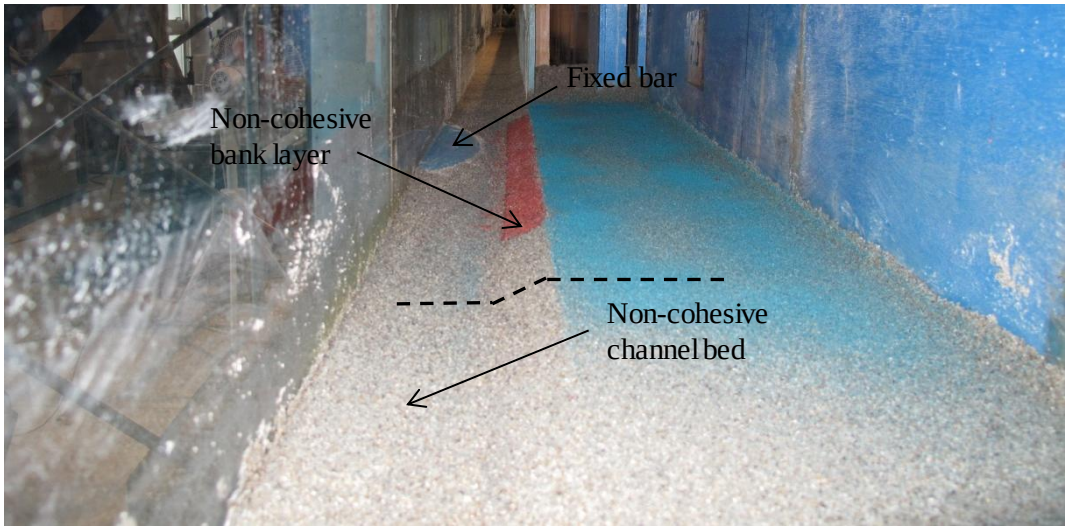

(a)

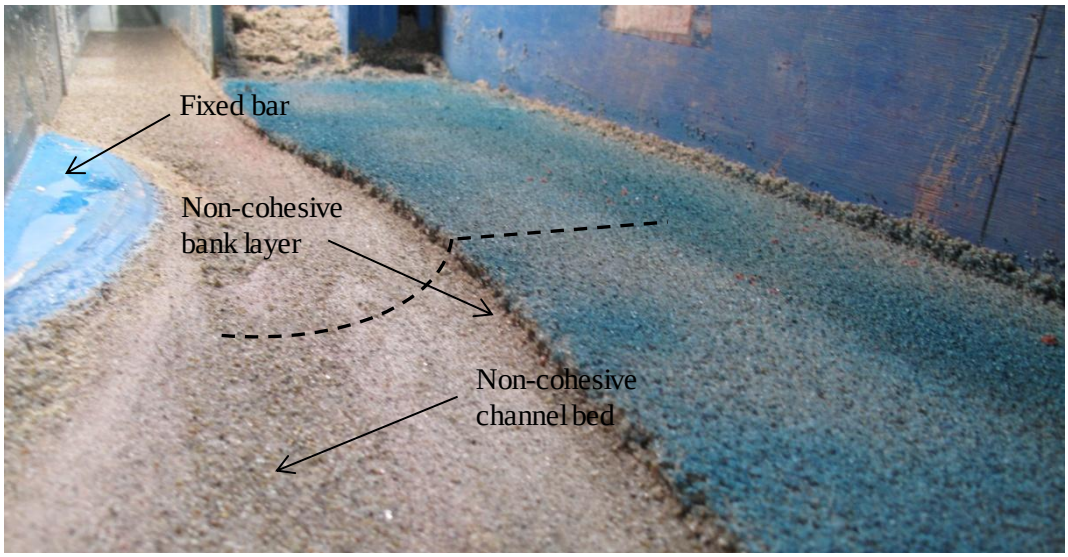

(b)

Photo 2.17 The bank surface at initial condition (a) and after experiment (b) in Case BE1

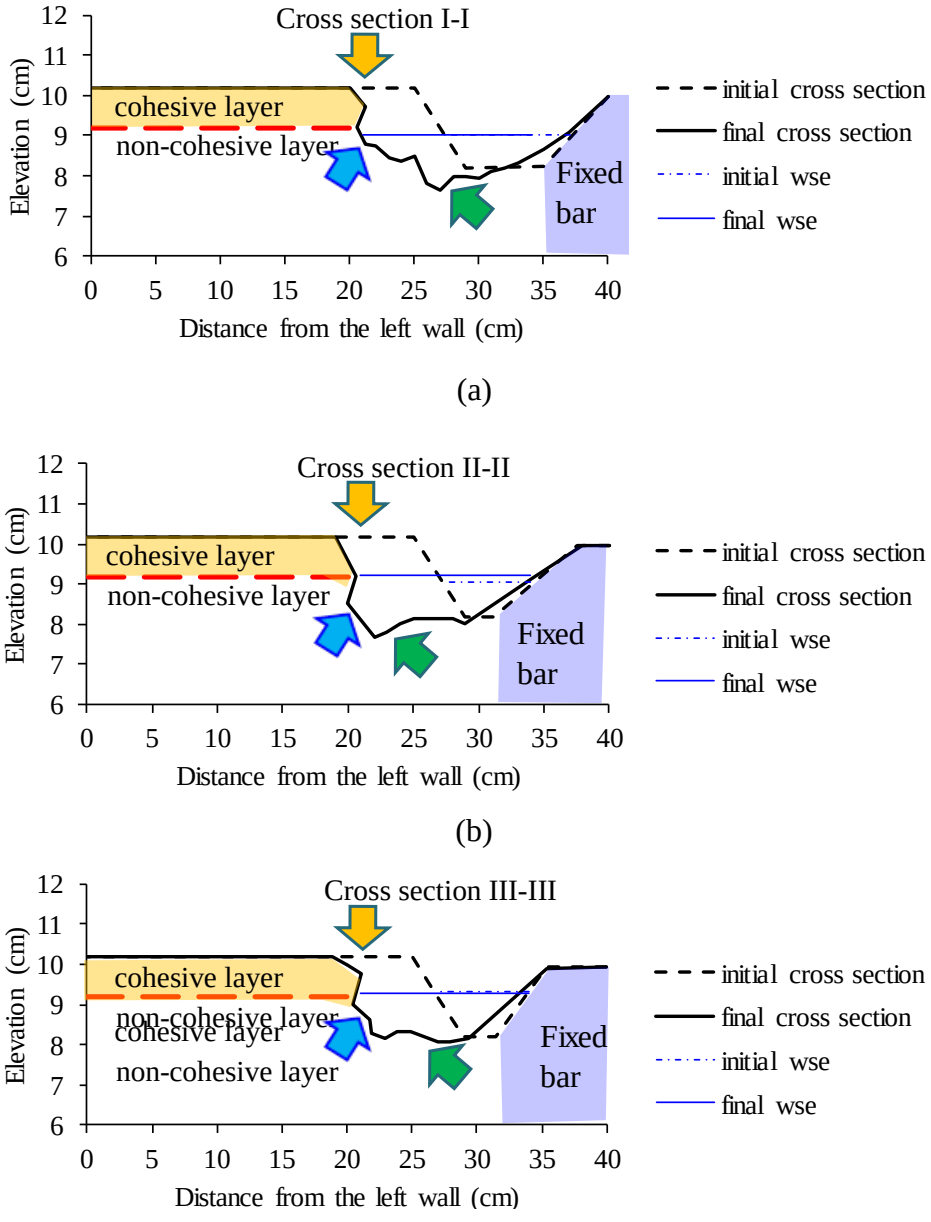

Figure 2.12 Water surface elevation (wse) and profiles of cross section I-I, II-II and III-III on the initial and final condition in Case BE2

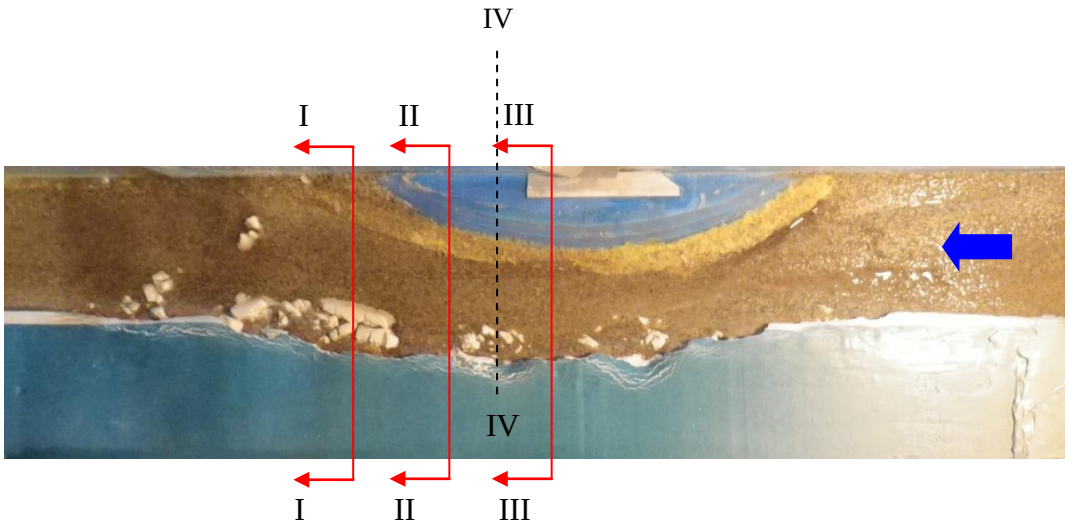

Figure 2.13 Location of the maximum bank line retreat (cross section IV-IV) in Case BE2

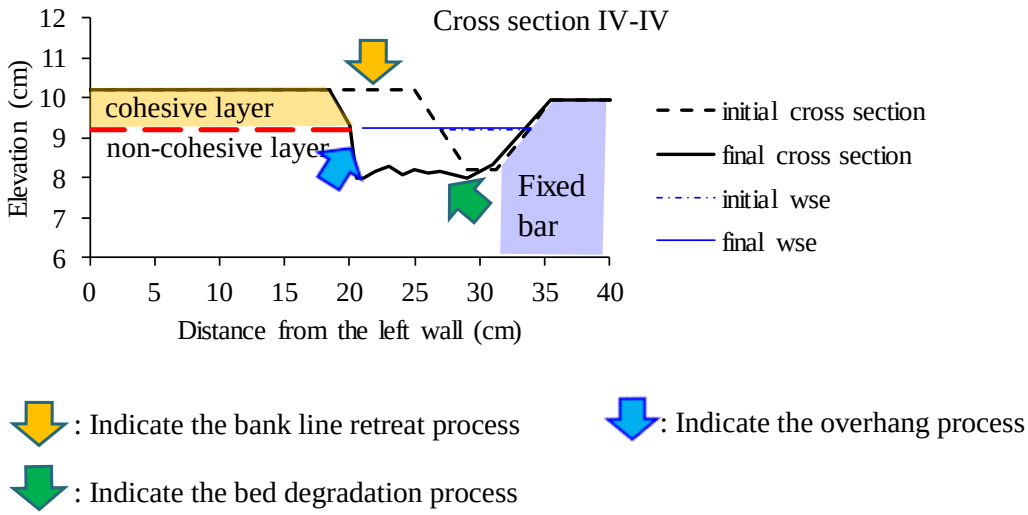

Figure 2.14 Water surface elevation (wse) and profiles of cross section IV-IV on the initial and end condition in Case BE2

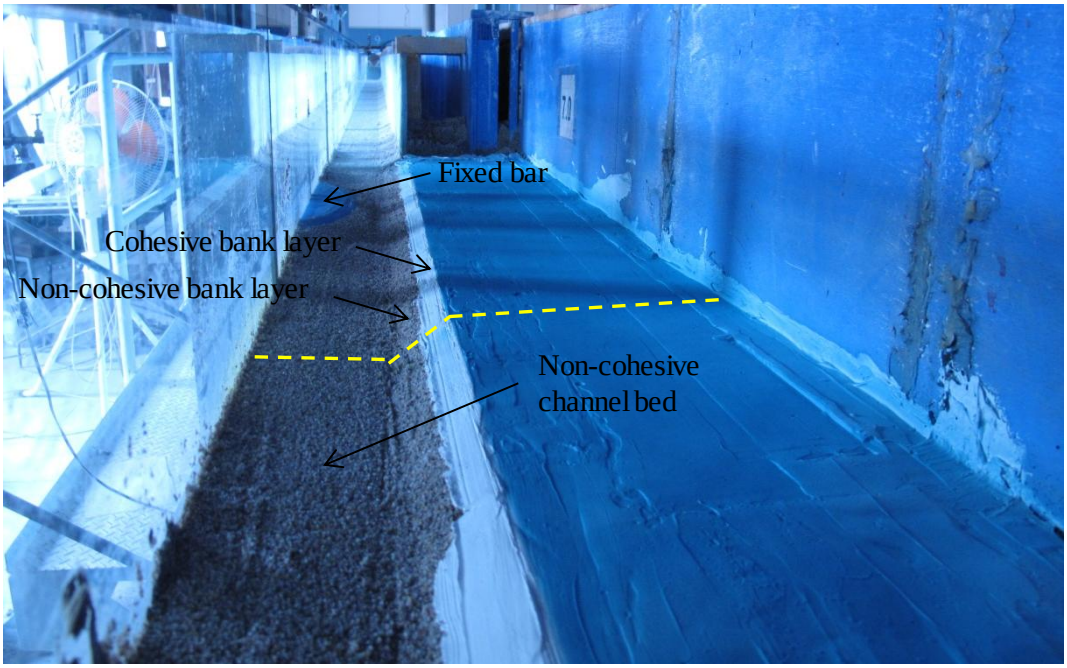

(a)

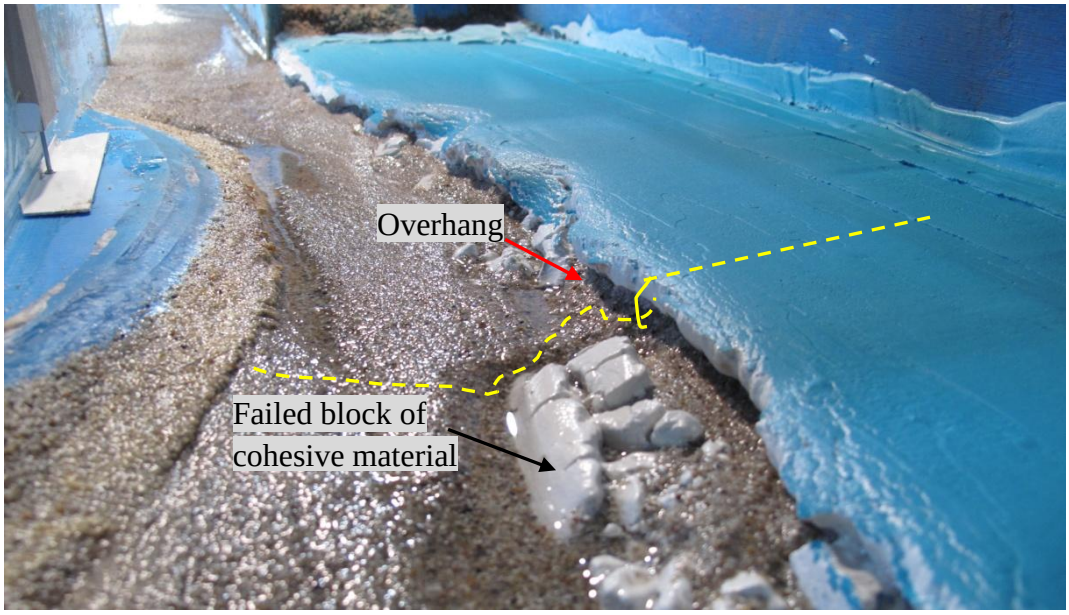

(b)

Photo 2.18 The bank surface at initial condition (a) and after experiment (b) in Case BE2

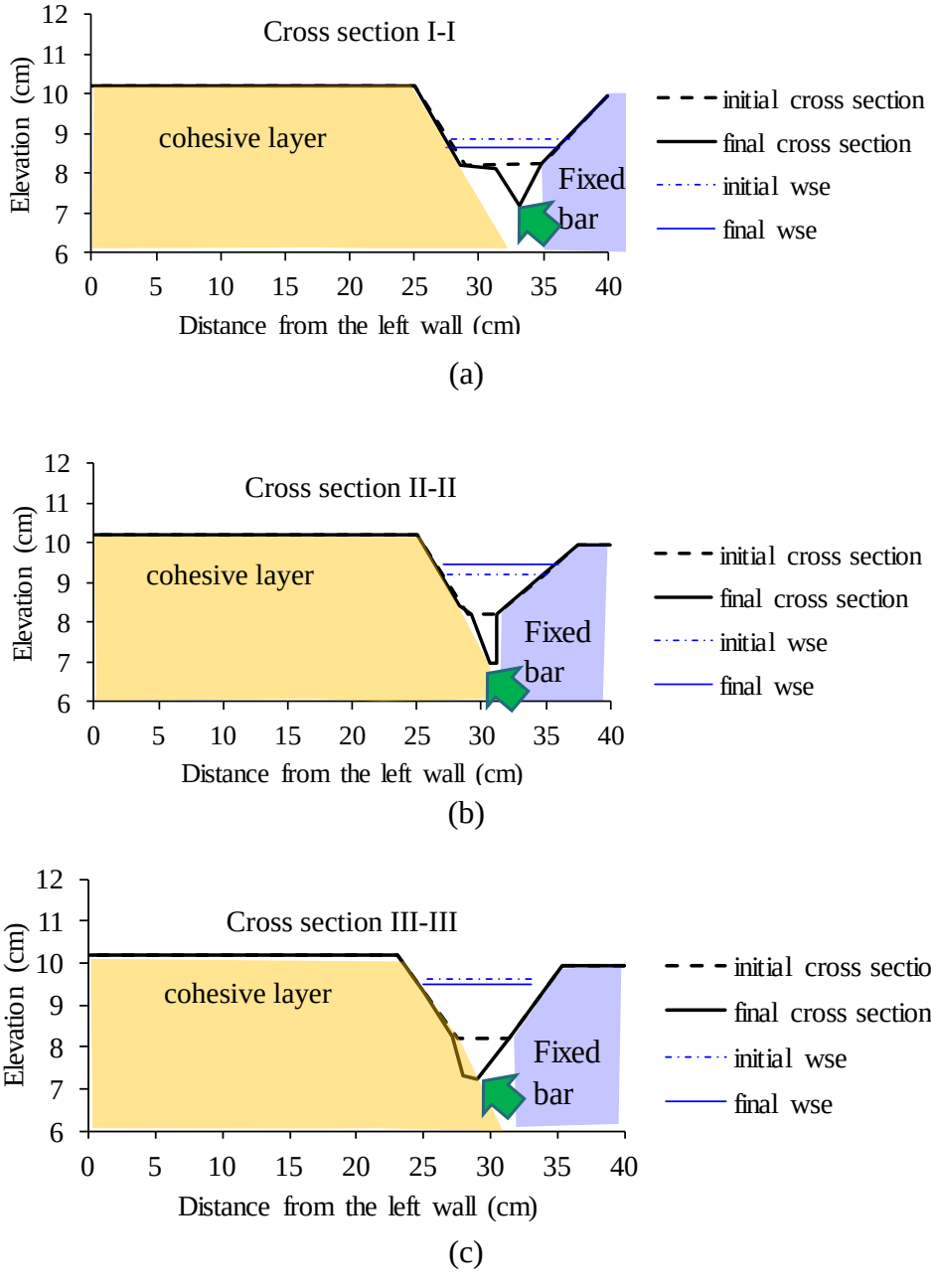

Figure 2.15 Water surface elevation (wse) and profiles of cross section I-I, II-II and III-III on the initial and final condition in Case BE3

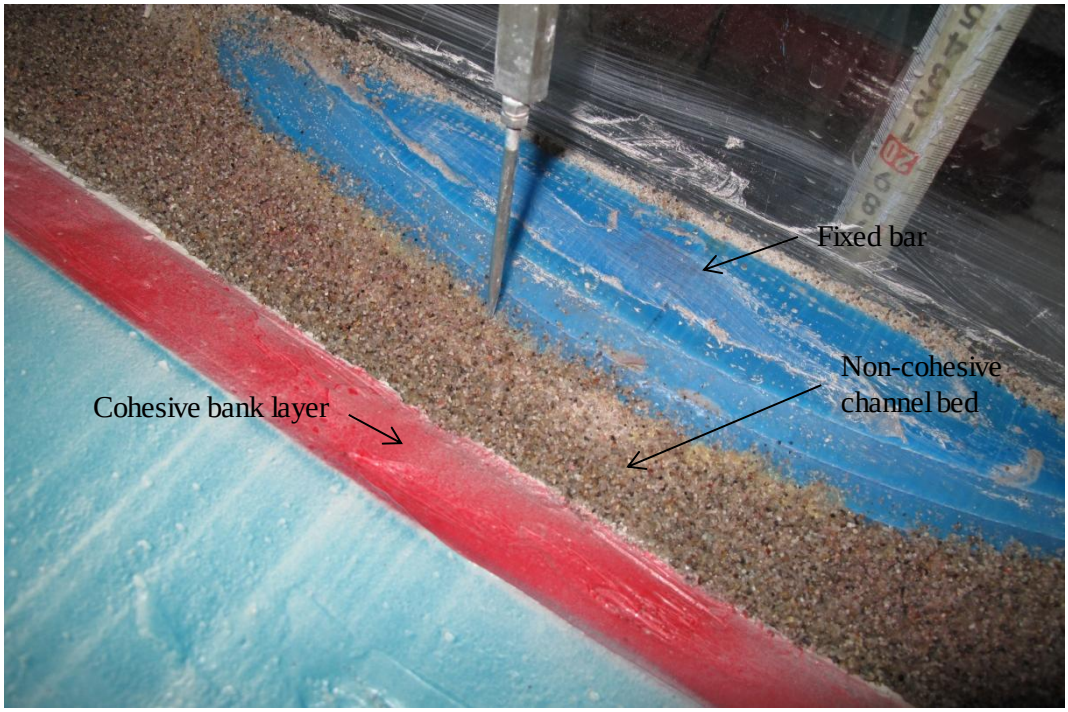

(a)

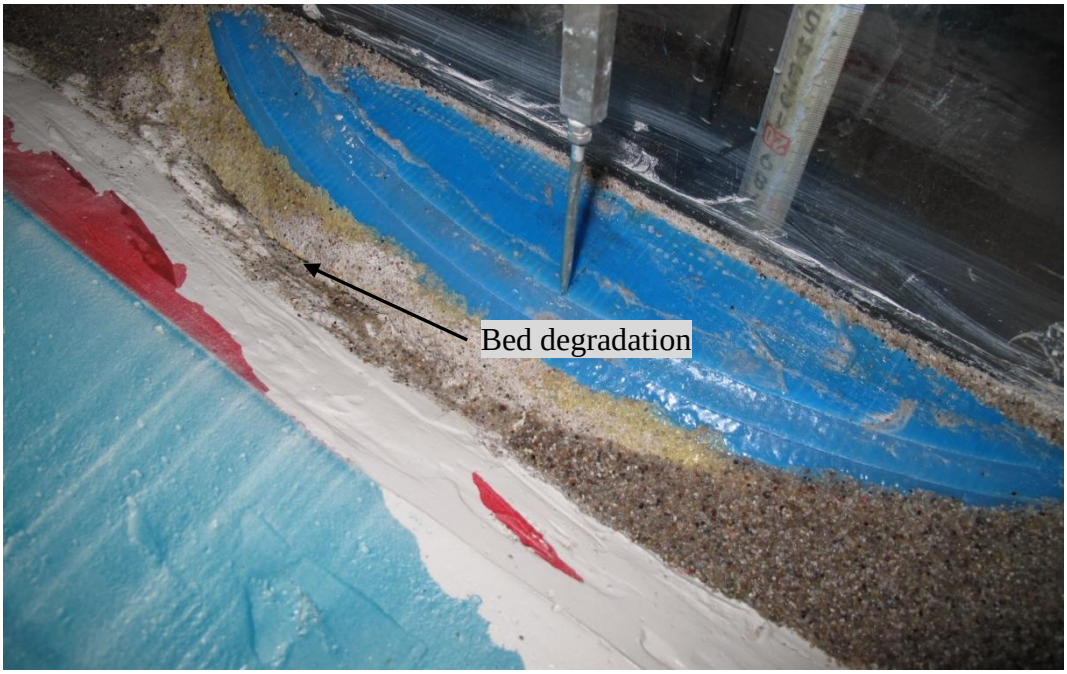

(b)

Photo 2.19 The bank surface at initial condition (a) and after experiment (b) in Case BE3

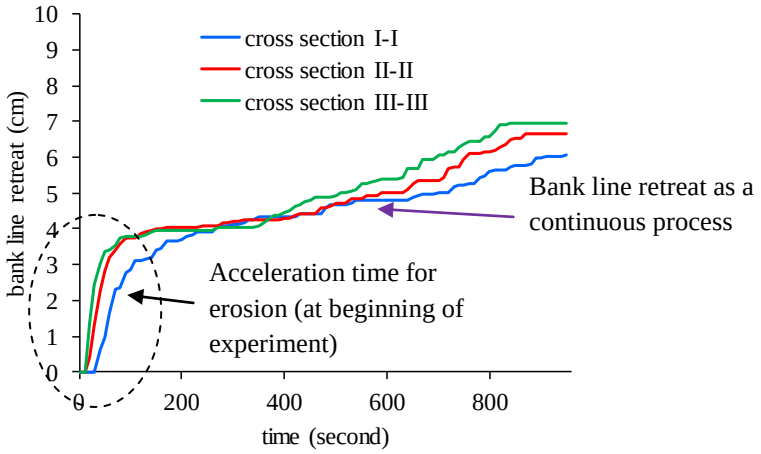

Figure 2.16 The bank line retreat in case bank composed of non-cohesive material only (Case BE1)

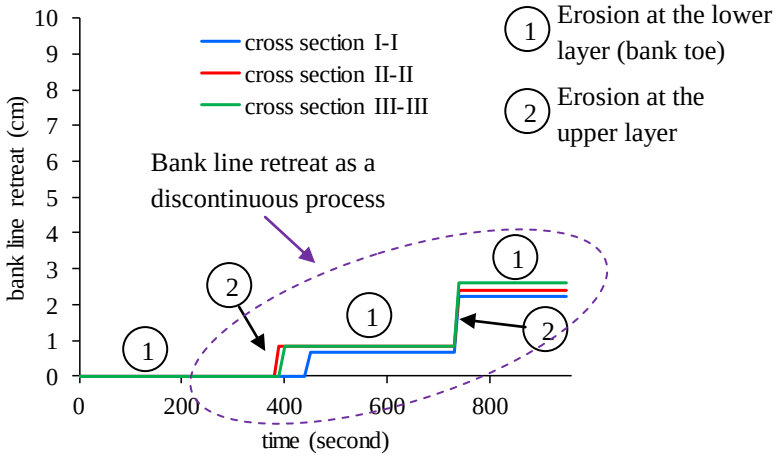

Figure 2.17 The bank line retreat in case bank composed of cohesive and non-cohesive material layers (Case BE2)

Figure 2.16 and Figure 2.17 show the bank line retreat in Case BE1 and Case BE2. In Case BE3 the bank line retreat is not occurs, so the graph of the relation between bank line retreat and time is not presented. The velocity of the bank line retreat under 100 second in Case BE1 (see Figure 2.16) is very fast. This is because the initial bank line is accelerated by the fixed bar. The bank line retreat is characterized by continuous line. However, the bank line retreat in Case BE2 is not continuous line. This is due to the bank composed of cohesive layer material.

2.9 Summary

The experiments of bank erosion processes using both the bank material, which have cohesive and non-cohesive material were conducted. The results show the different behavior on bank erosion processes and mechanism and are explained as follow:

- The erosion at the bank toe under the bank is composed of non-cohesive material is followed by the mass failure some part of the upper layer. The mass failure of the upper part of the bank is occurred immediately. The shape of bank line is a smooth and large radius curve.
- The erosion at the bank toe under the bank is composed of cohesive material on the upper layer and non-cohesive material at the bottom layer is followed by mass failure some part of the upper layer. However, the mass failure of the upper part of the bank occurred very late. The shape of bank line at the final experiment is not a smooth and small radius curve.
- The bank line retreat is a very small distance when the bank is totally composed of cohesive material. The dominant process is the bed degradation.

References

ASCE Task Committee on Hydraulics, Bank Mechanics, and Modeling of River Width Adjustment.: River width adjustment I, *Journal of Hydraulic Engineering*, ASCE, Vol. 124, pp. 881-902, 1998.

Couper, C., and Muddock, I.P.: Subaerial river bank erosion processes and their interaction with other bank erosion mechanisms on the River Arrow, Warwickshire, UK, *Earth Surf. Process. Landforms*, Vol. 26, pp. 631–646, 2001.

Darby, S.E., and Thorne, C.R.: Development and testing of riverbank stability analysis, *Journal of Hydraulic Engineering*, ASCE, Vol. 122, No. 8, pp. 443-454, 1996.

Duan, J.G., and Julien, P.Y.: Numerical simulation of meandering evolution, *Journal of Hydrology*, Vol. 391, pp. 34-46, 2010.

Duan, J.G., and Julien, P.Y.: Numerical simulation of the inception of channel meandering, *Earth Surf. Process. Landforms*, Vol. 30, pp. 1093-1110, 2005.

Fujita, Y.: Study on the process of bank erosion in straight stream channels, Annuals of Disas. Prev. Res. Inst., Kyoto Univ., No 22 B, pp. 537-552, 1979.

Hooke, J.M.: An analysis of the processes of river bank erosion, *Journal of Hydrology*, Vol. 42, pp. 39-62, 1979.

Iwagaki, Y.: Hydrodynamic study on critical shear stress. *Proc. of JSCE,* No. 41, pp. 1-21, 1956.

Lawler, D.M.: The impact of scale on the processes of channel-side sediment supply: a conceptual model, *IAHS Publ.*, No. 226, pp. 175-184, 1995.

Nagata, N., Hosoda, T., and Muramoto, Y.: Numerical analysis of river channel processes with bank erosion, *Journal of Hydraulic Engineering*, ASCE, Vol. 126, pp. 243-252, 2000.

Prosser, I.P., Hughes, A.O., and Rutherfurd, I.D.: Bank erosion of an incised upland channel by subaerial processes: Tasmania, Australia. *Earth Surface Processes and Landforms*, Vol. 25, pp. 1085-1101, 2000.

Simon, A., Curini, A., Darby, S.E., Langendoen, E.J.: Bank and near-bank processes in an incised channel, *Geomorphology*, Vol. 35, pp. 193-217, 2000.

Thorne C.R., and N. Keith Tovey, N.K.: Stability of composite river banks, *Earth Surf. Process. Landforms*, Vol. 6, pp. 469–484, 1981.

Thorne, C.R.: Bank erosion and meander migration of th red and mississippi river, USA, *IAHS, Proceed. of the Vienna Symp.*, No. 201, pp. 301-313, 1991.

Takebayashi, H., Fujita, M., Harsanto, P.: Numerical analysis of bank erosion process along bank composed of both cohesive and non-cohesive layers, *Int. Workshop on Multimodal Sediment Disasters Triggered by Heavy Rainfall and Earthquake and The Countermeasures*, Vol.1, pp. 77-86, 2010.

Chapter 3

Experimental Study on Erosion Characteristics of Cohesive Sediment by Non-cohesive Sediment Transport

3.1 Introduction

Generally, cohesive sediment is primarily composed of clay material (Huang *et al.*, 2006). Clay material has strong inter-particle forces due to their surface ionic charges. As the particle size decreases, the surface area per unit volume and the inter-particle's force increases. The gravitational force is not the dominant force for the smaller particle. The particle's size of cohesive sediment is smaller than 2 μm, and greater than 60 μm is non-cohesive sediment. The size between 2 μm and 60 μm is considered to be silt. The cohesiveness of silt is primarily due to the existence of clay. Therefore, in engineering practice, silt and clay are considered as cohesive sediment.

Erosion or re-suspension is one of the important processes in cohesive sediment's transport system (Mehta *et al.*, 1989a and Mehta *et al.*, 1989b). Erosion also one of the most studied aspects of cohesive sediment transport system. Many researchers have studied to clarify the erosion behavior of cohesive sediment, involving theoretical approaches, numerical analysis and field observations. They observed the erosion rate characteristics of cohesive sediments considering the physicochemical parameters. Those parameters are the salinity (Gularte *et al.*, 1980 and Parchure and Mehta, 1985), temperature (Gularte *et al.*, 1980 and Nishimori and Sekine, 2009), water content (Gularte *et al.*, 1980 and Sekine and Izuka, 2000) and bulk density (Aberlea *et al.*, and Parchure and Mehta, 1985). The results of those research show that the strength of the cohesive sediments is controlled by many parameters and explained as follow:

– the erosion resistance increases with increasing in salinity.
– the erosion resistance increases with increasing in temperature.

– the erosion resistance decreases with increasing in water content.

– the erosion resistance decreases with increasing in bulk density.

And also, they studied the erosion characteristics of cohesive sediment bed only using clear water as eroding media. However, the flow in natural rivers that containing only clear water are limited by the fact that most flows in rivers have sediment transport such as bed load, suspended or wash load. In other words, sediment transport is a common phenomenon in natural rivers and the transport rate depends on the flow characteristics. The presence of sediment transport changes the characteristics of the flow. This phenomenon also had observed by many researchers. The research's results on feedback effect of sediment transport on the flow characteristics are described below.

Kamphuis (1990) observed the influence of coarse sediment transport on erosion of cohesive bed. The test used both clear water and water containing sand as eroding media. The experiments show the importance of the variations of hydraulic condition to study the effect of bed-load transport in the flow. The various flow conditions are applied to analyze the effect of bed-load transport in erosion of cohesive bed. For an example, the samples hardly eroded at 20 Pa (shear stress in clear water) but easily eroded at 1.3 Pa (shear stress in flow containing sand). It indicates that, bed-load transport can increase the bed shear stress. The other results reported that, the small amounts of bed-load transport increases the erosion rate. The most rapid on condition rate is the condition when sand moving by saltation mode. The erosion rate decreases if the sand moves as pure bed-load that covers the bed at certain times. In this research, the characteristic of bed-load transport involving volume and size are not discussed yet.

Thompson and Amos (2004) conducted experiments to study the effect of sand movement on a cohesive substrate. The hydraulic conditions in these experiments are changed gradually to investigate the hydraulic condition under which the bed load transport will produce large erosion. They found that, the small size particles in saltating motions with small concentration will produce high erosion on the bed.

Song and Chin (1998) used various supplied sediment to investigate the effect of bed-load's movement to the flow friction factor. The experiments compared the frictions between the flow in clear water and the flow containing both water and sand. The results showed that the presence of bed-load increases the friction factor. In other words, the bed load decreases the mean flow velocity. He argued that, the bed load

transport extracts momentum from the flow and causes a reduction of flow velocity. These results give knowledge that the presence of bed-load transport can decreases the flow velocity and also the bed shear stress.

The results between Kamphuis (1990) and Song and Chin (1998) show that the bed load transports not only can decrease but also can increase the flow velocity. This phenomenon was agreed by Carbonneau and Bergeron (2000). In a given hydraulic condition, the flow that consist only clear water will produce different bed shear stress compare to the flow which has sediment transport. The magnitudes of the bed shear stress maybe higher or lower than the bed shear stress in clear water flow. From those investigations, author concludes that erosion of cohesive bed can increase or decrease due to the presence of bed-load transport. However, the investigations to observe in which condition the bed-load can increase or decrease still needed.

The experiments in this chapter are addressed to investigate the effect of the bed-load transport on the erosion rate characteristics of cohesive sediment bed. Flume test are performed under various sediment supply conditions. Due to the fact that, the sediment transport can decrease or increase the velocity, the sediment supply will be varied in size and volume. A given hydraulics condition is applied for allowing a comparison analysis. And also the bed-load sediment transports are flowing on the same cohesive sediment bed. Four basic conditions of the bed-load transport will be applied as illustrated in Figure 3.1. The bed-load conditions are explained as follow:

– The bed-load transport is equal to zero; the flow only clear water (see Figure 3.1. (a)).
– The bed-load transport is less than the equilibrium bed-load transport (see Figure 3.1. (b)).
– The bed-load transport is equal to the equilibrium bed-load transport (see Figure 3.1. (c)).
– The bed-load transport is larger than equilibrium bed-load transport (see Figure 3.1. (d)).

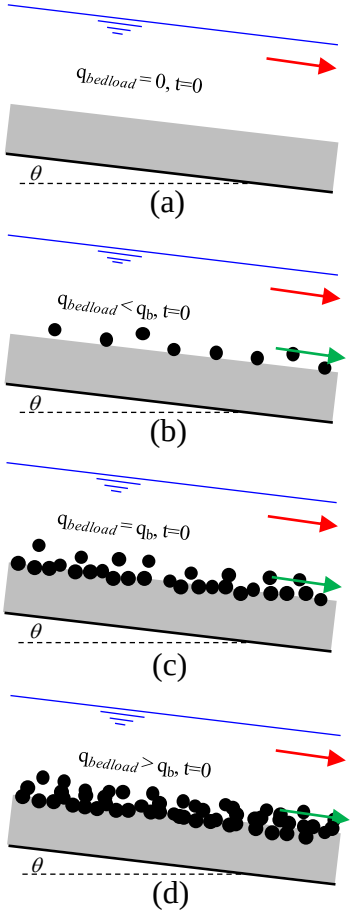

Figure 3.1 Concept of the experiment case

The Tonle Sap River in Cambodia is the natural river that has a phenomenon about the interaction between the coarse bed-load transport (non-cohesive material) and the cohesive sediment bed. This is due to a unique hydraulic and hydrology condition between Mekong River and Tonle Sap River. During dry season, the bed material in Tonle Sap River is fine and the bed material in Mekong River is coarse. During flood season, the coarse material from Mekong River flows on the fine material in Tonle Sap River. This phenomenon will be discussed in Chapter 5.

3.2 Experimental Methods

3.2.1 Flume Test Channel

Location of experiments is in Ujigawa Open Laboratory (UOL) of Disaster Prevention Research Institute (DPRI), Kyoto University, Kyoto, Japan. The experiments were conducted in a tilting flume channel with 8 m long. The channel has a rectangular cross section with 0.15 m wide and 0.25 m height. Both of walls have rails on the top. A moveable point gauge is installed on the rails. The point gauge can move in the longitudinal and the transverse directions. Figure 3.2 illustrates the experimental setup from right side. Photo 3.1 shows the top view of the channel.

This research is addressed for investigation of the effect of bed load transport in erosion characteristics of cohesive sediment bed. Thus, all experiments use the same hydraulic condition to allow comparative analysis. Several preliminary experiments are conducted to determine the appropriate slope, discharge and size of bed load material. The appropriate condition means that the coarse sediment particles can move as bed load transport over the cohesive sediment bed. Also the flow condition should be set to avoid the local erosion on the bed.

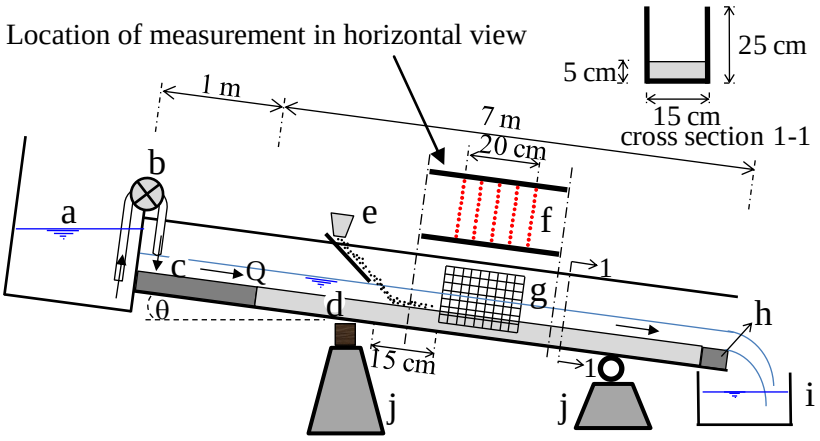

Figure 3.2 The experiment setup, where a) water tank, b) pump, c) rigid bed, d) cohesive sediment, e) sediment feeding location, f) horizontal view of cross sections, g) screen grid, h) downstream weir, i) downstream tank, and j) tilting machine)

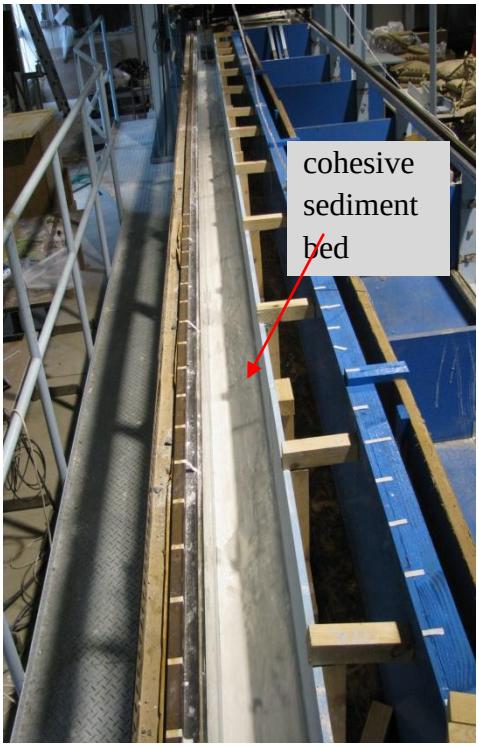

Photo 3.1 The flume test channel. The flow direction is to bottom side

3.2.2 Cohesive Sediment Sample

Photo 3.1 shows the cohesive sediment bed laid on the channel. The cohesive sediment beds for all experiments are prepared from industrially dry white kaolin powder. Figure 3.3 shows the grain size distribution of this material. The size distribution is between 0.328 μm and 68.973 μm. The mean diameter, D_{50} is around 4.616 μm.

Two different cohesive sediment beds (Type A and Type B) are used in these experiments. The preparation of cohesive sediment bed is divided into two steps and explained as follow:

(1) First step, the preparation of the cohesive sediment mud is explained as follow:

- Cohesive sediment bed Type A is composed of 100% kaolin. To prepare the cohesive sediment mud Type A, the dry kaolin powder and water with 1:1 volume ratio, are put into a bucket and mixed until the sample become mud and has a homogeneous condition.
- Cohesive sediment bed Type B is composed of 50% kaolin and 50% coarse

sand. To prepare cohesive sediment Type B, the water, kaolin and sand are put into a bucket with volume ratio is 1:1:1 (water : kaolin : sand). Mix until the sample become mud and has a homogeneous condition. The size distribution of the coarse sand in Type B is the sand size 2.

(2) Second step, the preparation of cohesive sediment bed on the channel is explained as follow:

- The mud samples (Type A or Type B) which are prepared in the first step is laid on the bed of the flume channel and pooled by water slowly.
- In order to allow the settling and consolidation naturally, the mud sample is kept in the pooled channel for one day. During settling and consolidation process, the flume slope is zero.
- The surface elevation of cohesive sediment bed is designed on the same level.
- The thickness of cohesive sediment bed is designed in 5 cm.

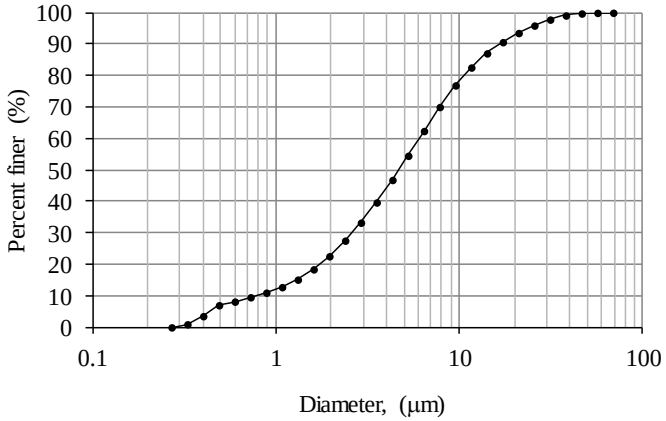

Figure 3.3 The size distribution of dry kaolin

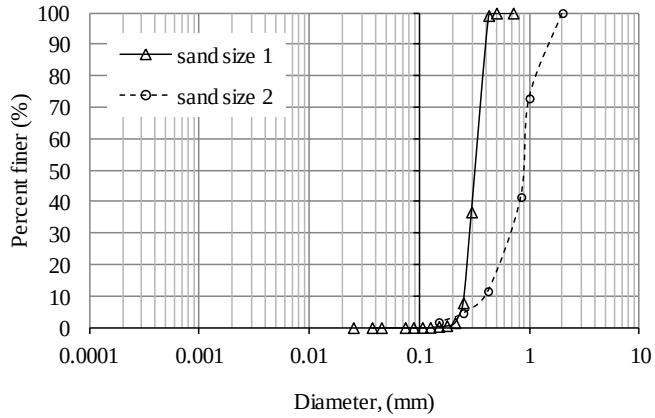

Figure 3.4 The size distribution of sand size 1 and sand size 2

3.2.3 Sediment Feeding

Location of sediment feeding is shown in Figure 3.2 (e). Sediment was released from the upstream side by hand. The location of the feeding sediment is located at 15 cm distance from measurement area. This distance is decided by preliminary experiment. The reasons for choosing the sediment feeding distance are explained as follow:

(1) Some of bed-load transport materials trapped during move on cohesive sediment bed. So, the distance should close to the observation area. If the trapped sediment on the surface of cohesive sediment bed at location before observation area is too much, the volume of bed-load transport that affect on the observation area will decrease and the volume is an unknown number. The fifteen cm is close enough because few sediment trapped along this distance. So that, the volume of bed-load transport that affects at observation area is equal to the volume of sediment feeding.

(2) The distance is enough for achieving an equilibrium condition of bed-load transport. This condition is hard to recognize. However, this can be evaluated by cross section profile at observation area. If the cross section profiles have a similar geometry, so the eroding media also in same condition. The cross section profiles from the observation area indicate that 15 cm is enough for achieving an equilibrium condition of the bed-load transport. Because all cross section profiles have a similar geometry. Its means that the bed deformation is affected by the same volume of bed-load transport.

This research used two kinds of sand (sand size 1 and sand size 2) for feeding material. Sand size 1 is fine material. Sand size 2 is coarse material. Both of them are sorted. The size distribution of sand size 1 and sand size 2 are shown in Figure 3.4. The mean diameter, d_{50} of sand size 1 and sand size 2 are 0.324 mm and 0.88 mm, respectively. The specific gravity of those sands is 2.65.

To generalize the volume of bed load transport, the potential equilibrium sediment transport, q_b in a given hydraulic condition is used for determination the variations of sediment feeding volume. The sediment feeding discharge is widely distributed from 0 (0%) to 1.5 (150%) times as the potential equilibrium sediment transport rate, q_b. Where, q_b is the potential bed-load transport rate in equilibrium condition on movable bed

composed of the supplied material and calculated using Ashida and Michiue's bed-load equation (Ashida and Michiue, 1973). So, in 0% q_b, the flow has no bed-load transport rate or only clear water. The 100% q_b is the condition that has bed-load transport with same volume to q_b. 150% q_b is the condition that the bed-load transport over than q_b.

Total of 18 cases are conducted in this research as shown in Table 3.1. In Case 1 until Case 13, the cohesive sediment bed Type A is used as eroded media. In Case 1a to Case 5a, the eroded media is cohesive sediment bed Type B. Case 1 is an experiment that eroding media only clear water. This case is used to make a comparison with all cases. In Case 2 until Case 7, the sediment feeding is fine sand (sand size 1). In Case 8 to Case 13, the sediment feeding is coarse sand (sand size 2). Case 1a is an experiment that the eroding media only clear water. In Case 2a to Case 5a, the sediment feeding is coarse sand (sand size 2).

The duration for each experiment is 6 minutes. During 6 minutes, sediment is fed continuously to produce bed-load transport at a constant rate. The sediment is fed at a certain volume of sediment by hand. The interval of feeding time is every 10 seconds.

Table 3.1 Experiment cases and volume of sediment feeding

No.	Case	d_{50} of sediment feeding (mm)	Sediment feeding discharge (gram/10 second)	Percent of bedload transport to q_b (%)	Type of cohesive sediment bed
1	Case 1	-	0	0	Cohesive sediment Type A
2	Case 2	0.324	15.96	15	
3	Case 3	0.324	26.59	25	
4	Case 4	0.324	37.23	35	
5	Case 5	0.324	53.19	50	
6	Case 6	0.324	106.37	100	
7	Case 7	0.324	159.56	150	
8	Case 8	0.88	0.65	15	
9	Case 9	0.88	1.09	25	
10	Case 10	0.88	1.53	35	
11	Case 11	0.88	2.18	50	
12	Case 12	0.88	4.36	100	
13	Case 13	0.88	6.54	150	
14	Case 1a	-	0	0	Cohesive sediment Type B
15	Case 2a	0.88	1.09	25	
16	Case 3a	0.88	2.18	50	
17	Case 4a	0.88	4.36	100	
18	Case 5a	0.88	6.54	150	

3.2.4 Experiment Condition

The hydraulic condition for all experiment is determined by the necessity for producing the flow condition capable to transport the feeding material. The water depth is 2.2 cm. The slope channel is 0.004. The discharge is 0.00145 m^3/s. The summary of the hydraulic conditions for all cases are shown in Table 3.2.

Table 3.2 Hydraulic condition for all experiments

Parameters	Value
Water discharge (m^3/s)	0.00145
Slope	0.004
Water depth (m)	0.022
Width (m)	0.15
Average flow velocity (m/s)	0.43
Aspect ratio	0.1467
Froude number	0.9256

As explained in Introduction of this chapter that the physicochemical parameters will affect in the erosion rate of the cohesive sediment bed. Those parameters are water content of cohesive sediment bed, temperature and salinity of water. Therefore, those parameters should be controlled in the same magnitude for all experiments to allow the comparative analysis. The water content is measured by sampling from cohesive sediment bed after experiment. The average of water content for all experiments, which using cohesive sediment Type A is 52.19%. The average of water content for all experiments, which using cohesive sediment Type B is 31.91%. Deviations of water content for cohesive sediment samples Type A and Type B are 0.996% and 1.82%, respectively. Due to the presence of coarse material in the cohesive sediment bed, the water content in cohesive sediment Type B is lower than in Type A. Furthermore, the analyses of erosion rate are separated. The water temperature is measured during experiment. The temperature is around 30 degrees centigrade. In this research, the salinity is not observed. However, to ensure the salinity in the same condition, all experiments used the same water source.

3.3 Measurement Methods

In order to evaluate erosion rate characteristics, the bed elevation at initial condition and final condition were measured. The location of observation area is set in the middle of the flume channel as shown in Figure 3.2 (f). Although, the observation area is only 20 cm long, the total sample of cohesive sediment bed were made on 8 m long to reduce the effect of boundary condition at upstream and downstream end. The distance between observation area and the location of sediment feeding is around 15 cm. The 15 cm is enough long to get the spatially equilibrium erosion speed that was explained in Subchapter 3.2.3. Bed elevations are measured at five cross sections spaced 5 cm apart along 20 cm observation area. In each cross section, eleventh points are measured. Thus, for each experiment around fifty five points are measured in the initial and the final stage of the experiment.

Along both sides of the channel a point gauge is installed on the rail for leveling the bed and measuring bottom topography. The accuracy of the point gauge is 0.1 mm. The bed elevation and water surface are also monitored during experiments by a digital high speed camera from beside the wall. The camera shots through the acrylics wall which has grids on it as shown in Figure 3.1 (g). The floated particles are put on the surface of the water flow and tracked them with a high speed camera in order to have sample measurements of surface flow velocities.

3.4 Dynamic Shear Stress on Cohesive Bed Surface

The bed load transport affects the bed shear stress magnitude. The excess of the bed shear stress produces erosion on the bed. Therefore, the erosion rate should be estimated by considering the presence of bed-load transports. In order to analyze the effect of the bed-load transport on the bed shear stress magnitude, two layer flows concept is applied here (see Figure 3.5). This concept is chosen by considering that the flow has bed-load transport. The flow where Reynold's stress is a dominant force is assumed in the upper flow layer. Laminar flow that consists of the bed-load and water is assumed in the lower flow layer. In this concept, the sediment is transported under non-equilibrium conditions.

At the lower layer, the flow consists of water and bed-load material. Thus, the flow mixture at the lower layer is assumed as a debris flow. Egashira *et al*. (1997) proposed the constitutive equations for calculating the shear stress distribution of debris flow. Therefore, these constitutive equations are applied for the lower layer phenomenon. Hence, the vertical distribution of both water and sediment velocity must be reproduced to obtain the dynamic shear stress on the surface of cohesive sediment bed.

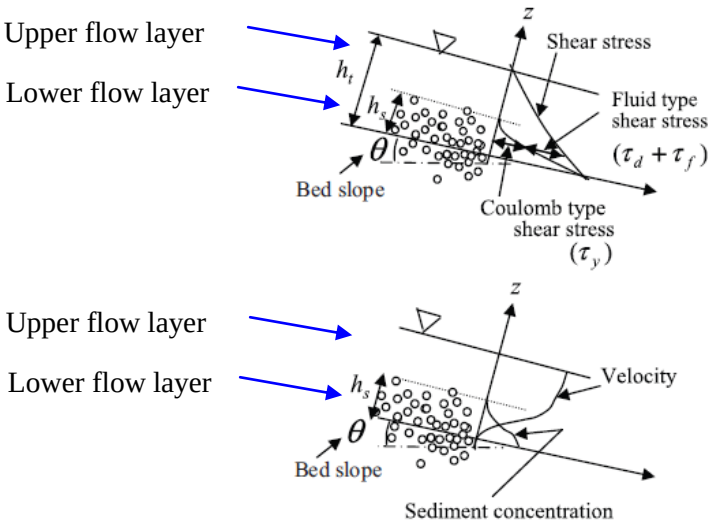

Figure 3.5 Schematic diagrams of the shear stress distribution promoted by Egashira *et al.* (1997) and corresponding profiles for velocity and sediment concentration

Base on Figure 3.5, shear stress τ and pressure *p* in the upper flow layer ($h_s \le z \le h_t$) are calculated as follows:

$$\tau = \int_{h_s}^{h_t} \rho g \sin\theta dz \tag{3.1}$$

$$p = \int_{h_s}^{h_t} \rho g \cos\theta dz \tag{3.2}$$

where, *z* is the vertical axis, h_t is the total flow depth, h_s is the flow depth of the lower layer, ρ is the density of water, *g* is the gravity acceleration, θ is the channel slope. Shear stress τ and pressure *p* in the lower flow layer ($0 \le z \le h_s$) are calculated as follows (Ashida *et al.*, 1982),

$$\tau = \tau_s + \tau_d + \tau_f = \int_0^{hs} \rho_m g \sin\theta dz \tag{3.3}$$

$$p = p_s + p_d + p_f = \int_0^{hs} \rho_m g \cos\theta dz \tag{3.4}$$

Here, the pressure and shear stress in the upper layer are the same as those in the lower layer at the boundary. τ_s and p_s are the shear stress and the pressure due to the static intergranular contact, respectively, τ_d and p_d are the shear stress and the pressure due to interparticle collisions, respectively, and τ_f and p_f are the shear stress and the pressure supported by the interstitial liquid phase, ρ_m is the density of mixed material of sediment and water. The constitutive equations proposed by Egashira *et al*. (1997) are as follows:

$$\tau_s = p_s \tan\phi_s \tag{3.5}$$

$$\tau_d = k_d \left(1 - e^2\right) \sigma d^2 c^{1/3} \left(\frac{\partial u}{\partial z}\right)^2 \tag{3.6}$$

$$\tau_f = \rho k_f d^2 \frac{(1-c)^{5/3}}{c^{2/3}} \left(\frac{\partial u}{\partial z}\right)^2 \tag{3.7}$$

$$p_s = \left(\frac{c}{c_*}\right)^{1/5} (p_s + p_d) \tag{3.8}$$

$$p_d = k_d \sigma e^2 d^2 c^{1/3} \left(\frac{\partial u}{\partial z}\right)^2 \tag{3.9}$$

where, ϕ_s is the friction angle, e is the restitution coefficient, c is the volumetric sediment concentration and c_* is the volumetric sediment concentration in stationary state, σ is the density of sediment, u is the longitudinal flow velocity, k_d (=0.0828) and k_f (=0.16) are the empirical constants. Equations (3.5) to (3.9) are substituted to equations (3.3) and (3.4) and following velocity and sediment concentration profiles are obtained.

$$\left(h_t - z\right)\frac{\partial F}{\partial z} = F - c \tag{3.10}$$

$$\frac{\partial u}{\partial z} = \frac{1}{d}\sqrt{\frac{g\left(G - Y\right)}{f_d + f_f}} \tag{3.11}$$

where, d is the mean diameter of sediment. F, G, Y, f_d and f_f are calculated as follows.

$$F = \frac{f_{pd} \tan\theta}{\left(\sigma/\rho - 1\right)\left(F_1 - F_2\right)} \tag{3.12}$$

$$G = \sin\theta \int_z^{h_s} \left(\sigma/\rho - 1\right) c dz + \sin\theta \int_z^1 dz \tag{3.13}$$

$$Y = \left(\frac{c}{c_*} \right)^{1/5} \cos\theta \tan\phi \int_z^{h_s} (\sigma/\rho - 1) c dz \tag{3.14}$$

$$f_d = k_d \left(1 - e^2\right)(\sigma/\rho) c^{1/3} \tag{3.15}$$

$$f_f = k_f \left(1 - c\right)^{5/3} \Big/ c^{2/3} \tag{3.16}$$

$$f_{pd} = k_d e^2 (\sigma/\rho) c^{1/3} \tag{3.17}$$

$$F_1 = f_f + f_d - f_{pd} \tan\theta \tag{3.18}$$

$$F_2 = \left(\frac{c}{c_*} \right)^{1/5} \left(f_f + f_d - f_{pd} \tan\phi_s \right) \tag{3.19}$$

Logarithmic velocity profile is applied to the upper flow layer as follows:

$$\frac{u}{u_*} = \frac{u_i}{u_*} + \frac{1}{\kappa} \ln\left(\frac{z - h_s + \eta_0}{\eta_0} \right) \tag{3.20}$$

Where, $u_* = \sqrt{g h_w \sin\theta}$, u_i is the velocity at the interface, κ is the Karman constant, h_w is the depth of the upper flow layer. η_0 is the particle interstitial scale and estimated as follows:

$$\eta_0 = a \sqrt{k_f} \left(\frac{1 - c}{c} \right)^{1/3} d \qquad (a \cong 1.0) \tag{3.21}$$

The height at c=0.05 is assumed for the interface height between the upper flow and the lower flow. Water velocity between the upper flow layer and the lower flow layer is connected at the interface.

The dynamic shear stress, τ_{dy}, in the lower flow layer is calculated to discuss the effect of the volume or concentration of bed-load transport rate on the erosion rate of cohesive material bed. The dynamic shear stress, does not consider energy dissipation by the collision between the bed and the sediment in the vertical movement. Hence, here, we discuss the phenomena focusing on the erosion process by the shear in longitudinal direction. So, the dynamic shear stress is calculated by use of the following equation.

$$\tau_{dy} = \tau - \tau_s \tag{3.22}$$

Here, there is no sediment for the upper layer. Hence, τ_s is equal to 0, The dynamic shear stress can be obtained for both layers. The experimental sediment transport

condition in the paper is non-equilibrium condition. These equations are made to reproduce equilibrium and non-equilibrium sediment transport phenomena and can be applied to non-equilibrium sediment transport (Egashira *et al.*, 1997).

3.5 Erosion Rate Characteristics and Dynamic Shear Stress

3.5.1 Cohesive Sediment Bed Type A

Sediment Supply Using Fine Material

Figure 3.10 shows cross section profiles of the bed at initial and final conditions. Figure 3.10 (a) is the bed elevation profile in experiment, which flowing by water only. Figure 3.10 (b) to (g) are the results from Case 3 to Case 7 that the flow water containing fine sediment transport (sand size 1). To analyze the effect of the concentration of bed-load transport, the comparison of the cross section profile among the experimental cases were done.

Figure 3.10 (c) shows the result of experiment Case 3. The bed degradation depth with sediment supply (25% q_b) is more than that without sediment supply (Case 1, Figure 3.10 (a)). This result shows that the bed composed of the cohesive sediment bed will be eroded more by the addition of the non-uniform sediment transport in the flow under the same hydraulic conditions. This case indicates that the bed-load transport can increase the dynamic shear stress on the surface of cohesive sediment bed.

Figure 3.10 (d) shows the result of the experiment in Case 4. The erosion process of cohesive sediment has been stopped, and the aggradation process occurs in this case. This case indicates that the sediment supply reduces the flow velocity near the bed surface. The supplied sediment was trapped much by the cohesive material due to the small velocity of the sediment transport.

The water discharge is constant under all experiments. Hence, the velocity of the sediment transport near the bed decreases with the increase in the bed-load transport rate. This result indicates that the bed-load transport can decrease the dynamic shear stress on the surface of cohesive sediment bed. When sediment supply exceeds 35% q_b, Case 5 to Case 7, the velocity of the sediment transport becomes enough small to be trapped. In these cases, all the surface area of cohesive sediment bed covered by the

bed-load transport material (see Figure 3.10 (e) to (g)). The average of bed deformations in these experiments are presented in Table 3.3.

Sediment Supply Using Coarse Material

Figure 3.10 (h) to (m) are the results from Case 8 to Case 13. These experiments used coarse sediment (sand size 2) for producing bed-load transport. Figure 3.10 (i) and (j) show the result of experiment Case 9 and Case 10, respectively. The bed degradation with sediment supply (Case 9 and Case 10) is more than without sediment supply (Case 1). Case 9 and Case 10 indicate that the volume of bed-load transport can increase the dynamic shear stress on the surface of cohesive sediment bed. However, the bed degradation decreases with adding the sediment supply as shown in Figure 3.10 (k) to (m). These results show that using coarse material for sediment supply, the phenomenon of the bed deformation is same as in case using fine material for sediment feeding. The average of bed deformations in these experiments are presented in Table 3.4.

Effect of the sediment size is clearly observed in this research. In case using fine sediment feeding (sand size 1), bed aggradated when sediment feeding is more than 35 % q_b. This is due to the fact that the supplied sediment trapped by cohesive material. However, for coarse sediment feeding (sand size 2), bed does not aggradated. This due to the fact that the supplied sediment is not trapped so much by cohesive material. In case sediment supply is fine material, during the saltating motion, the momentum energy is smaller than if the sediment supply is coarse material. So, the fine sediment supply is easier to trap on the bed due to the cohesiveness than the coarse sediment supply. The coarse sediment supply also produces a higher impact on the bed than the fine sediment supply. It can be seen that the maximum erosion is larger in case the sediment supply is coarse material. The effect of the cohesiveness of the bed is strong enough in cases with fine material of bed-load transport.

Table 3.3 Average of bed deformations using fine sediment feeding

Case	Percent volume of bed-load transport to q_b ($\% q_b$)	Bed deformation during six minutes (cm)
Case 1	0	0.430
Case 2	15	0.254
Case 3	25	1.055
Case 4	35	-0.213
Case 5	50	-0.093
Case 6	100	-0.368
Case 7	150	-1.235

Table 3.4 Average of bed deformations using coarse sediment feeding

Case	Percent volume of bed-load transport to q_b ($\% q_b$)	Bed deformation during six minutes (cm)
Case 1	0	0.430
Case 8	15	0.210
Case 9	25	0.450
Case 10	35	1.242
Case 11	50	0.409
Case 12	100	0.105
Case 13	150	0.049

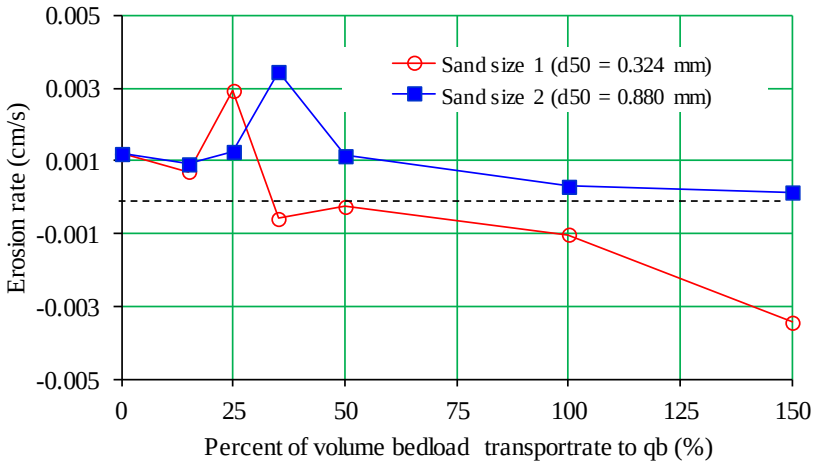

Figure 3.6 The erosion rate on cohesive sediment Type A

All results show that the erosion rate will increase when the volume of the sediment feeding increase under the small rate condition. However, after achieving a certain volume of the sediment transport, the erosion rate of cohesive sediment bed will decrease.

To analyze the effect of sediment concentration on bed shear stress, three cases are chosen. The three cases are Case 9, 11 and 12 that showing the increasing and decreasing on erosion rate. The amount of sediment feeding in Case 9, Case 11 and Case 12 are 25% *qb*, 50% *qb* and 100% *qb*, respectively. The Equation 3.1 to Equation 3.22 are applied in Case 9, Case 11 and Case 12. Figure 3.9 shows the vertical distribution of the longitudinal velocity, the sediment concentration and the dynamic shear stress in Cases 9, Case 11 and Case 12.

When sediment feeding rate is 100% q_b, the thickness of the bed load layer becomes maximum and velocity near bed is smaller than in Case 9 and Case 11. The dynamic shear stress on the bed is equal to zero. Hence, the erosion rate of the cohesive material is equal to zero in the calculation. On the other hand, when sediment feeding rate is equal to 25% q_b, the thickness of the bed load layer becomes thin and velocity near bed is larger than other two cases. The dynamic shear stress on the bed is also larger than the other two cases. Hence, it is considered that the erosion rate of the cohesive material becomes largest among the three cases. These results indicate that after achieves on a certain volume of the bed-load transport, the erosion rate will decrease during increasing of bed-load transport, as shown in Figure 3.6 because of the small dynamic shear stress.

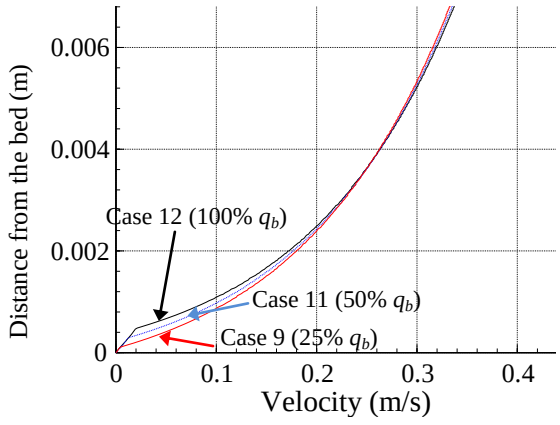

(a) Longitudinal velocity

Figure 3.7 The vertical distribution of velocity

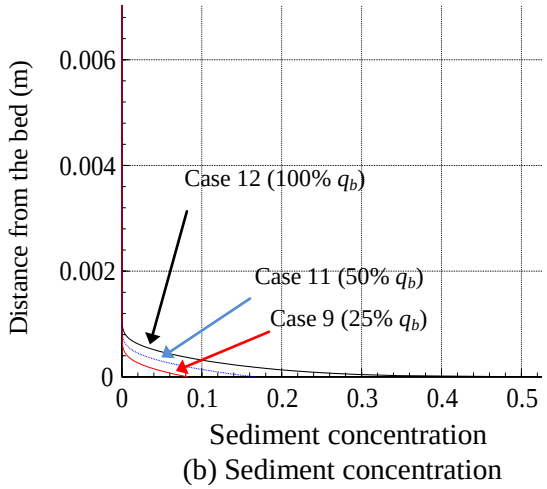

(b) Sediment concentration

Figure 3.8 The vertical distribution of sediment concentration

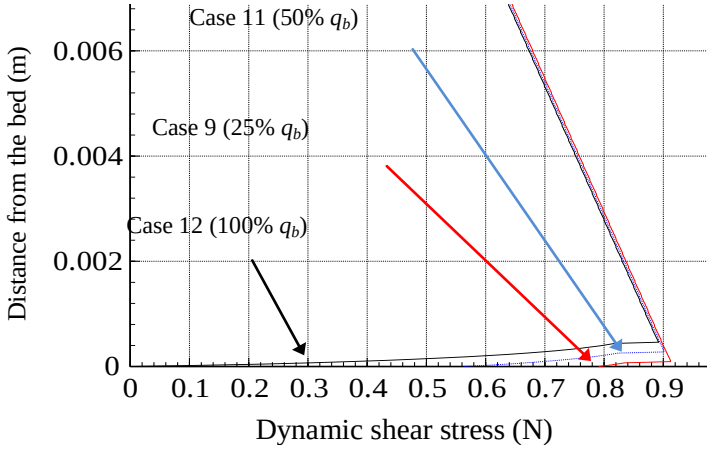

(c) Dynamic shear stress

Figure 3.9 The vertical distribution of dynamic shear stress

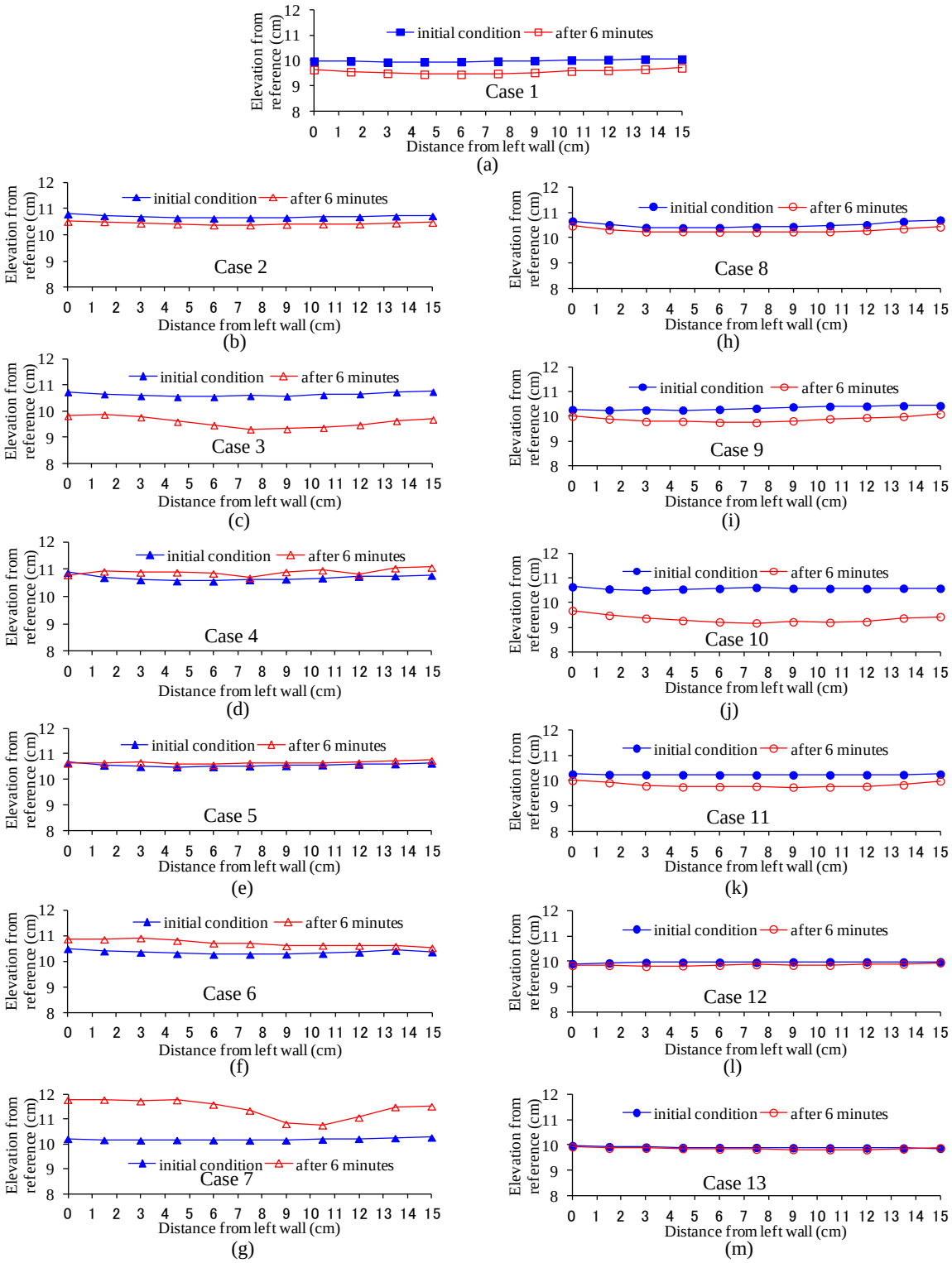

Figure 3.10 The cross section profiles for Case 1 to Case 13

3.5.2 Cohesive Sediment Bed Type B

Figure 3.11 is the results of erosion rate in experiment using cohesive sediment Type B. In these experiments, the cohesive sediment bed contains the coarse material and eroded by flowing water. These become another bed-load transport source in the observation area. The erosion rate in Case 1a is the largest among other cases. Sediment supply due to the bed erosion between the upstream end and the observation place affects on the result. In Case 1a, coarse material is only supplied from the bed and the effect of the erosion by non-cohesive material is introduced in this case. However, the non-equilibrium characteristics of coarse material in cohesive material are strong (Egashira *et al*., 1997). The distance from the upstream end of cohesive material layer and the measurement location, which is 4 m, is not enough to get the equilibrium sediment transport rate. As a result, the erosion rate of cohesive sediment decreases with increasing in the sediment supply. This phenomenon will be applied in numerical simulation that presented in Chapter 5.

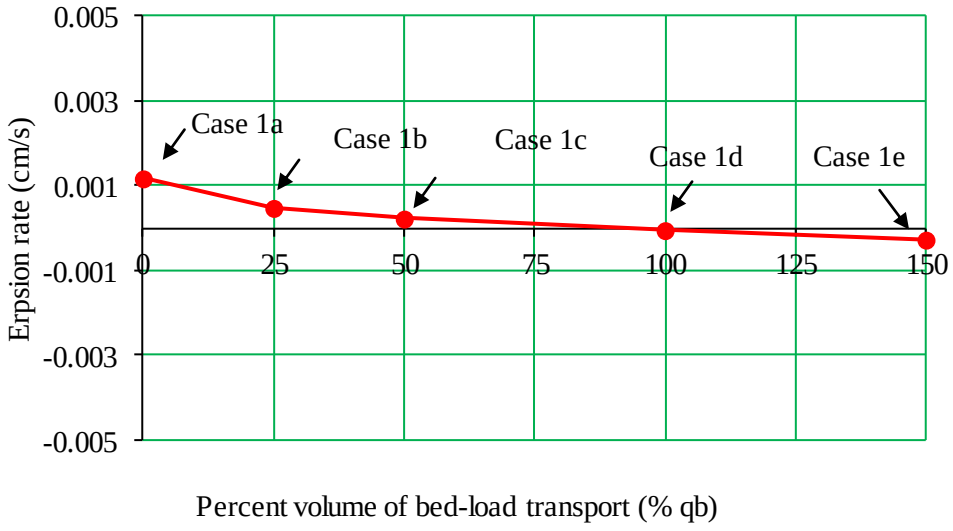

Figure 3.11 The erosion rate on cohesive sediment Type B

3.6 Summary

The erosion rate characteristics of cohesive sediment bed were studied experimentally. The obtained results are summarized as below.

The erosion rate of cohesive sediment composed of 100 % kaolin will increase

when the volume of the bed load transport increased under small sediment supply conditions. In case that the supplied sediment is fine material, the maximum erosion occurs at 25 % q_b. In case that the supplied sediment is coarse material, the maximum erosion occurs at 35 % q_b. However, after achieving on a certain volume of the bed load transport, the erosion rate will decrease with increase in bed load transport because of the decreasing in the dynamic shear stress on the bed.

For fine non-cohesive material, the bed is aggradated when sediment supply is large, because the supplied sediment is trapped by cohesive material. However, for coarse non-cohesive material, the bed is not aggradated when sediment supply is large, because the supplied sediment is not trapped so much by cohesive material. This is one of the reasons why the maximum erosion rate of the cohesive material by coarse material is larger than that by fine material.

Generally, the results show that the volume of sediment feeding increases the erosion rate of cohesive sediment when under the small rate conditions. However, after achieving a certain volume of sediment feeding, the erosion rate of cohesive sediment will decrease. This tendency indicates that the relation between the volume of bed-load transport and erosion rate of cohesive sediment is a non-linear function. It is well known that the calculation of the shear stress considers only in clear water flow. In fact, the volume or concentrations of the bed-load transport effects on the magnitude of the shear stress on the surface of bed. This phenomenon should be considered in the calculation of the bed deformation, if the flow contents of bed-load transport. The shear stress on the bottom should be calculated by including the effect of the concentration of bed-load transport.

In cohesive sediment composed of 50% kaolin and 50% coarse sand, the erosion rate of cohesive sediment decreases with increase in the sediment supply. The volume of bed-load transport at observation area is affected by bed-load transport from eroded bed. These conditions make the erosion rate on the bed not only caused by sediment feeding but also sediment from the bed itself. The presence of coarse material on the cohesive sediment bed becomes another interesting phenomenon that need to observe more detail.

References

Aberlea J, Nikorab V, and Waltersb R, Effects of bed material properties on cohesive sediment erosion, *Marine Geology*, Vol. 207, pp. 83-93, 2004.

Ashida, K., Egashira, S., and Kamoto, M.: Study on the erosion and variation of mountain streams, *Bulletine of DPRI, Kyoto University*, Vol. 25, B-2, pp. 349-360, 1982.

Carbonneau, P.E., and Bergeron, N.E.: The effect of bed-load transport on mean and turbulent flow properties, *Geomorphology*, Vol. 35, pp. 267-278, 2000.

Egashira, S., Miyamoto, K., and Itoh, T.: Constitutive equations of debris flow and their applicability, *Proc. 1st Int. Conf. on Debris-Flow Hazards Mitigation, New York*: ASCE: pp.340-349, 1997.

Gularte, R.C., Kelly, W.E., and Nacci, V.A.: Erosion of cohesive sediments as a rate process, *Ocean Engng*, Vol. 7, pp. 539-551, 1980.

Kamphuis, J.W.: Influence of sand or gravel on the erosion of cohesive sediment, *J. of Hyd. Research*, Vol. 28, No. 1, pp. 43-53, 1990.

Mehta, A.J., Hayter, E.J., Parker, W.R., Krone, R.B., and Teeter, A.M.: Cohesive sediment transport. I: Process description, *J. of Hyd. Eng.*, ASCE, Vol. 115, No. 8, pp. 1076-1093, 1989.

Mehta, A.J., McAnally, W.H.J., Hayter, E.J., Teeter, A.M., Schoellhamer, D., Heltzel, S.B., and Carey, W.P.: Cohesive sediment transport. I: Application, *J. of Hyd. Eng*., ASCE, Vol. 115, No. 8, pp. 1094-1112, 1989.

Nishimori, K., and Sekine, M.: Studies on soil erosion processes and erosion kinetics sticky, *Journal Japan Society of Civil Engineers*, B JSCE, Vol. 65 No. 2, pp. 127-140, 2009. (in Japanese)

Parchure T.M, and Mehta A.J, Erosion of soft cohesive sediment deposit, *Journal of Hydraulic Engineering*, ASCE, Vol. 111, No. 10, pp.1308-1326, 1985.

Sekine M and Iizuka N, Erosion rate of cohesive sediment, *Proceeding Int. Confernce, Hamburg*, 2000.

Song, Y.M., and Chin, C.O.: Effect of bed-load movement on flow friction factor, *Journal of Hydraulic Engineering*, ASCE, Vol. 124, No. 2, pp. 165-175,1998

Thompson, C.E.L., and Amos, C.L.: Effect of sand movement on a cohesive substrate, *Journal of Hydraulic Engineering*, ASCE, Vol. 130, No. 11, pp. 1123-1125, 2004.

Chapter 4

Numerical Analysis on Countermeasures of Bank Erosion

4.1. Introduction

Bars in a river are classified according to position, shape and size. The size of the bar can vary from several meters square until hundred or thousand meters square. There are various types of bar formation in river systems. One of them is a mid-channel bar. The mid-channel bar becomes an obstruction in the middle of a river cross section. The presence of it increases the flow velocity and local scouring around banks. It is widely known that the mid-channel bar accelerates of bank erosion. Therefore, it is closely related to the occurrence of bank erosion.

Many training works such as groin, revetment, spur dike and so on are applied at rivers to prevent bank erosion. Those structures are installed on the bank body to prevent mass failure and also to improve bank stability. It will be successful in protecting the riverbank locally. However, usually the structures will change the cross-sectional geometry, in which leads to change the flow pattern and others hydraulic parameters. In an extreme case, the structure will produce bank erosion problem at the other places. Therefore, the countermeasure by installing a structure to increase bank stability may not work all the time. Hence, study on the bank erosion problem considering the flow patterns and bed deformations under the channel width scale are important for achieving a successful countermeasure.

In a river with banks composed of non-cohesive material in the bottom layer, the bed deformation near the bank toe is an important parameter in triggering the bank erosion. The prevention of erosion on the bed near the bank toe is a basic solution to reduce the possibility of bank failure. This can be done by controlling the flow velocity in the river. The bed deformation near the bank is one of the input parameters to predict the bank line retreat. The increase in relative height of riverbank that caused by bed

scour has a strong influence on the stability of riverbank. Therefore, the prediction of bed deformation near the bank with accurate calculation becomes an important analysis. The results of experimental cases as explained in Chapter 2 show that the cohesive material in the bank affects on the bank line migration process. The effects of the cohesive material are also discussed in this chapter.

Numerical simulation is one of the methods to predict the future condition. It is useful for planning or designing in river regulation works. In this research, the numerical simulation was performed to analyze the future condition of flow pattern, bed deformation and bank line retreat. These simulations are done to investigate the effect of the cohesive material in the bank and also the effectiveness of countermeasures on bank erosion problem. This analysis will be applied in Sesayap River. The river located in East Kalimantan Indonesia. The river reach at Malinau has a problem related to the bank erosion. The presence of a huge mid-channel bar accelerates the bank erosion by flow. It is considered that the the deflected flow around the bar is a primary cause of the bank erosion problem. Hence, to control the flow by dredging of the bars may give the significant difference of the results. A general countermeasure structure is also simulated to counteract the bank erosion. Revetment structure is chosen as the general structure for countermeasure method here.

The purpose of this chapter is to elucidate the relationship of the flow pattern, the velocity distribution, bed deformation near the bank toe and bank line retreat. Using numerical analysis, the flow pattern, flow velocity, bed deformation near the bank and the bank line retreat will be analyzed.

4.2. Outline of Study Area

4.2.1. General Condition and Bank Erosion Problem

Sesayap River in East Kalimantan is chosen in order to examine the interaction of channel geometry, water flow, and bed. The watershed area is around 17,432 square kilometers. The headwaters are located in the mountain forest on the national boundary between Indonesia and Malaysia. This river is one of the largest rivers in East Kalimantan. The main function of the river is a navigation channel. The channel stream

passes through in three regencies, Nunukan. Malinau and Bulungan regencies (see Figure 4.1). The average temperature in East Kalimantan is 26^{o}C, which has fluctuation 5^{o}C-7^{o}C. The rainfall intensity is 2000-4000 mm/year and the amount of rain days are 130-150 days/year. This general description of the climate indicates that the rivers in East Kalimantan have large discharge within a half year.

During the last ten years, the flood and bank erosion occur intensively in Sesayap River, especially at Malinau reach. Photo 4.1 (a) shows the floodwater from Sesayap River on November 2008 and many villages have been inundated during this time. Bank erosions were occurred at some reaches of the river as shown in Photo 4.1 (b). The bank erosion gives damages on the road structure. The main structure of the road around 2 meters width and 40 m long was collapsed. This is the main road for transportation in Malinau Regency. Due to this hazard, the bank erosion in Malinau reach becomes main issue in this regency.

Understanding the processes and mechanisms of bank failure, their causes, and spatial extent is crucial for the identification of stabilization measures and management of bank erosion problems. Prediction of stable bank geometry as a function of material properties and river stage should represent a fundamental part of projects involving the riverbank stabilization and mitigation measures (Dapporto, *et al*., 2003). Accordingly, to accomplish the bank erosion problems, it is important to understand and consider the geology, geomorphology and hydraulic aspects of the river. Hence, in this study, field investigations were conducted to obtain: (1) the geological characteristics of the bank, (2) flow characteristics of the river, (3) geometry and morphology characteristics of riverbed and (4) erosion characteristics of the river. Furthermore, sampling of bank material, measurement of river stages, topography, and investigation of the bank surface are conducted.

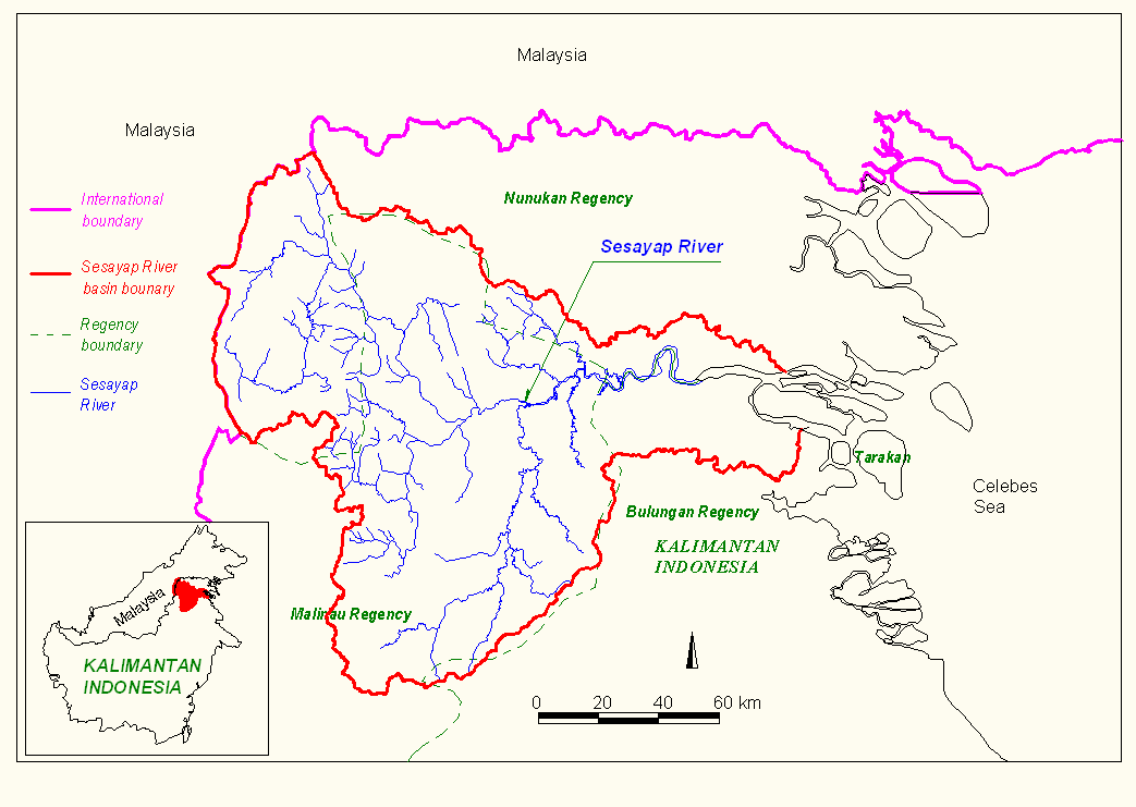

Figure 4.1 Location of study site in Sesayap River basin. (Source: Satuan Kerja Bina Pengelolaan SDA, Direktorat Bina Penatagunaan SDA, Public Work Ministry of Indonesia)
http://www.polapsda.net/?act=detail_ws&wid=15

(a) Inundated water on the bank (b)Bank erosion

Photo 4.1 Inundated water and bank erosion in Sesayap River at Malinau reach

4.2.2. Water Levels

Most of bank erosion with the mass failure takes place in the high soil moisture level. The cohesive material becomes erodible under the high moisture (Hooke, 1979). The water from the river influences the soil moisture condition in the bank. Therefore, to understand the bank erosion processes needs to evaluate the river flow properties such as water level (Lawler, *et al.*, 1997). Hence, the water surface measurements were conducted to analyze the flow characteristics of the river. The location of measurement points is shown in Figure 4.2. Although the distance between study site and the estuary is about 70 km, the sea tide still influences the flow in the study site. It is due to the small slope of riverbed. Three stage gauge meter are installed in the river (P1, P2 and P3). The water levels were measured every hour within three days, simultaneously.

Figure 4.3 shows the characteristics of water stages at P1, P2 and P3. The influence of sea tide can be seen clearly at location P1 and P2. In these locations, fluctuation of water level similar to the typical fluctuation from the sea. However, the sea tide does not influence the water stages at location P3 because of the high bed elevation. The water stages during one month at P1 are shown in Figure 4.4.

The influence of sea tide makes the hydraulic conditions in the river reach has a contrastive flow as described below.

(1) During the water level from the sea getting high, the sea water entrance to the river through the estuary. The flow reverses to the upstream area. In case Sesayap River, the reversed flow until at Malinau reach than against the flow from upstream area. In this condition, the flow velocity in Malinau reach becomes small or even zero. Sediment transports from the upstream area are deposited on the riverbed and then form a bar. The size of the bar becomes higher and wider during this period.

(2) As an opposite condition of point (1), during the lowest level of sea water, the energy height in the river becomes maximum and lead to a condition where the flow velocity is a high value. The high flow velocity causes the large erosion of the bed. The bed degradation near the bank steepens the bank surface slope and triggers the bank failure.

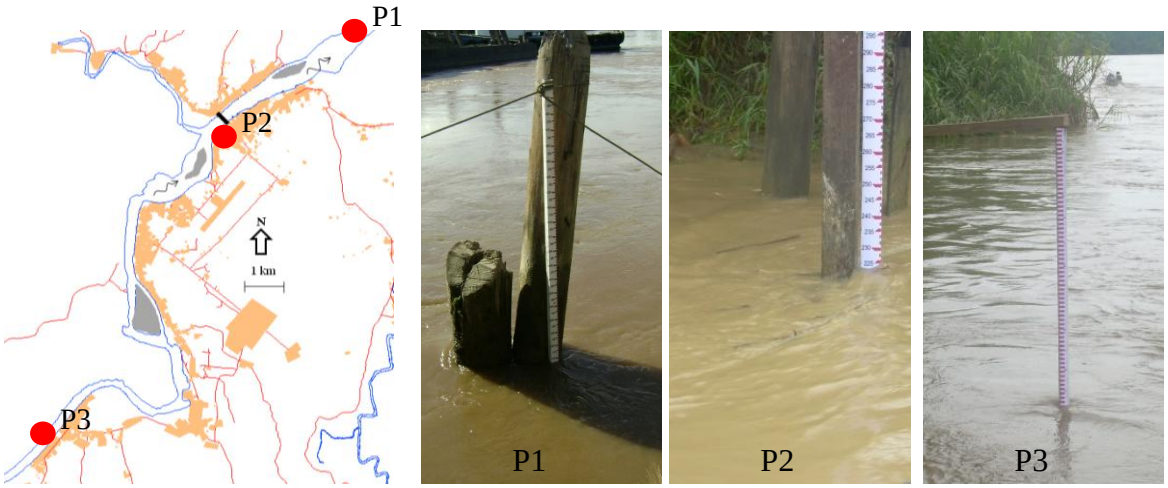

Figure 4.2 Water surface elevation measurement

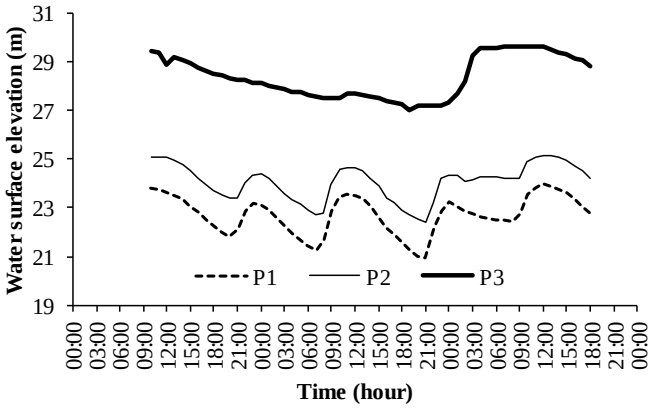

Figure 4.3 Temporal change of water surface elevation at location P1, P2 and P3

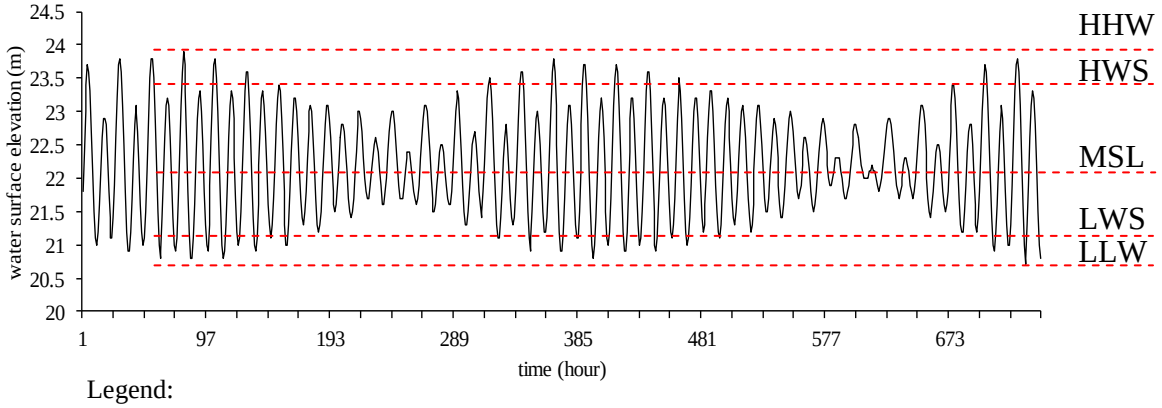

Legend:
HHW: highest high water, HWS: high water springtide, MSL: mean sea level
LWS: low water springtide, LLW: lowest low water

Figure 4.4 Temporal change of water surface elevation in one month (location P1)

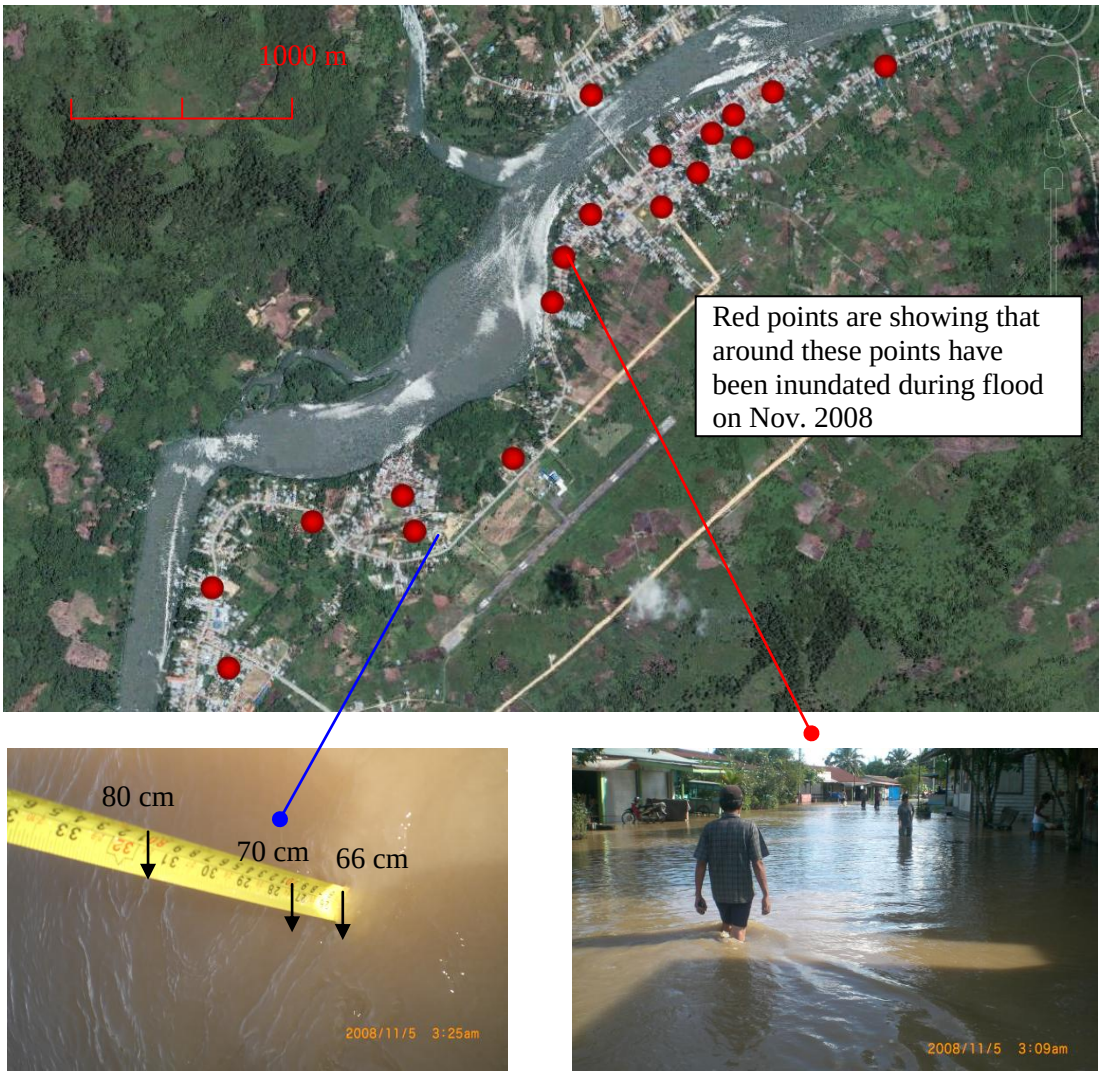

Photo 4.2 Floodwater form Sesayap River in Malinau Kota. The depth of flood is around 50 cm – 100 cm

4.2.3. River Topography

The channel pattern type of Sesayap River in the study site is a combination of meandering river and mid-channel bar. The bar is composed of sand and gravel material. The sinuosity of the river is around 1.3 to 1.5. Because of the flow conditions as explained in the previous section, the location of the study site becomes a sediment deposition place. The deposition material forms bars. Figure 4.5 shows the mid-channel bar formation in the river channel.

The significance of mid-channel bar in lateral migration of a river has studied using field observation by several researchers, for example; Hooke (1986), Gabel and Bridge (1992), and Jiongxin (1996). Their results show that, the mid-channel bar is an important factor in rapid erosion process of the bank. Using experimental laboratory, Ashworth (1996) explained that lateral migration of the bank has strong relation to the bar aggradation and changes of wetted cross-sectional area. These give knowledge that, during the bar growth, the bank erosion will occur intensively. From this point of view, controlling the bar growth may become a solution to stop bank erosion.

The effect of mid-channel bar on hydraulic parameters related to the bank erosion will be discussed in the next sub-chapter using numerical simulations. The simulations need data involving topography of riverbed and floodplain. Therefore, topography of river bed and floodplain were measured. The floodplain is around 12 km long and 50 meters perpendicular wide from the riverbank line. Riverbed topography was measured using GPS-map 178 Sounder that has accuracy 0.01 m. This equipment is installed on the ship as shown in Photo 4.3. In order to obtain contour that cover all surface of river bed, the observation is conducted during high water level. During low water level the bar merges on the water surface, so the ship cannot cover all surface of the bar. The GPS equipment is only for measurement the depth of water, so water level during bathymetry survey is also observed to obtain riverbed elevation. This data is also used to connect between the topography of the floodplain and riverbed elevation. So, the overall elevation data have one point reference. Figure 4.6 shows the tracking points during observation of riverbed in Sesayap River at Malinau reach. The result of this observation is presented in numerical analysis section.

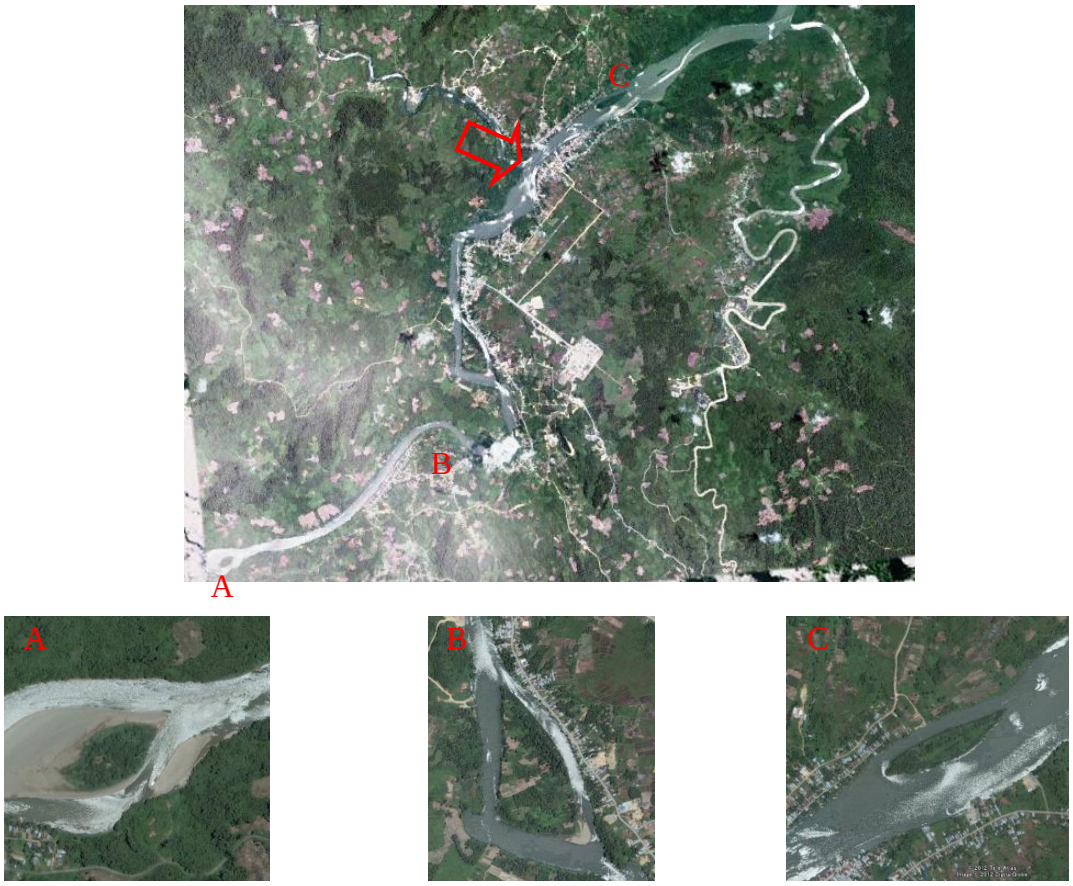

Figure 4.5 Aerial photograph showing large mid-channel bars in the Sesayap River (Google Image)

Photo 4.3 GPS-map 178 Sounder

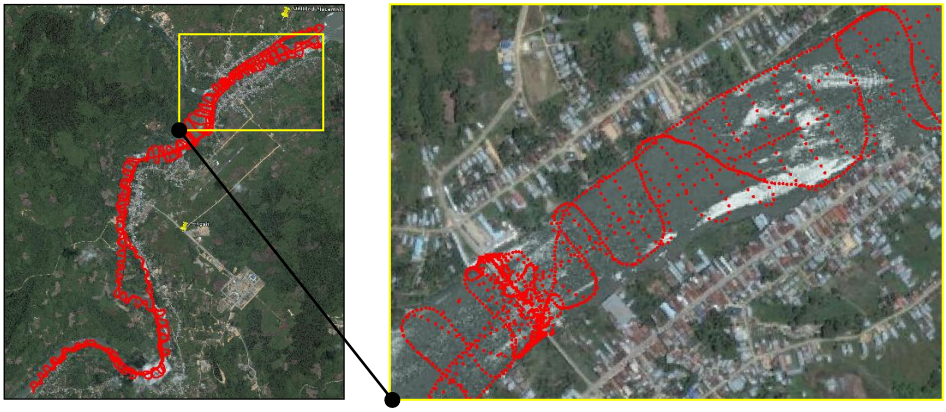

Figure 4.6 Tracking points in river bathymetry observation

4.2.4. Type of Bed Materials

Bed material is also observed in this research. There are three point locations for sampling data. Two samples data are collected from each location. The volume of each sample is around 2 liter. These data were collected from mid-channel bar near the location of bank erosion. The size distribution is analyzed by sieving method in laboratory. Photo 4.4 shows the type of bed material and Figure 4.7 shows the grain size distributions. Gravel and sand are the dominant in the bed material. The presence of the gravel material on the bed indicates that the bed shear stress is high values.

Photo 4.4 Riverbed material

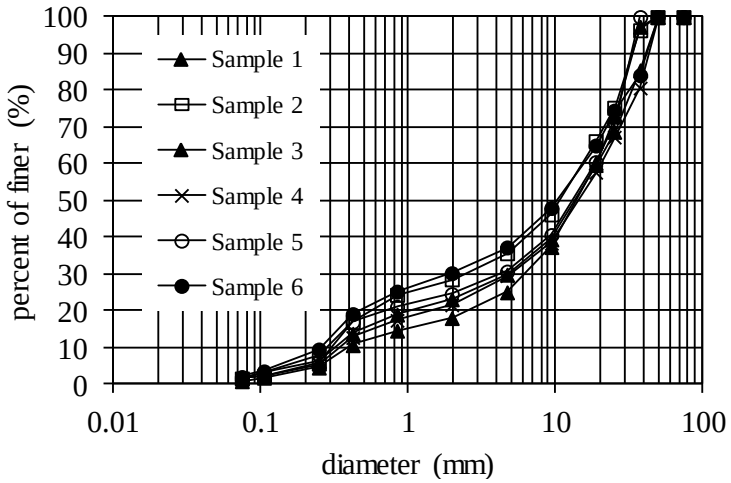

Figure 4.7 Grain size of riverbed material in Sesayap River

4.2.5. Stratification in Bank

This chapter presents the in-situ soil investigation to identify, classify and obtain the information on physical engineering properties of the bank. Furthermore, to clarify the bank-failure mechanism with associated to bank stratification. The sampling points are located in the floodplain area and around the location of bank erosion. Also, the locations of sampling points should close to the river channel.

In this field observation, the total numbers of sampling point are four locations. The methods for sampling data are cone penetration test (CPT), hand auger and spit test. Laboratory tests are conducted to analyze mechanical properties of the samples. In the sampling of the cone penetration test, the undisturbed soil samples are also collected. From these data can be obtained by the physical and mechanical characteristics of the soil at the site along the river reach. Figure 4.8 and Table 4.1 show the location and detailed coordinate of sampling points. Location sampling points for these observations are namely by S1, S2, S4 and S5. S1 and S2 are located at the right bank. S4 and S5 are located at the left bank. The distance of the sampling points is less than 30 m from the riverbank line, perpendicularly. The activities during the cone penetration test and spit sampling are shown in Photo 4.5 and Photo 4.6, respectively.

Figure 4.8 Locations of soil observation in Sesayap River at Malinau reach

Table 4.1 Coordinates of the sampling point

Points name	Coordinates	
	Latitude	Longitude
S1	03^{o} 35’10.2”	116^{o}37’08.4”
S2	03^{o}34’55.9”	116^{o}37’06.6”
S4	03^{o}35’30.5”	116^{o}37’11.7”
S5	03^{o}35’32.6”	116^{o}37’14.6”

Photo 4.5 Activity of CPT sampling at S1,S2, S4 and S5

Photo 4.6 Activity of spit test at S1,S2, S4 and S5

Table 4.2 Characteristics of undisturbed soil of riverbank material

Parameters	Unit	Location sampling point							
		S1		S2		S4		S5	
Depth	(m)	0-2	> 2	0-3.4	> 3.4	0-2.5	> 2.5	0-3.5	> 3.5
Soil Classification	-	CL/CH	SM/SC-SM	CL/CH	SM/SC-SM	CL/CH	SM/SC-SM	CL/CH	SM/SC-SM
Specific Grafity	-	2.61	2.67	2.59	2.65	2.57	2.64	2.62	2.62
Soil moisture	(%)	70	18.5	56	30.7	61	32	46	39
Density	kN/m3	16	17	17.5	17	16	16	17.5	17
Cohesion	kN/m2	8	5	10	5	50>	10	50>	20

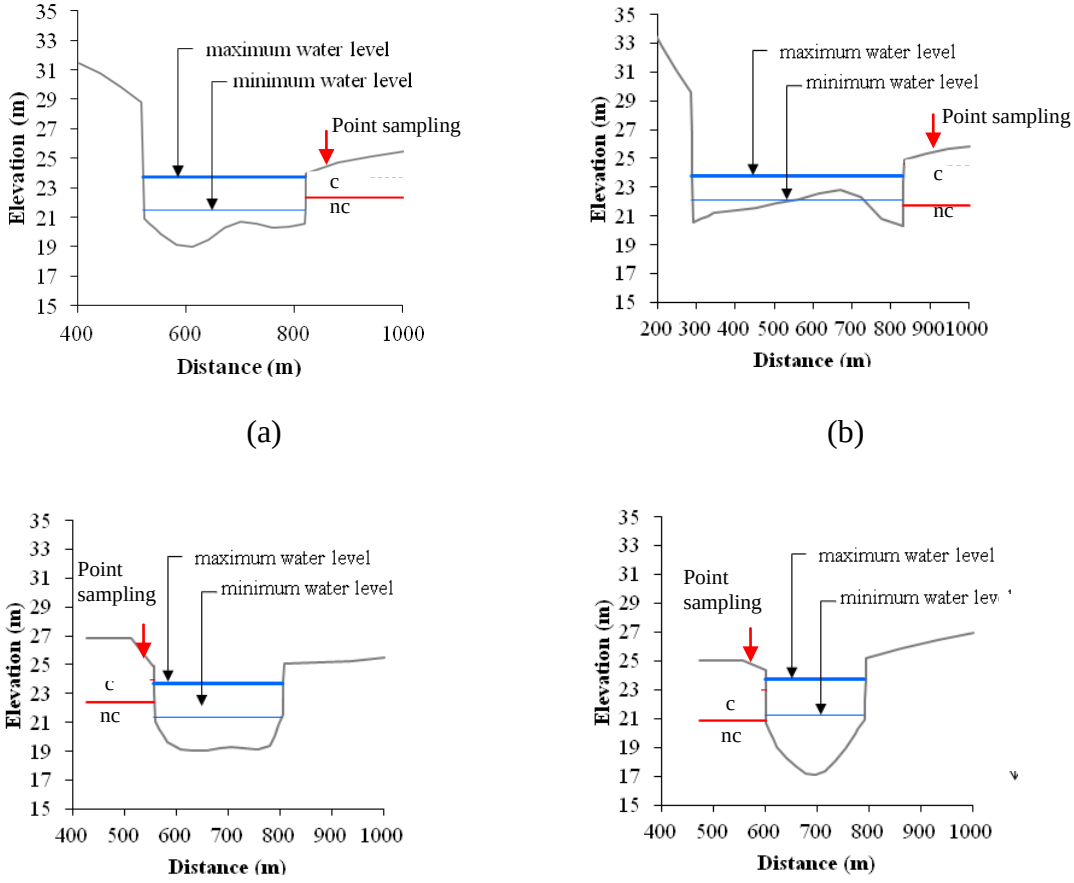

Figure 4.9 Bank stratification from soil test at point S1 (a), S2 (b), S3 (c), and S5 (d)

The results from the soil sampling test are explained as follows:

- The top soil is composed of silty clay. The depth of this soil at S1, S2, S4 and S5 are 0-0.6 m, 0-0.6 m, 0-1.0 m and 0-1.4 m, respectively.
- Under the top soil is clay. The depth of this soil at S1, S2, S4 and S5 are 0.6-2.0 m, 0.6-3.4 m, 1.0-2.5 m and 1.4-3.5 m, respectively.
- Under the clay layer is silty sand or sand. The depth of this soil at S1, S2, S4 and S5 are >2.0 m, >3.4 m, >2.5 m and >3.5 m, respectively.

Generally, the soil investigation shows that the bank is composed of cohesive material on the upper layer and non-cohesive material at the bottom layer. Figure 4.9 shows the vertical bank stratification at S1, S2, S4, and S5. And also the water levels at maximum

and minimum stage are illustrated. During the low stages, the flow velocity is high due to the large difference of water level at upstream and downstream area. The surface of the bank toe is always exposed by flow even in low water level and lead to the undercutting process.

4.2.6. Factors of Triggering Bank Erosion in Malinau Reach

The characteristics of riverbed topography, water stages, riverbed material, riverbank stratification, and riverbank erosion in Sesayap River at Malinau reach were analyzed as follows:

(1) The Sesayap River reach at Malinau is the meeting place between the river flow from the upstream area and the tides from the sea. During the high tide, the flow velocity becomes small and the excessive deposition of sediment occurs and the mid-channel bars are formed. While the bar grows, the flow capacity decreases. Furthermore, the flow will find the new balance conditions by eroding the riverbank.

(2) Mid-channel bar splits the flow into two parts and the flow velocity concentrated at the lee area and leads to erode much volume of the riverbed, especially near the bank toe. Furthermore, the relative bank height will increase. This condition triggers the bank failure with planar mechanism. The controlling level of mid-channel bar may suppress the bank erosion.

(3) The stratification of the riverbank is composed of the cohesive sediment layer on the non-cohesive sediment layer. The thickness of cohesive sediment is around 4 meters. The bank height is more than 5 meters. It means that the non-cohesive sediment layer always exposed with the flow. During the lowest low water (LLW), the water flow with high velocity causes erosion at the bank toe which is the part of non-cohesive material layer. The erosion at non-cohesive material layer develops cantilever of cohesive layers or steepen the relative bank height on riverbanks. The failure block material slide or fall toward the toe of the bank. It will remain until broken down or entrained by the flow. The failed block, in turn, may temporarily protect the toe of the bank from erosion.

(4) To prevent the excessive erosion near bank toe becomes basic treatment to counteract bank erosion. The erosion at near the bank toe is caused by the mid-channel bar, so controlling the height of bars is one of the solutions to prevent river bank erosion in river reach in Sesayap River at Malinau reach.

4.3. Numerical Simulation

4.3.1. Simulation Conditions

The field analyses of bank erosion in Sesayap River at Malinau reach were discussed. The results show that the flow pattern was changed due to the presence of mid-channel bar. The flow pattern and the bed deformation near the bank toe become important parameters on triggering the initial bank erosion process. This agreed with investigations that have been done by Simon *et al.*, (2000). The flow pattern and the bed deformation near the bank toe, especially during lowest low water (LLW) in Malinau reach are discussed in this chapter. During this time, the flow condition may produce high energy due to the different water level between upstream and downstream. The results from this simulation will be used for discussion on the countermeasure of bank erosion problem in Sesayap River.

The horizontal two-dimensional bed deformation analysis model is used in the numerical analysis. Two main cases were conducted in these simulations and described as follow:

(1) Controlling the height of mid-channel bar by dredging or removal a part of volume that higher than a certain level. The dredging area is between Sta. 1650 km and Sta. 2700 km as shown in Figure 4.11.

(2) Installing a general structure of bank protection. In this case, the revetment is chosen as a structure for the bank protection. This structure is a common structure to prevent bank erosion in Malinau.

Figure 4.10 shows the domain of numerical simulation in Malinau reach. The domain model is indicated with a dashed line. Figure 4.11 shows the topography of the calculation domain and the detailed map contour of the mid-channel bar. The mid-channel bar is located between Sta. 1650 km and Sta. 2700 km.

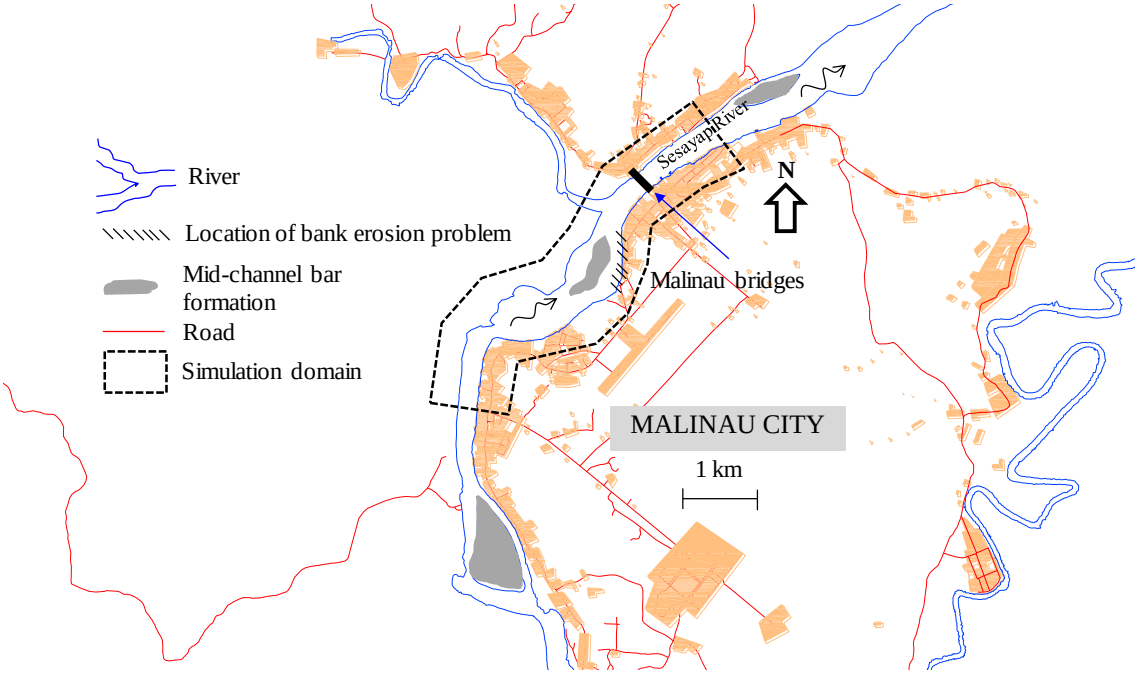

Figure 4.10 Domain of the model for numerical simulation

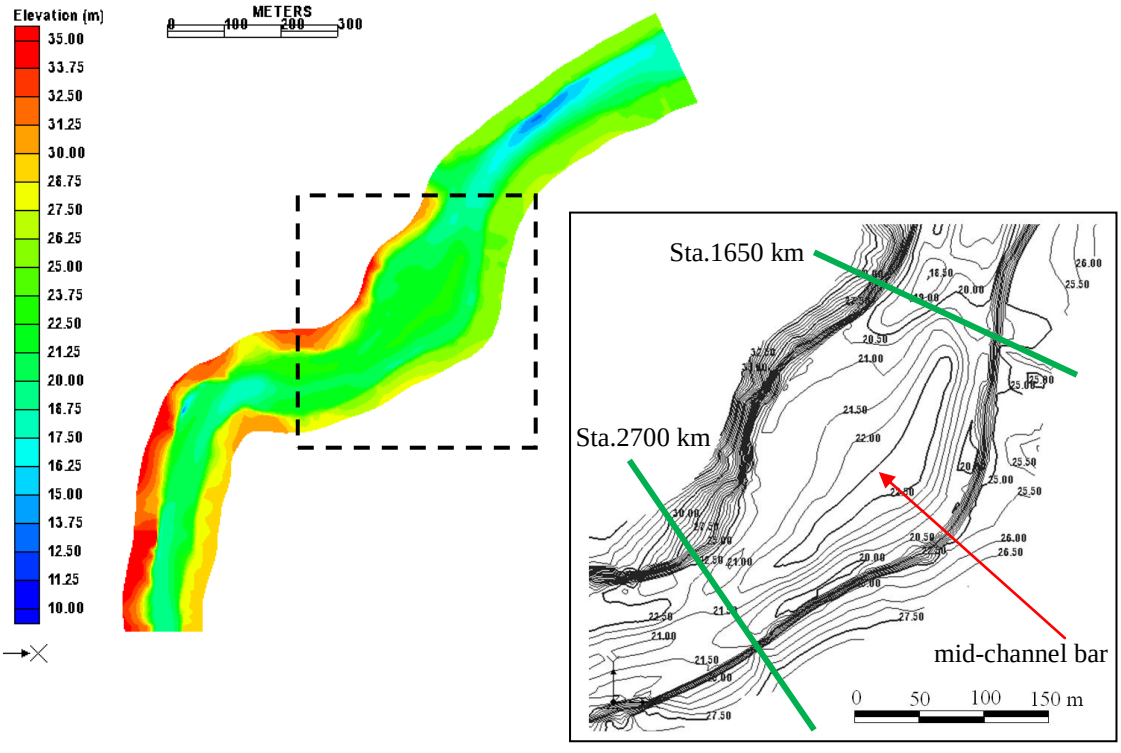

Figure 4.11 Topography of riverbed, floodplain and detailed contour of mid-channel bar

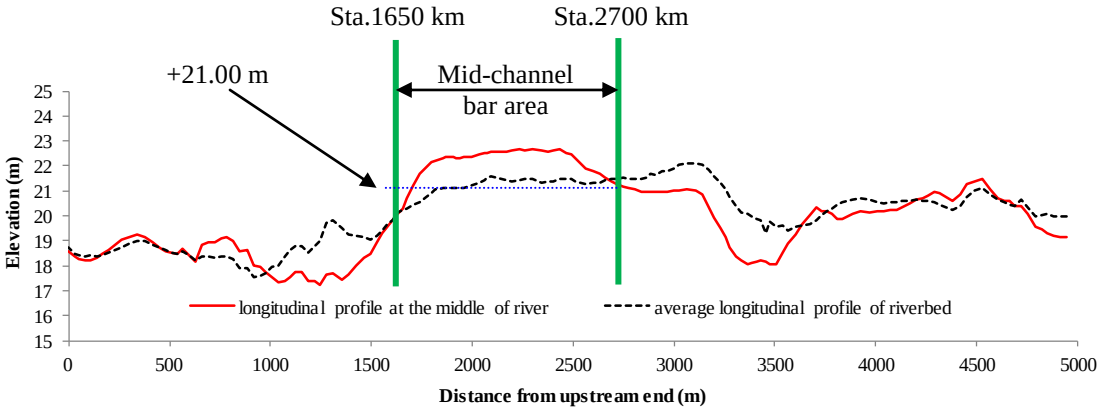

Figure 4.12 Longitudinal profile at the middle line and the average slope of the Sesayap River at Malinau reach

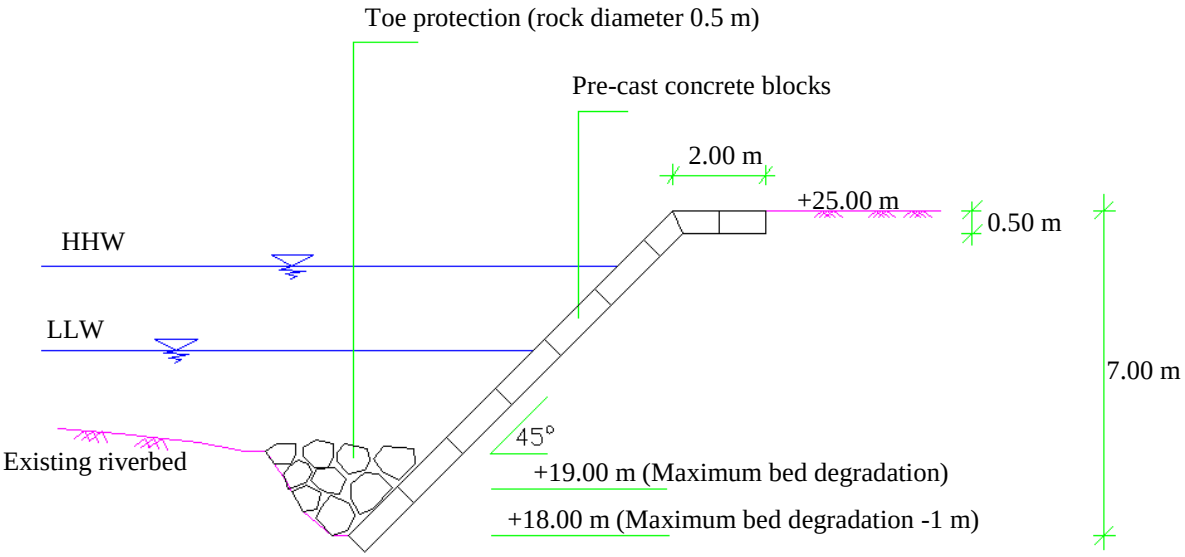

Figure 4.13 The type of revetment structure for bank protection in Sesayap River

4.3.2. Simulation Case

The simulation cases are Case 1a, Case 1d, Case 1e, Case 1h, Case 2a, Case 2d, Case 2e and Case 2h. The bed geometry for each case is explained as follow:

(1) Case 1a is the original condition. The bed geometry of the original condition was measured in 2008. Figure 4.15 (a) shows the bed geometry in Case 1a. Bank material of the upper layer (higher than +22.00m) is composed of cohesive

material and bank material of the lower layer is composed of non-cohesive material.

(2) Case 1d is the simulation considering the dredging of the mid channel bar. The bed material higher than +21.00 m in area "A" (see Figure 4.15 (b)) is removed. The +21.00 m is a level that similar as average slope of the river as shown in Figure 4.12. Bank material of the upper layer (higher than +22.00m) is composed of cohesive material and bank material of the lower layer is composed of non-cohesive material.

(3) Case 2a is the simulation considering the structure of preventing the bank from the erosion. In this case, the revetment is installed along the bank, where the bank was collapsed. Figure 4.15 (a) show s the bed geometry in Case 2a and the dashed blue line in this figure indicates the location of the revetment.

(4) Case 2d is the simulation considering combination methods in Case 1d and Case 2a. Figure 4.15 (b) shows the bed geometry in Case 2d.

(5) Case 1e is the simulation considering the dredging method. In this case, the bed material higher than +20.50 m in area "A" is removed (see Figure 4.16 (a)). The +20.50 m is a level that deeper than average elevation. Bank material of the upper layer (higher than +22.00m) is composed of cohesive material and bank material of the lower layer is composed of non-cohesive material.

(6) Case 1h is the simulation considering the dredging method. In this case, the bed material higher than +19.00 m in area "A" is removed (see Figure 4.16 (b)). This case is performed to discuss the effect the excessive dredging. Bank material of the upper layer (higher than +22.00m) is composed of cohesive material and bank material of the lower layer is composed of non-cohesive material.

(7) Case 2e is the simulation considering method in Case 2a and Case 1e. Figure 4.17 (a) shows the bed geometry in Case 2e.

(8) Case 2h is the simulation considering method in Case 2a and Case 1h. Figure 4.17 (b) shows the bed geometry in Case 2h.

(9) Bank material of both the upper layer and the lower layer is composed of non-cohesive material in Case 3a. The other hydraulic conditions are the same as those in Case 1a.

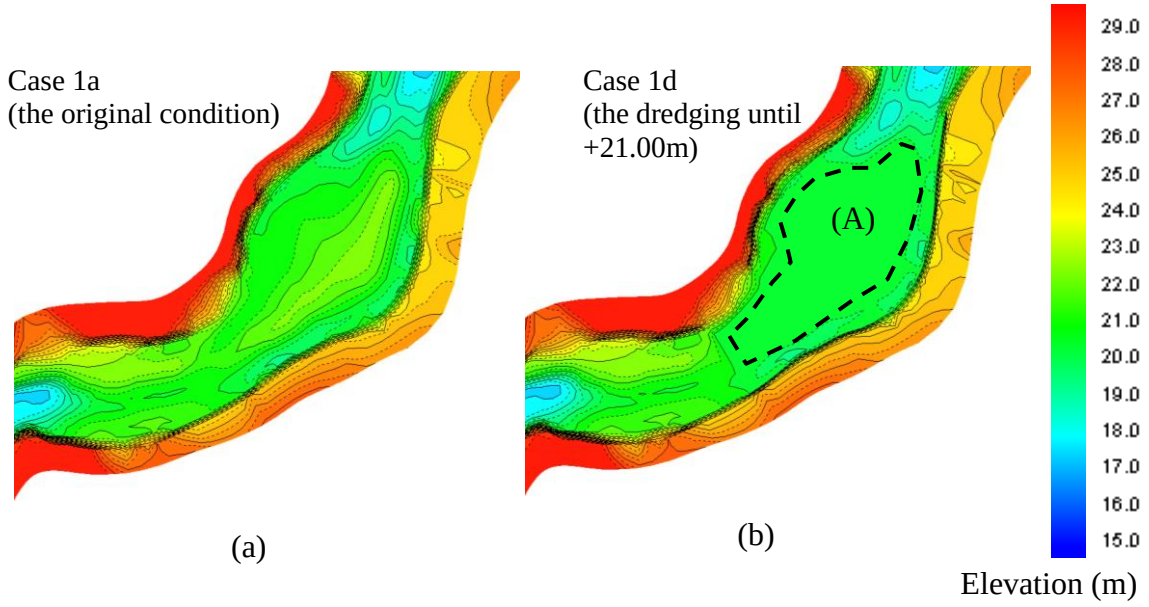

Figure 4. 14 Bed geometry for Case 1a and Case 1d

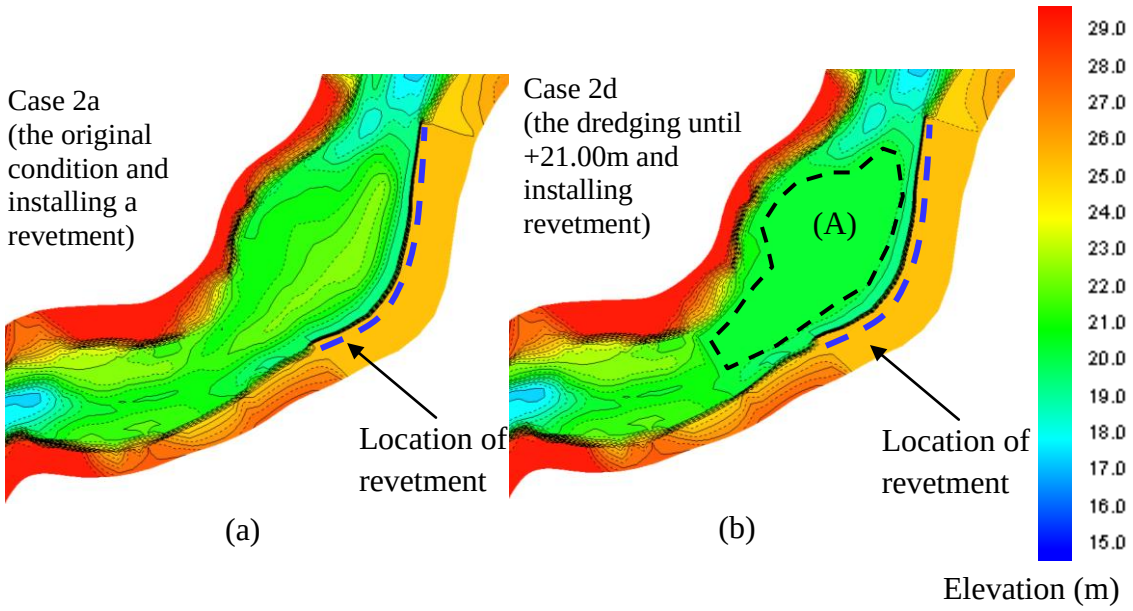

Figure 4.15 Bed geometry for Case 2a and Case 2d

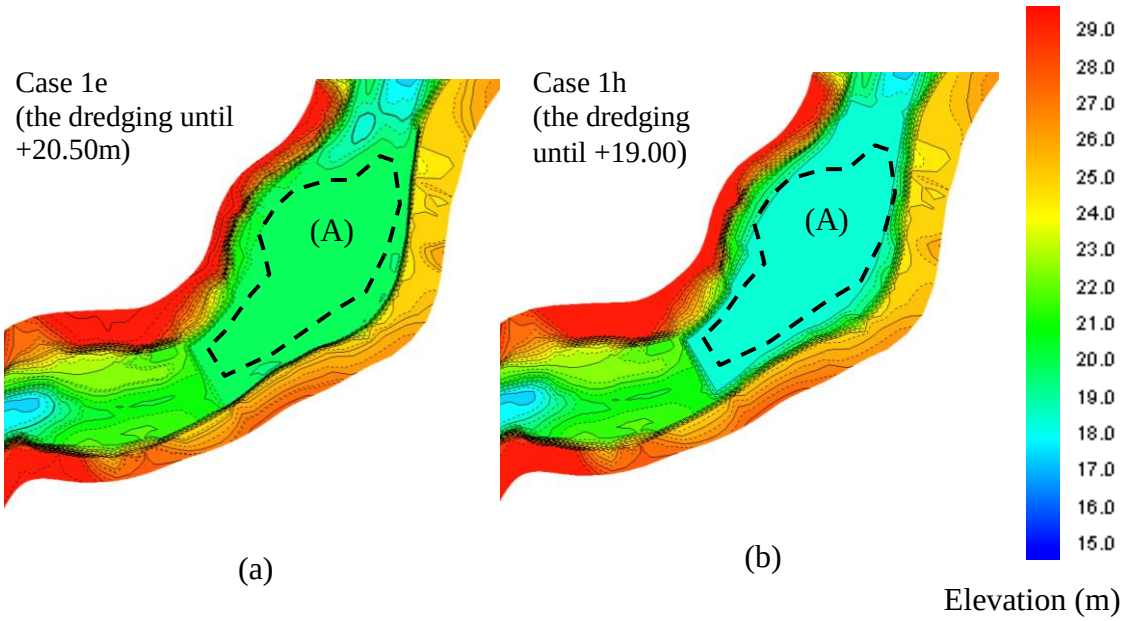

Figure 4.16 Bed geometry for Case 1e and Case 1h

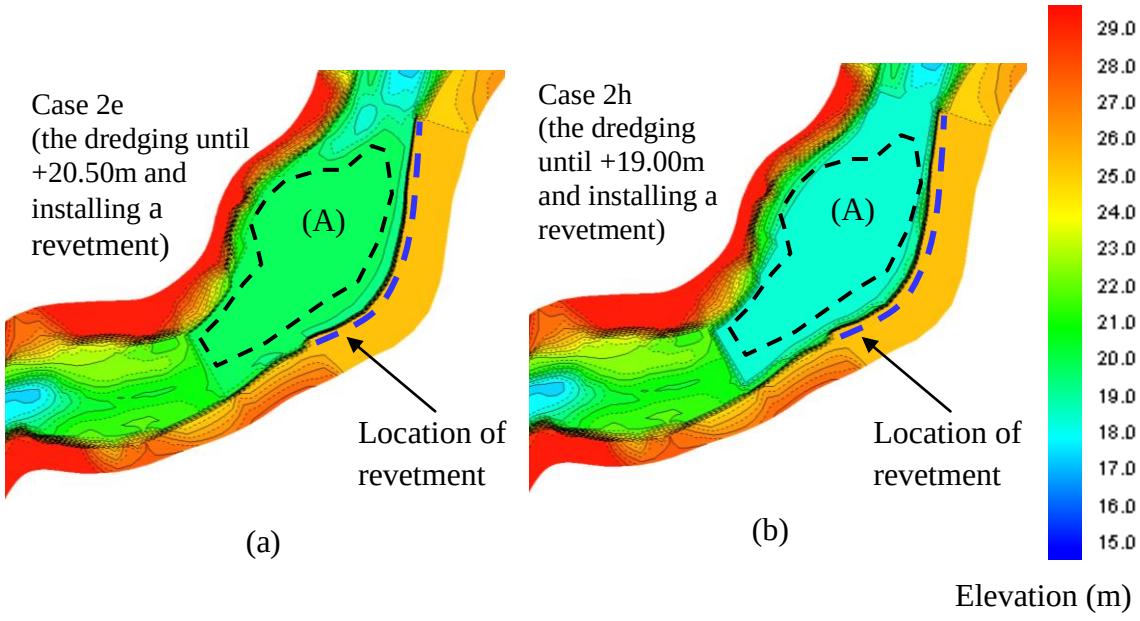

Figure 4.17 Bed geometry for Case 2e and Case 2h

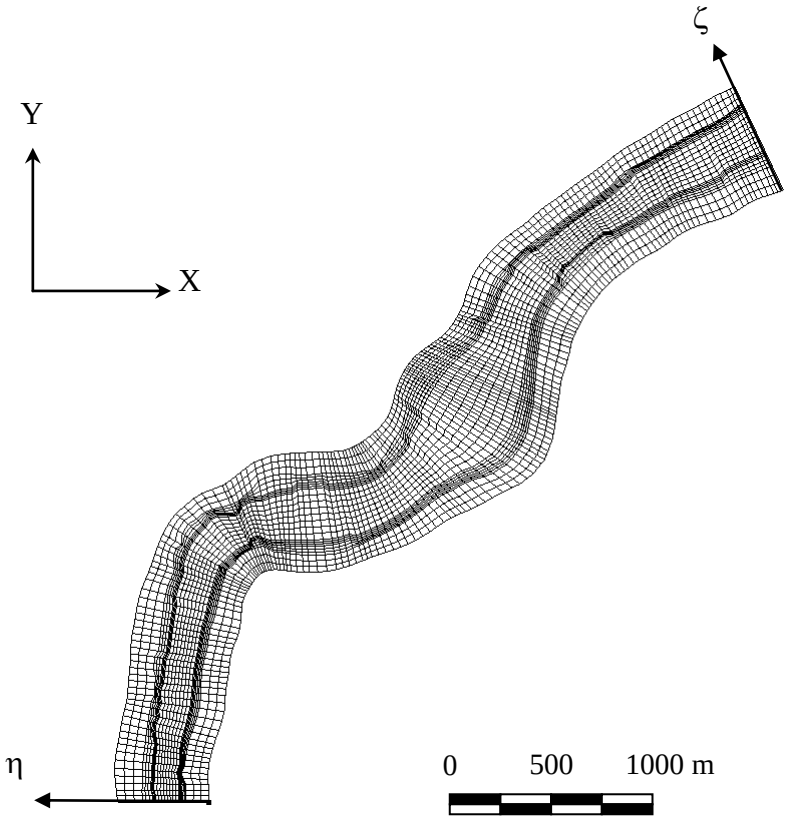

Figure 4.18 Grid for numerical simulation

This research is to understand the hydraulic phenomena, estimate the possibility of bank failure, and make a countermeasure of the bank erosion. As explained in Chapter 1 that bed deformation is one of important parameters on triggering of bank erosion by mass failure process. The numerical simulations are conducted to estimate the bed deformation near the bank toe considering to an existing and countermeasures condition. According to this objective, some cases of numerical simulation were conducted. The simulations are divided into three types. Type 1 is simulation in existing or original condition. Type 2 is simulation with the typical counteract A (dredging method). Type 3 is simulation with typical counteract B (bank protection method). The cases of simulation can be seen in Table 4.3.

Table 4.3 Cases of simulation

Case	Countermeasure	Bank material	Upstream discharge (m^3/s)	Downstream stages condition (m)
1a	No countermeasure	Cohesive+Non-cohesive	434.64	Unsteady
1d	The bed material higher that +21.00 m removed	Cohesive+Non-cohesive	434.64	Unsteady
1e	The bed material higher that +20.50 m removed	Cohesive+Non-cohesive	434.64	Unsteady
1h	The bed material higher that +19.00 m removed	Cohesive+Non-cohesive	434.64	Unsteady
2a	Install a revetment	Cohesive+Non-cohesive	434.64	Unsteady
2d	The bed material higher that +21.00 m removed and install a revetment	Cohesive+Non-cohesive	434.64	Unsteady
2e	The bed material higher that +20.50 m removed and install a revetment	Cohesive+Non-cohesive	434.64	Unsteady
2h	The bed material higher that +19.00 m removed and install a revetment	Cohesive+Non-cohesive	434.64	Unsteady
3a	No countermeasure	Non-cohesive	434.64	Unsteady

4.4. Governing Equations

Numerical simulations are performed using the horizontal two-dimensional flow model which the equations are written in general coordinate system. The model uses the finite difference method to solve the different equations. Relationship between Cartesian coordinate system and General coordinate system is as follows.

$$J = \frac{1}{\left(\frac{\partial x}{\partial \xi}\frac{\partial y}{\partial \eta} - \frac{\partial x}{\partial \eta}\frac{\partial y}{\partial \xi}\right)} \tag{4.1}$$

$$\frac{\partial \xi}{\partial x} = J \frac{\partial y}{\partial \eta} \tag{4.2}$$

$$\frac{\partial \eta}{\partial x} = -J \frac{\partial y}{\partial \xi} \tag{4.3}$$

$$\frac{\partial \xi}{\partial y} = -J \frac{\partial x}{\partial \eta} \tag{4.4}$$

$$\frac{\partial \eta}{\partial y} = J \frac{\partial x}{\partial \xi} \tag{4.5}$$

Where, ξ and η are the coordinates along the longitudinal and the transverse directions in generalized coordinate system, respectively, x and y are the coordinates in Cartesian coordinate system. Computation of surface flow is carried out using the governing equation of the horizontal two-dimensional flow averaged with depth. The conservation of mass, i.e., inflow and outflow of mass by seepage flow, is taken into consideration as shown in the following equation (Takebayashi, 2005).

$$\Lambda \frac{\partial}{\partial t}\left(\frac{z}{J}\right) + \frac{\partial}{\partial \xi}\left(\left(\frac{\partial \xi}{\partial t} + U\right)\frac{h}{J}\right) + \frac{\partial}{\partial \eta}\left(\left(\frac{\partial \eta}{\partial t} + V\right)\frac{h}{J}\right) + \frac{\partial}{\partial \xi}\left(\left(\frac{\partial \xi}{\partial t} + U_g\right)\frac{h_g}{J}\right) + \frac{\partial}{\partial \eta}\left(\left(\frac{\partial \eta}{\partial t} + V_g\right)\frac{h_g}{J}\right) = 0 \tag{4.6}$$

Where, t is the time, z is the water surface level. Surface flow depth is represented as h, seepage flow depth is h_g. U and V represent the contravariant depth averaged flow velocity on bed along ξ and η coordinates, respectively. These velocities are defined as

$$U = \frac{\partial \xi}{\partial x} u + \frac{\partial \xi}{\partial y} v \tag{4.7}$$

$$V = \frac{\partial \eta}{\partial x} u + \frac{\partial \eta}{\partial y} v \tag{4.8}$$

where, u and v represent depth averaged flow velocity on bed along x and y coordinates, respectively. U_g and V_g represent the contravariant depth averaged seepage flow velocity along ξ and η coordinates, respectively. These velocities are defined as

$$U_g = \frac{\partial \xi}{\partial x} u_g + \frac{\partial \xi}{\partial y} v_g \tag{4.9}$$

$$V_g = \frac{\partial \eta}{\partial x} u_g + \frac{\partial \eta}{\partial y} v_g \tag{4.10}$$

where, depth averaged seepage flow velocities along x and y coordinates in Cartesian coordinate system are shown as u_g, v_g, respectively. Λ is a parameter related to the porosity in the soil, wherein $\Lambda = 1$ as $z \gamma z_b$, and $\Lambda = \lambda$ as $z < z_b$, where z_b is the bed

level and λ is the porosity in the soil. Seepage flow is assumed as horizontal two-dimensional saturation flow. Momentum equations of surface water are as follows.

$$\begin{aligned}
&\frac{\partial}{\partial t}\left(\frac{hU}{J}\right)+\frac{\partial}{\partial \xi}\left(\left(\frac{\partial \xi}{\partial t}+U\right)\frac{hU}{J}\right)+\frac{\partial}{\partial \eta}\left(\left(\frac{\partial \eta}{\partial t}+V\right)\frac{hU}{J}\right)\\
&\quad-\frac{hu}{J}\left(\frac{\partial}{\partial t}\left(\frac{\partial \xi}{\partial x}\right)+\left(\frac{\partial \xi}{\partial t}+U\right)\frac{\partial}{\partial \xi}\left(\frac{\partial \xi}{\partial x}\right)+\left(\frac{\partial \eta}{\partial t}+V\right)\frac{\partial}{\partial \eta}\left(\frac{\partial \xi}{\partial x}\right)\right)\\
&\quad-\frac{hv}{J}\left(\frac{\partial}{\partial t}\left(\frac{\partial \xi}{\partial y}\right)+\left(\frac{\partial \xi}{\partial t}+U\right)\frac{\partial}{\partial \xi}\left(\frac{\partial \xi}{\partial y}\right)+\left(\frac{\partial \eta}{\partial t}+V\right)\frac{\partial}{\partial \eta}\left(\frac{\partial \xi}{\partial y}\right)\right)\\
&\quad=-gh\left(\frac{1}{J}\left(\left(\frac{\partial \xi}{\partial x}\right)^2+\left(\frac{\partial \xi}{\partial y}\right)^2\right)\frac{\partial z_s}{\partial \xi}+\frac{1}{J}\left(\frac{\partial \xi}{\partial x}\frac{\partial \eta}{\partial x}+\frac{\partial \xi}{\partial y}\frac{\partial \eta}{\partial y}\right)\frac{\partial z_s}{\partial \eta}\right)-\frac{\tau_{b\xi}}{\rho J}\\
&\qquad+\frac{1}{J}\left(\frac{\partial \xi}{\partial x}\right)^2\frac{\partial}{\partial \xi}\left(h\sigma_{xx}\right)+\frac{1}{J}\frac{\partial \xi}{\partial x}\frac{\partial \eta}{\partial x}\frac{\partial}{\partial \eta}\left(h\sigma_{xx}\right)+\frac{1}{J}\frac{\partial \xi}{\partial y}\frac{\partial \eta}{\partial x}\frac{\partial}{\partial \eta}\left(h\tau_{yx}\right)+\frac{1}{J}\frac{\partial \xi}{\partial y}\frac{\partial \xi}{\partial x}\frac{\partial}{\partial \xi}\left(h\tau_{yx}\right)\\
&\qquad+\frac{1}{J}\frac{\partial \xi}{\partial x}\frac{\partial \eta}{\partial y}\frac{\partial}{\partial \eta}\left(h\tau_{xy}\right)+\frac{1}{J}\frac{\partial \xi}{\partial x}\frac{\partial \xi}{\partial y}\frac{\partial}{\partial \xi}\left(h\tau_{xy}\right)+\frac{1}{J}\left(\frac{\partial \xi}{\partial y}\right)^2\frac{\partial}{\partial \xi}\left(h\sigma_{yy}\right)+\frac{1}{J}\frac{\partial \xi}{\partial y}\frac{\partial \eta}{\partial y}\frac{\partial}{\partial \eta}\left(h\sigma_{yy}\right)
\end{aligned} \tag{4.11}$$

$$\begin{aligned}
&\frac{\partial}{\partial t}\left(\frac{hV}{J}\right)+\frac{\partial}{\partial \xi}\left(\left(\frac{\partial \xi}{\partial t}+U\right)\frac{hV}{J}\right)+\frac{\partial}{\partial \eta}\left(\left(\frac{\partial \eta}{\partial t}+V\right)\frac{hV}{J}\right)\\
&\quad-\frac{hu}{J}\left(\frac{\partial}{\partial t}\left(\frac{\partial \eta}{\partial x}\right)+\left(\frac{\partial \xi}{\partial t}+U\right)\frac{\partial}{\partial \xi}\left(\frac{\partial \eta}{\partial x}\right)+\left(\frac{\partial \eta}{\partial t}+V\right)\frac{\partial}{\partial \eta}\left(\frac{\partial \eta}{\partial x}\right)\right)\\
&\quad-\frac{hv}{J}\left(\frac{\partial}{\partial t}\left(\frac{\partial \eta}{\partial y}\right)+\left(\frac{\partial \xi}{\partial t}+U\right)\frac{\partial}{\partial \xi}\left(\frac{\partial \eta}{\partial y}\right)+\left(\frac{\partial \eta}{\partial t}+V\right)\frac{\partial}{\partial \eta}\left(\frac{\partial \eta}{\partial y}\right)\right)\\
&\quad=-gh\left(\frac{1}{J}\left(\frac{\partial \xi}{\partial x}\frac{\partial \eta}{\partial x}+\frac{\partial \xi}{\partial y}\frac{\partial \eta}{\partial y}\right)\frac{\partial z_s}{\partial \xi}+\frac{1}{J}\left(\left(\frac{\partial \eta}{\partial x}\right)^2+\left(\frac{\partial \eta}{\partial y}\right)^2\right)\frac{\partial z_s}{\partial \eta}\right)-\frac{\tau_{b\eta}}{\rho J}\\
&\qquad+\frac{1}{J}\frac{\partial \eta}{\partial x}\frac{\partial \xi}{\partial x}\frac{\partial}{\partial \xi}\left(h\sigma_{xx}\right)+\frac{1}{J}\left(\frac{\partial \eta}{\partial x}\right)^2\frac{\partial}{\partial \eta}\left(h\sigma_{xx}\right)+\frac{1}{J}\frac{\partial \eta}{\partial y}\frac{\partial \xi}{\partial x}\frac{\partial}{\partial \xi}\left(h\tau_{yx}\right)+\frac{1}{J}\frac{\partial \eta}{\partial y}\frac{\partial \eta}{\partial x}\frac{\partial}{\partial \eta}\left(h\tau_{yx}\right)\\
&\qquad+\frac{1}{J}\frac{\partial \eta}{\partial x}\frac{\partial \xi}{\partial y}\frac{\partial}{\partial \xi}\left(h\tau_{xy}\right)+\frac{1}{J}\frac{\partial \eta}{\partial x}\frac{\partial \eta}{\partial y}\frac{\partial}{\partial \eta}\left(h\tau_{xy}\right)+\frac{1}{J}\frac{\partial \eta}{\partial y}\frac{\partial \xi}{\partial y}\frac{\partial}{\partial \xi}\left(h\sigma_{yy}\right)+\frac{1}{J}\left(\frac{\partial \eta}{\partial y}\right)^2\frac{\partial}{\partial \eta}\left(h\sigma_{yy}\right)
\end{aligned} \tag{4.12}$$

Where, g is the gravity, ρ is the water density. $\tau_{b\xi}$ and $\tau_{b\eta}$ represent the contravariant shear stress along ξ and η coordinates, respectively. These shear stresses are defined as

$$\tau_{b\xi}=\frac{\partial \xi}{\partial x}\tau_{bx}+\frac{\partial \xi}{\partial y}\tau_{by} \tag{4.13}$$

$$\tau_{b\eta}=\frac{\partial \eta}{\partial x}\tau_{bx}+\frac{\partial \eta}{\partial y}\tau_{by} \tag{4.14}$$

where, τ_x and τ_y are the shear stress along x and y coordinates, respectively as follows.

$$\tau_x = \tau_b \frac{u_b}{\sqrt{u_b^2 + v_b^2}} \tag{4.15}$$

$$\tau_y = \tau_b \frac{v_b}{\sqrt{u_b^2 + v_b^2}} \tag{4.16}$$

$$\frac{\tau_b}{\rho} = u_*^2 \tag{4.17}$$

$$u_*^2 = \frac{n_m^2 g}{R^{1/3}}\left(u^2 + v^2\right) \tag{4.18}$$

Where, u_* is the friction velocity, n_m is the Manning's roughness coefficient, R is the hydraulic radius, k_s is the roughness height. u_b and v_b represent velocity near the bed surface along x and y coordinates, respectively. Velocities near the bed are evaluated using curvature radius of streamlines as follows.

$$u_b = u_{bs}\cos\alpha_s - v_{bs}\sin\alpha_s \tag{4.19}$$

$$v_b = u_{bs}\sin\alpha_s + v_{bs}\cos\alpha_s \tag{4.20}$$

$$u_{bs} = 8.5u_* \tag{4.21}$$

$$v_{bs} = -N_* \frac{h}{r} u_{bs} \tag{4.22}$$

Where, $\alpha_s = \arctan(v/u)$, N_* is 7.0 (Engelund, 1974) and r is the curvature radius of stream lines obtained by depth integrated velocity field as follows (Shimizu and Itakura, 1991).

$$\frac{1}{r} = \frac{1}{\left(u^2 + v^2\right)^{3/2}}\left\{u\left(u\frac{\partial v}{\partial x} - v\frac{\partial u}{\partial x}\right) + v\left(u\frac{\partial v}{\partial y} - v\frac{\partial u}{\partial y}\right)\right\} \tag{4.23}$$

σ_{xx}, σ_{yy}, τ_{xy} and τ_{yx} are turbulence stresses as follows.

$$\sigma_{xx} = 2\nu\frac{\partial u}{\partial x} \tag{4.24}$$

$$\sigma_{yy} = 2\nu\frac{\partial v}{\partial y} \tag{4.25}$$

$$\tau_{xy} = \tau_{yx} = \nu\left(\frac{\partial v}{\partial x} + \frac{\partial u}{\partial y}\right) \tag{4.26}$$

$$\nu = \frac{\kappa}{6} u_* h \tag{4.27}$$

Where, ν is the coefficient of kinematics eddy viscosity, κ is the Karman constant, k_t is the depth-averaged turbulence kinetic energy (Takebayashi, 2005).

$$u_g = -k_{gx}\left(\frac{\partial \xi}{\partial x}\frac{\partial z_b}{\partial \xi} + \frac{\partial \eta}{\partial x}\frac{\partial z_b}{\partial \eta}\right) \tag{4.28}$$

$$v_g = -k_{gy}\left(\frac{\partial \xi}{\partial y}\frac{\partial z_b}{\partial \xi} + \frac{\partial \eta}{\partial y}\frac{\partial z_b}{\partial \eta}\right) \tag{4.29}$$

Where, k_{gx} and k_{gy} is the coefficient of permeability along the longitudinal and the transverse directions, respectively. When the water depth of surface flow becomes less than the mean diameter of the bed material, the surface flow is computed only in consideration of the pressure term and bed shear stress term in the momentum equation of surface flow (Nagata, 1999).

Grain size distribution is evaluated using the sediment transport multilayer model as follows (Takebayashi, *et al*,. 2003):

$$\begin{aligned}&\frac{\partial}{\partial t}\left(\frac{c_b E_b f_{bk}}{J}\right) + (1-\lambda) F_{bk}\frac{\partial}{\partial t}\left(\frac{z_b}{J}\right) \\ &\quad + \left(\frac{\partial}{\partial \xi}\left(\frac{\partial \xi}{\partial t}\frac{c_b E_b f_{bk} r_b}{J} + \frac{q_{b\xi k}}{J}\right) + \frac{\partial}{\partial \eta}\left(\frac{\partial \eta}{\partial t}\frac{c_b E_b f_{bk} r_b}{J} + \frac{q_{b\eta k}}{J}\right)\right) = 0\end{aligned} \tag{4.30}$$

$$\begin{cases} F_{bk} = f_{d1k}, \ \partial z_b/\partial t \le 0 \\ F_{bk} = f_{bk}, \ \partial z_b/\partial t \ge 0 \end{cases}$$

$$\frac{\partial}{\partial t}\left(\frac{E_{d1} f_{d1k}}{J}\right) - F_{dk}\frac{\partial}{\partial t}\left(\frac{E_{d1}}{J}\right) = 0 \qquad \begin{cases} F_{dk} = f_{d1k}, \ \partial z_b/\partial t \le 0 \\ F_{dk} = f_{bk}, \ \partial z_b/\partial t \ge 0 \end{cases} \tag{4.31}$$

In the formulae above, fbk is the concentration of bed load of size class k in the bed load layer, fdmk is the sediment concentration of size class k in the mth bed layer, cb is the depth-averaged concentration of bed load. Ebe is the equilibrium bed load layer thickness; it is estimated by the following equation (Egashira and Ashida, 1992):

$$\frac{E_{be}}{d_m} = \frac{1}{c_b \cos\theta(\tan\phi - \tan\theta)}\tau_{*m} \tag{4.32}$$

where d_m is the mean diameter of bed load, ϕ is the angle of repose, and τ_{*m} is the non-dimensional shear stress of mean diameter. E_{sd} is the sediment layer thickness on cohesive sediment bed. E_b is the bed load layer thickness, $q_{b\xi k}$ and $q_{b\eta k}$ are the bed load

of size class k in ξ and η directions, respectively, q_{bxk} and q_{byk} are the bed load of size class k in x and y directions, respectively as follows (Ashida and Michiue, 1972; Kovacs and Parker, 1994 and Liu, 1991).

$$q_{bxk} = q_{bk}\cos\beta_k \tag{4.33}$$

$$q_{byk} = q_{bk}\sin\beta_k \tag{4.34}$$

$$q_{bk} = 17\frac{\rho u_{*e}^3}{(\rho_s-\rho)g}\left(1-\sqrt{K_c}\frac{u_{*ck}}{u_*}\right)\left(1-K_c\frac{u_{*ck}^2}{u_*^2}\right)f_{bk} \tag{4.35}$$

Therein, ρ_s is the sediment density, u_{*e} is the effective shear velocity, the non-dimensional critical friction velocity of size class k is evaluated as follows (Ashida and Michiue, 1972).

$$u_{*ck}^2 = u_{*cm}^2\left[\frac{\log_{10}19}{\log_{10}(19d_k/d_m)}\right]^2\frac{d_k}{d_m} \qquad d_k/d_m \geq 0.4 \tag{4.36}$$

$$u_{*ck}^2 = 0.85u_{*cm}^2 \qquad d_k/d_m \leq 0.4 \tag{4.37}$$

Iwagaki's formula (Iwagaki, 1956) which is formulated for uniform bed material is used for evaluating u_{*cm}. K_c is the correction factor due to the influence of bed inclination on sediment motion.

$$K_c = 1+\frac{1}{\mu_s}\left[\left(\frac{\rho}{\rho_s-\rho}+1\right)\cos\alpha\tan\theta_x+\sin\alpha\tan\theta_y\right] \tag{4.38}$$

where α is the angle of deviation of near-bed flow from the x direction as follows.

$$\alpha = \arctan\left(\frac{v_b}{u_b}\right) \tag{4.39}$$

μ_s is the coefficient of static friction. θ_x and θ_y are bed inclinations in x and y directions, respectively. These inclinations are evaluated as follows,

$$\theta_x = \arctan\left(\frac{\partial\xi}{\partial x}\frac{\partial z_b}{\partial\xi}+\frac{\partial\eta}{\partial x}\frac{\partial z_b}{\partial\eta}\right) \tag{4.40}$$

$$\theta_y = \arctan\left(\frac{\partial\xi}{\partial y}\frac{\partial z_b}{\partial\xi}+\frac{\partial\eta}{\partial y}\frac{\partial z_b}{\partial\eta}\right) \tag{4.41}$$

Hence, the local bed slope along direction of bed load of sediment mean diameter (θ) is obtained as follows.

$$\sin\theta = \cos\beta_m\sin\theta_x+\sin\beta_m\sin\theta_y \tag{4.42}$$

where β_m is the deviation angle of bed load of mean diameter to the x direction. The deviation angle of bed load of size class k to the x direction (β_k), which depends on the flow near bed and inclination of the bed, is calculated by the following relation.

$$\tan\beta_k = \frac{\sin\alpha - \Pi\Theta_y\left(\frac{u_{*ck}^2}{u_*^2}\right)\tan\theta_y}{\cos\alpha - \Pi\Theta_x\left(\frac{u_{*ck}^2}{u_*^2}\right)\tan\theta_x} \tag{4.43}$$

$$\Pi = K_{ld} + 1/\mu_s \tag{4.44}$$

$$\Theta_y = \frac{1}{1+\tan^2\theta_x+\tan^2\theta_y} \tag{4.45}$$

$$\Theta_x = \Theta_y + \frac{\rho}{\rho_s-\rho}\cos^2\theta_x \tag{4.46}$$

Evolution of bed elevation is estimated by means of the following formulae.

$$\frac{\partial}{\partial t}\left(\frac{c_b E_b}{J}\right)+(1-\lambda)\frac{\partial}{\partial t}\left(\frac{z_b}{J}\right)+\left(\frac{\partial}{\partial\xi}\left(\frac{\partial\xi}{\partial t}\frac{c_b E_b}{J}+\sum_{k=1}^{n}\frac{q_{b\xi k}}{J}\right)+\frac{\partial}{\partial\eta}\left(\frac{\partial\eta}{\partial t}\frac{c_b E_b}{J}+\sum_{k=1}^{n}\frac{q_{b\eta k}}{J}\right)\right)=0 \tag{4.47}$$

In them, n represents the number of the size class of sediment.

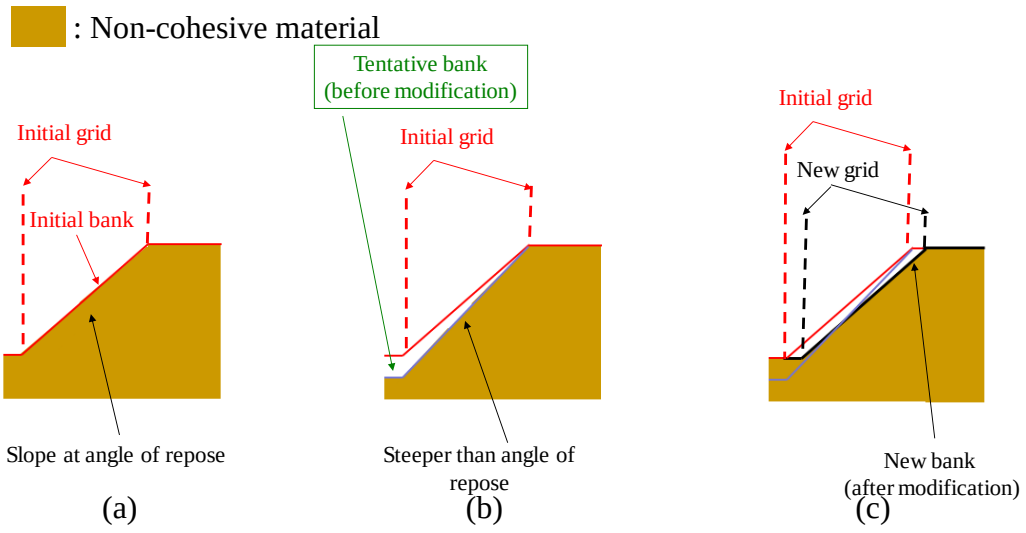

Figure 4.19 Conceptual diagram of bank erosion model in case the bank composed of the non-cohesive material only

Figure 4.19 shows the conceptual diagram of bank erosion model in case the bank composed the non-cohesive material. When bank is composed of non-cohesive material and bed near bank is eroded (see Figure 4.19 (a)), bank line is shifted as

keeping the slope geometry at the angle of repose (see Figure 4.19 (c)). The location of numerical grids will be shifted as shown in Figure 4.19 (c). When bank is composed of cohesive material, bank line is shifted at the speed of erosion velocity of the cohesive material. The conceptual diagram of bank erosion model is shown in Figure 4.20.

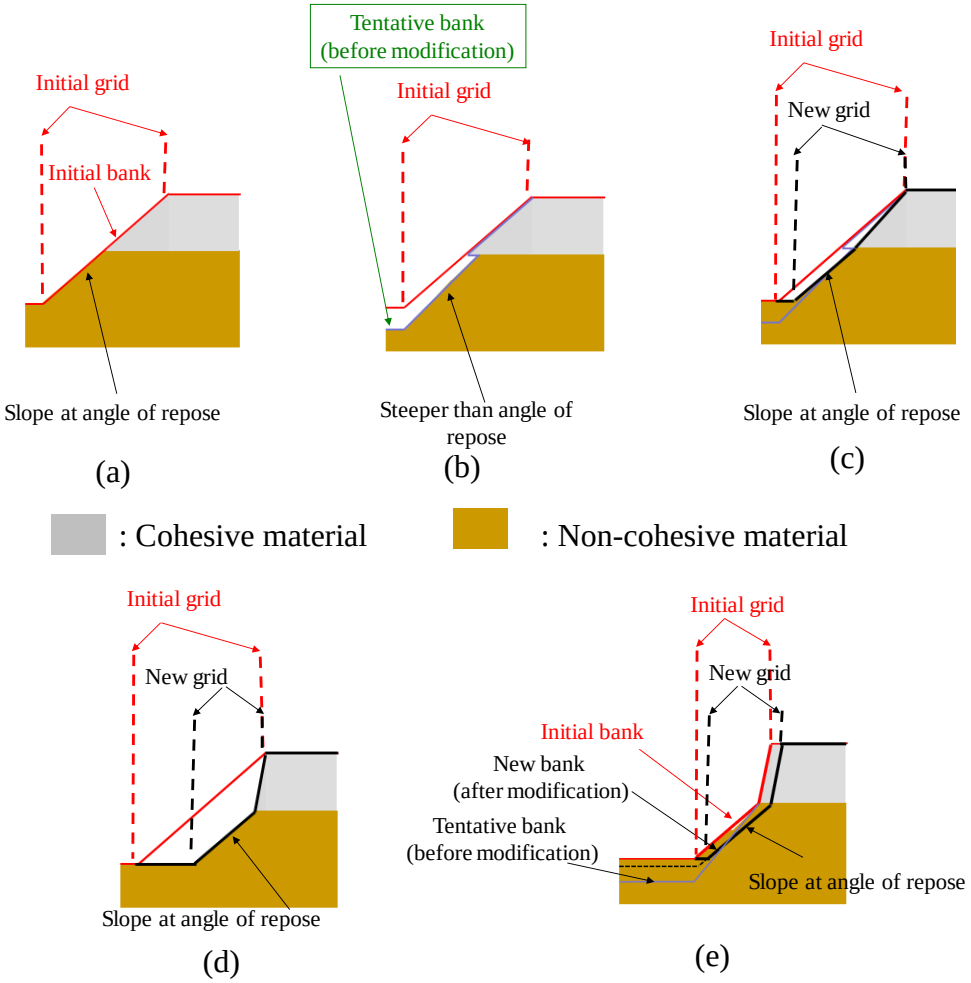

Figure 4.20 Conceptual diagram of bank erosion model in case the bank composed of cohesive material on the top layer and the non-cohesive material at the bottom layer

The erosion velocity of cohesive sediment (V_e) is estimated as follows (Sekine et al, 2003).

$$V_e = \alpha_c R_{wc}^{2.5} u_*^3 \tag{4.48}$$

where, α_c is the coefficient related on kinds of cohesive sediment, R_{wc} is the water content rate. When bank material is composed of cohesive material, the bed degradation near bank does not affect on the bank erosion. When bank material is composed of both

non-cohesive material and cohesive material, the treatment of the bank erosion becomes more complex. In this research, the bank which has the upper bank layer composed of cohesive material and the lower bank layer with non-cohesive material, as shown in Figure 4.20, is treated. When the water level near the bank is lower than the bottom level of cohesive material layer, the lower part of bank is composed of non-cohesive material. Hence, the bank erosion process is the same as Figure 4.20 (a) to (d) at the beginner time and after the long time the process is the same as Figure 4.20 (d) to (e). The bank composed of non-cohesive material forms the slope at the angle of repose. Hence, the cohesive layer will be overhanged because of the erosion of lower layer composed of non-cohesive material and it is assumed here that the overhanged cohesive material is collapsed immediately. When the water surface level near the bank is higher than the bottom level of cohesive material layer, the bank erosion process is determined by the erosion of the cohesive material on the top layer. The non-cohesive material at the bottom layer is eroded considering the repose angle with the starting point is the bottom of the cohesive layer. The bank shape is the same as Figure 4.20 (e).

4.5. Results and Discussions

4.5.1. Channel Geometry

The effect of the cohesive characteristics of bank material on the channel geometry is discussed here. Furthermore, the effects of the dredging and installing revetment will be discussed considering on the erosion rate at the bank toe. Figure 4.21 shows the channel geometry at 48h in Case 1a, Case 1d, Case 2a, Case 2d and Case 3a, respectively. Figure 4.22 to Figure 4.26 are the cross section at C1 (see Figure 4.27 to Figure 4.30) for Case 1a, Case 1d, Case 2a Case 2d and Case 3a, respectively. The maximum erosion near the right bank toe for Case 1a, Case 1d, Case 2a and Case 2d as shown in Table 4.4.

In Case 1a, the bed near the bank toe (at right bank) was eroded well. The erosion depth in Case 1a is deeper than that in Case 3a, because the upper bank has the high surface slope in Case 1a and flow tends to be concentrated near the bank. The transvers erosion width of the bank line in Case 1a and Case 3a is about 12m and 32m,

respectively. The cohesive characteristics and the high surface slope of the upper layer course the difference. This result indicates that the cohesive characteristics of the material in banks must be considered, when the bank erosion process is reproduced by mathematical models.

As shown in the results of Case 1d, the bed degradation is reduced significantly by the dredging of the mid channel bar. The dredging of the bar reduces the concentration of the flow along the right bank and suppress the bed degradation and the bank erosion along the right bank.

The bed degradations occur very much in Case 2a in spite of the installation of revetment. Its means that after installing the revetment, the bed degradations near the bank toe still occurs, and will affect on the stability of the structure. This condition is similar with Case 1a. By considering the cost of the structure of revetment, it seems that this structure is not necessary.

Table 4.4 Elevation near the right bank toe

Case	Elevation (m)
Case 1a	+17.88
Case 1d	+20.03
Case 2a	+17.97
Case 2d	+19.97
Case 3a	+18.88

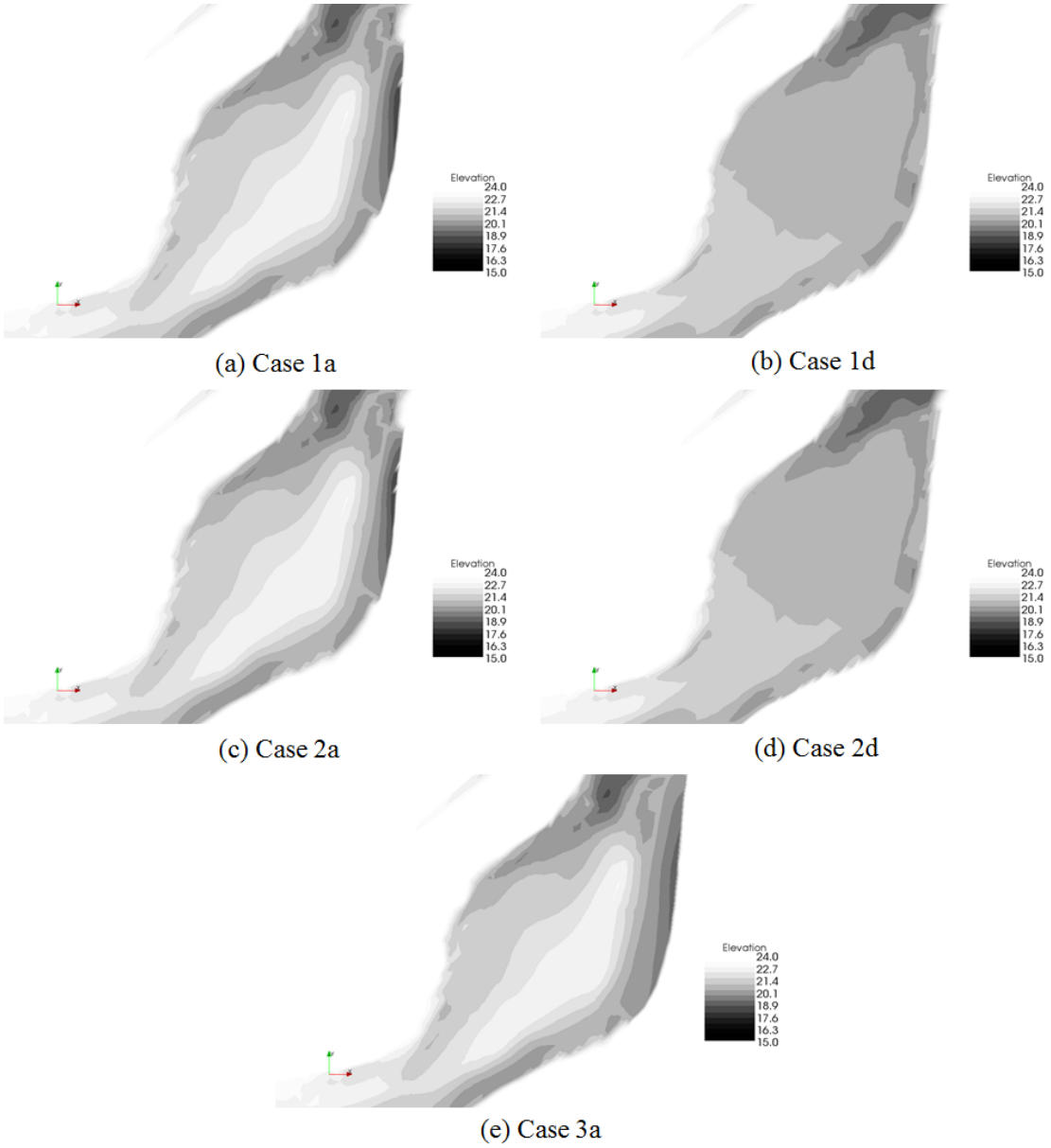

(a) Case 1a

(b) Case 1d

(c) Case 2a

(d) Case 2d

(e) Case 3a

Figure 4.21Bed geometry at 48h in Case 1a, Case 1d, Case 2a, Case 2d and Case 3a

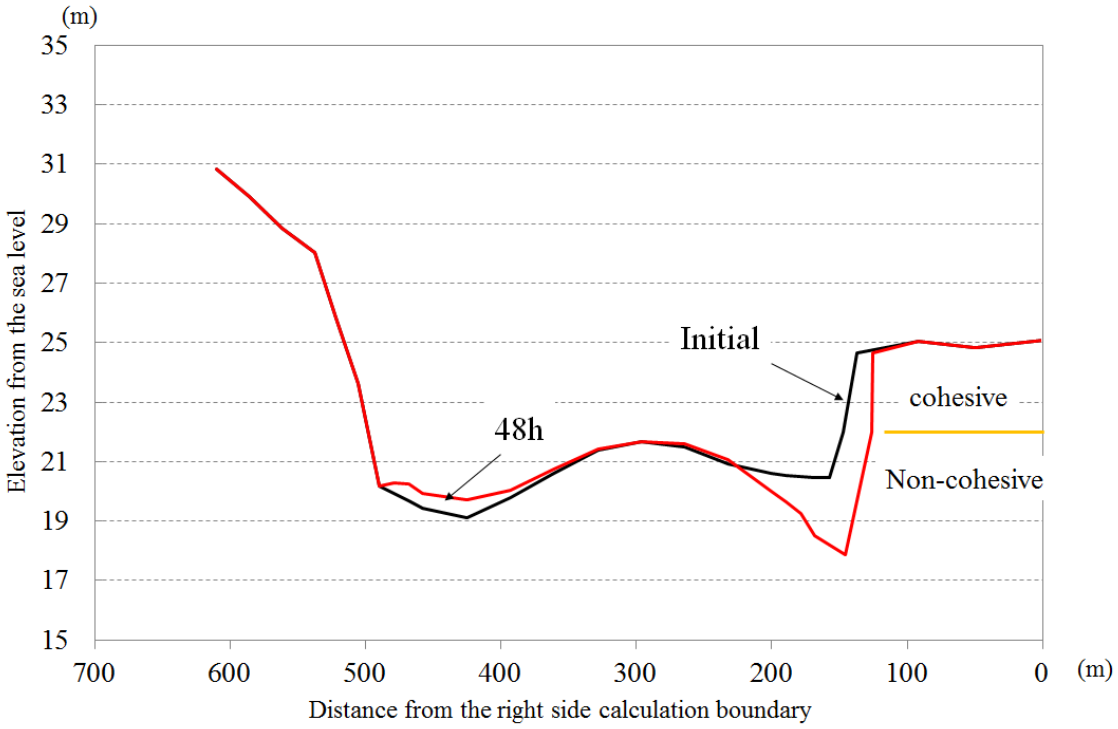

Figure 4.22 The temporal cross sectional change at the downstream of the bar (cross section C1) in Case 1a

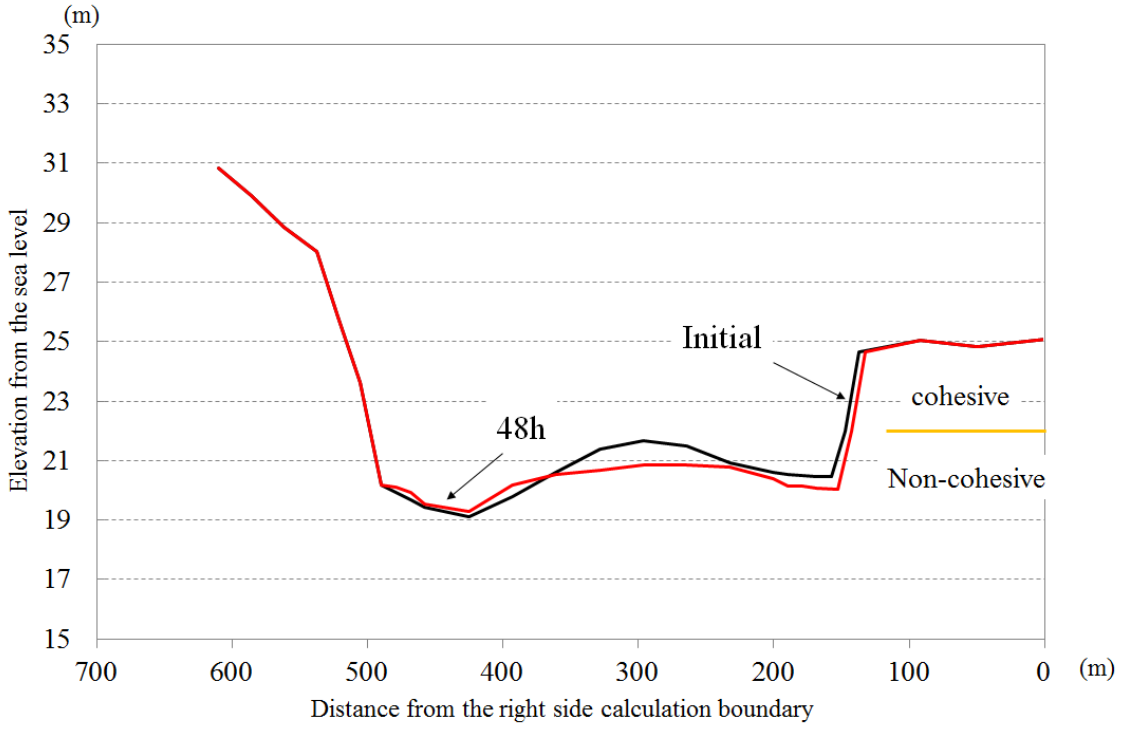

Figure 4.23 The temporal cross sectional change at the downstream of the bar (cross section C1) in Case 1d

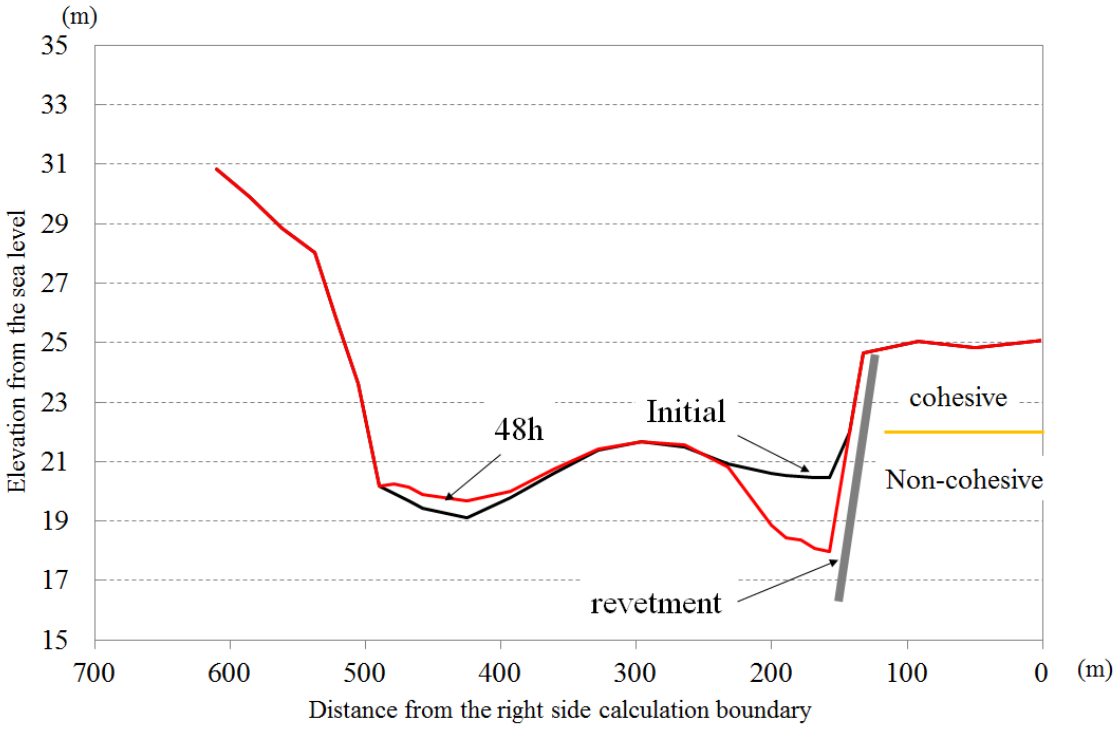

Figure 4.24 The temporal cross sectional change at the downstream of the bar (cross section C1) in Case 2a

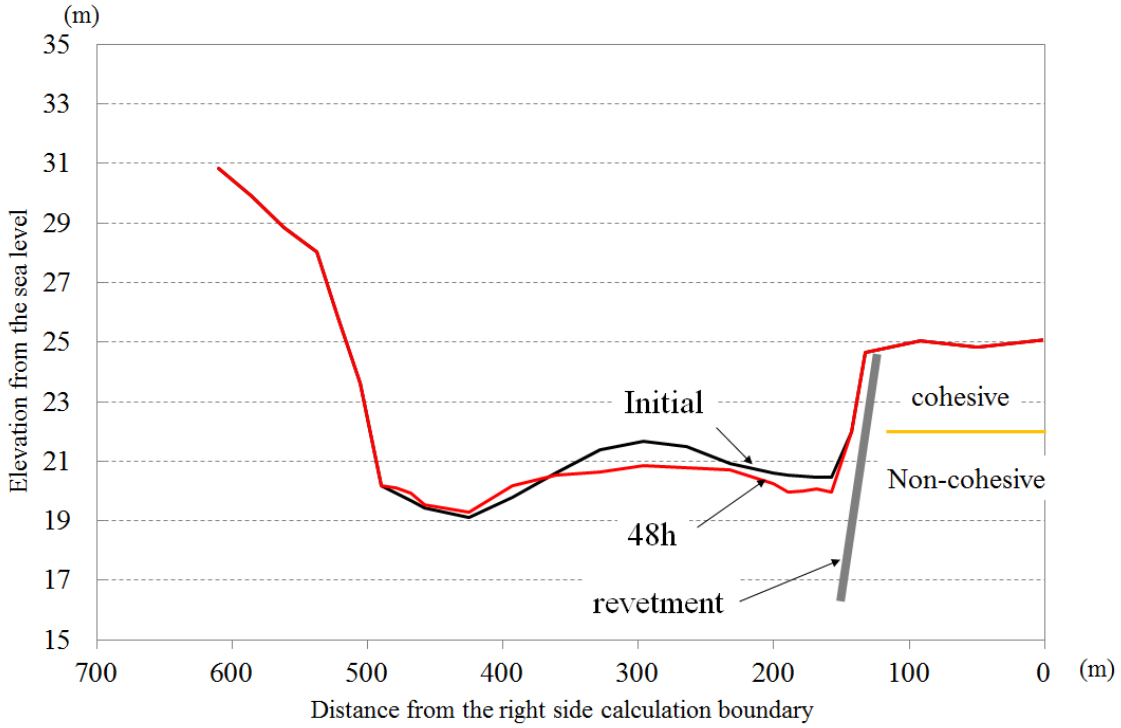

Figure 4.25 The temporal cross sectional change at the downstream of the bar (cross section C1) in Case 2d

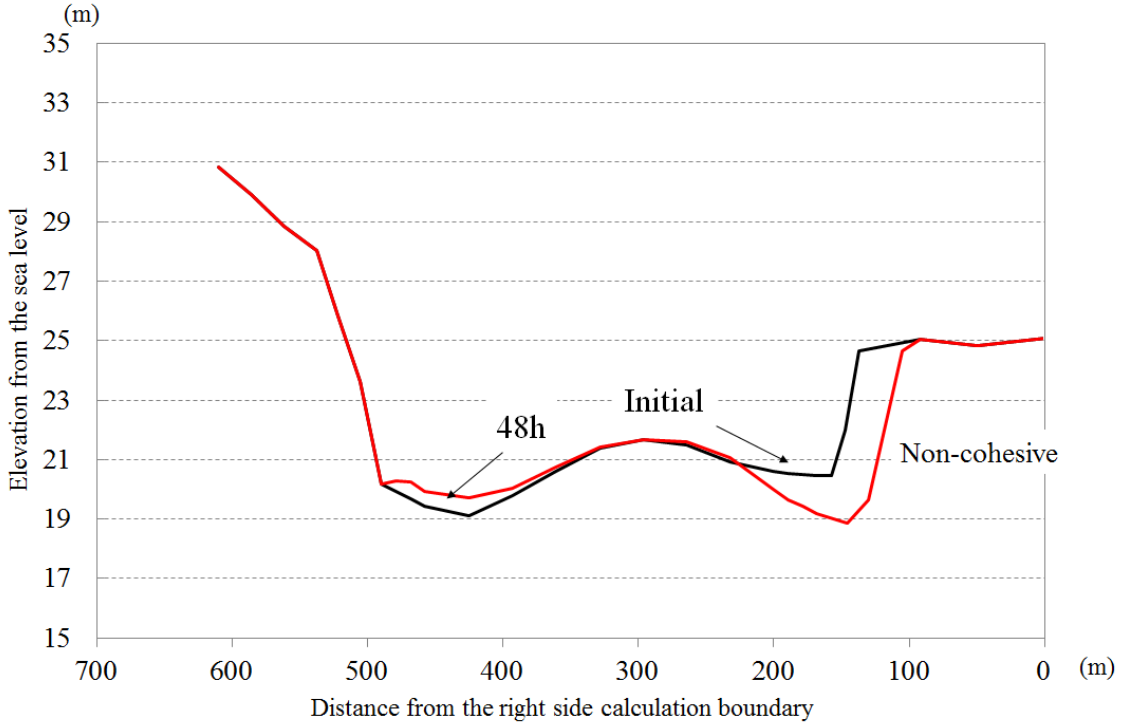

Figure 4.26 The temporal cross sectional change at the downstream of the bar (cross section C1) in Case 3a

4.5.2. Flow Pattern

Figure 4.27 to Figure 4.30 show the horizontal distributions of velocity vector under the lowest low water (LLW) condition at the downstream area before the bank erosion. The small size of the vector indicates the low velocity and the big size indicates the high velocity. The effect of the excessive dredging method is presented in Figure 4.31 and Figure 4.32.

In Case 1a (see Figure 4.27), the flow divided into two parts by the presence of the mid channel bar and produce high and convergence velocity at lee area (the downstream of the bar which is indicated by the blue circle). This may become a strong reason that bank erosion occurred there. The bank erosion in Sesayap River as shown in Photo 4.1 (b) is located in this area. However, after the mid channel bar was dredged (see Figure 4.28), the flow velocity in this area decreases significantly. This means that the dredging method can control the flow velocity near the bank. In case a countermeasure only installing a revetment as shown in Figure 4.29, the flow velocity around the downstream of the bar still has high magnitude. And also tend to increase the

velocity at opposite side as indicated by red circle. In this area, the flow velocity will decrease significantly after the dredging of the mid channel bar (see Figure 4.30). These results show that the horizontal distribution of velocity on Case 1d and Case 2d are similar. According to the horizontal distribution of flow velocity, the revetment seems unnecessary for a countermeasure of the bank erosion problem in this river each.

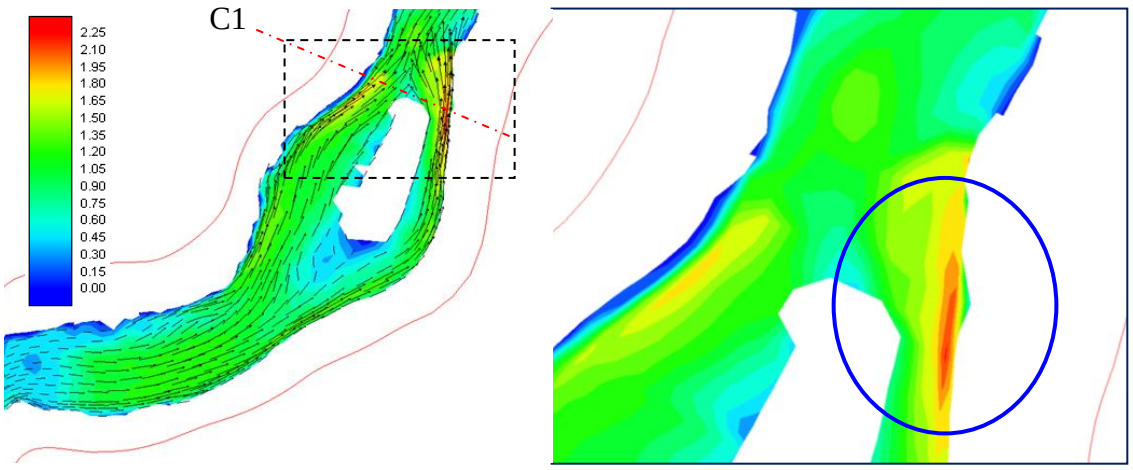

Figure 4.27 Horizontal distribution of velocity vector and detailed velocity contour around the downstream of the bar in Case 1a

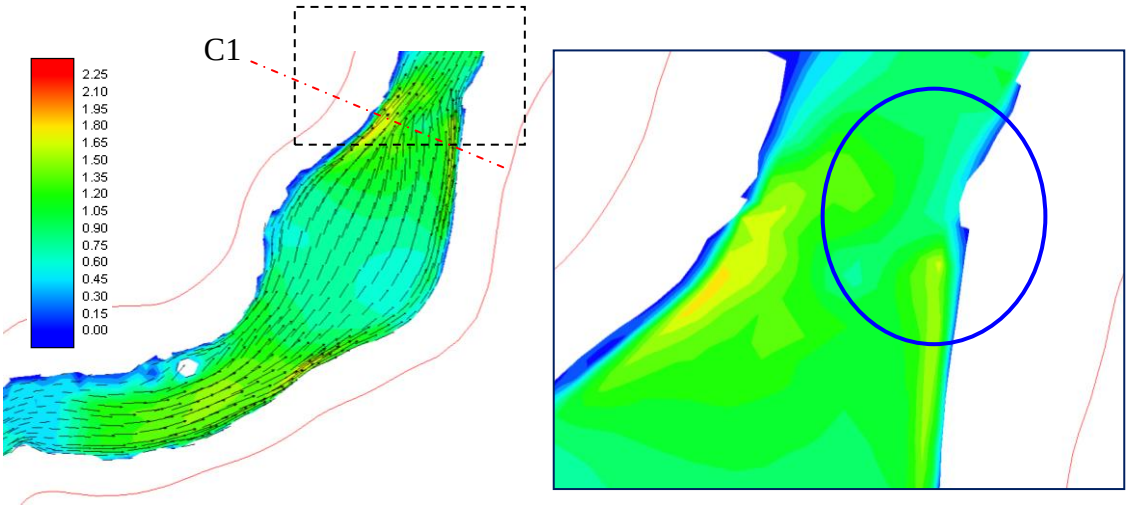

Figure 4.28 Horizontal distribution of velocity vector and detailed velocity contour around the downstream of the bar in Case 1d

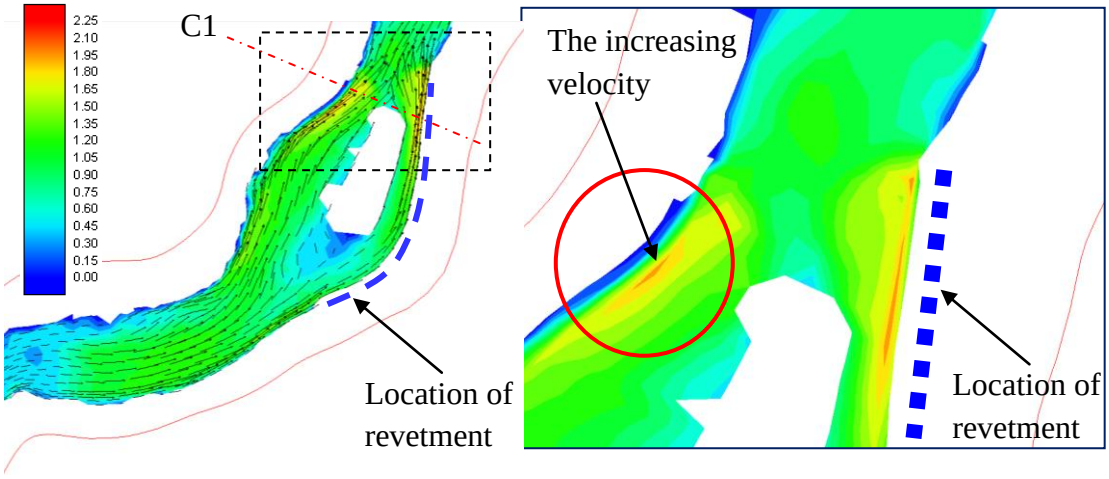

Figure 4.29 Horizontal distribution of velocity vector and detailed velocity contour around the downstream of the bar in Case 2a

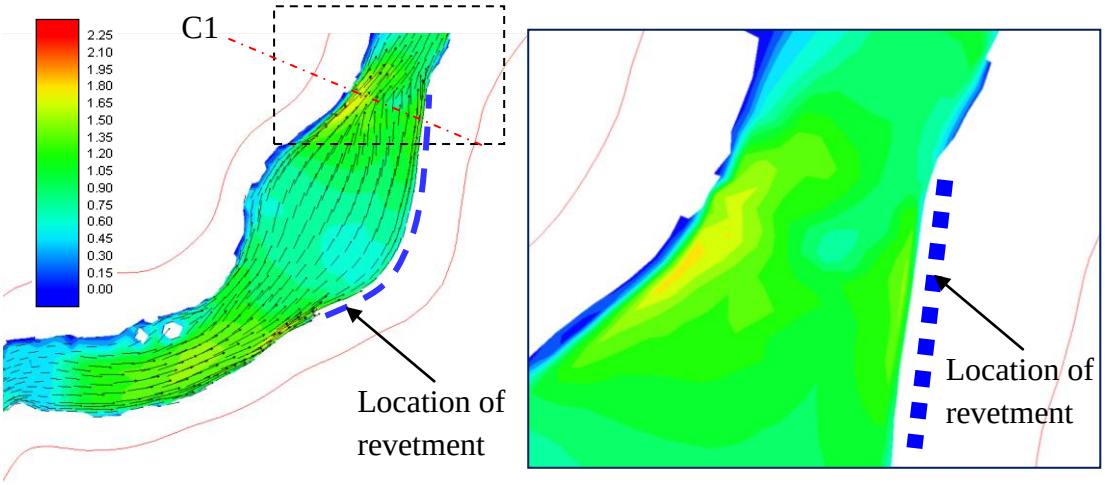

Figure 4.30 Horizontal distribution of velocity vector and detailed velocity contour around the downstream of the bar in Case 2d

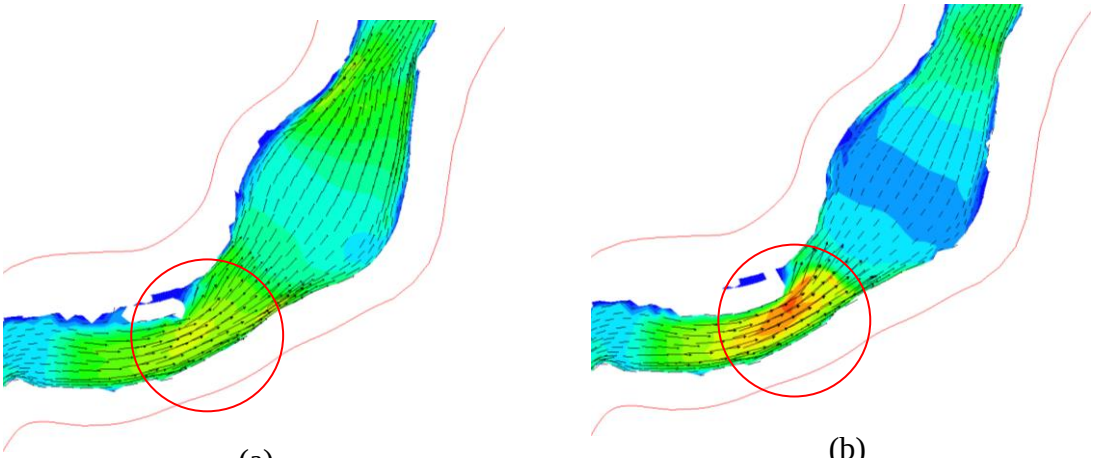

(a) (b)

Figure 4.31Horizontal distribution of velocity vector in Case 1e and Case 1h

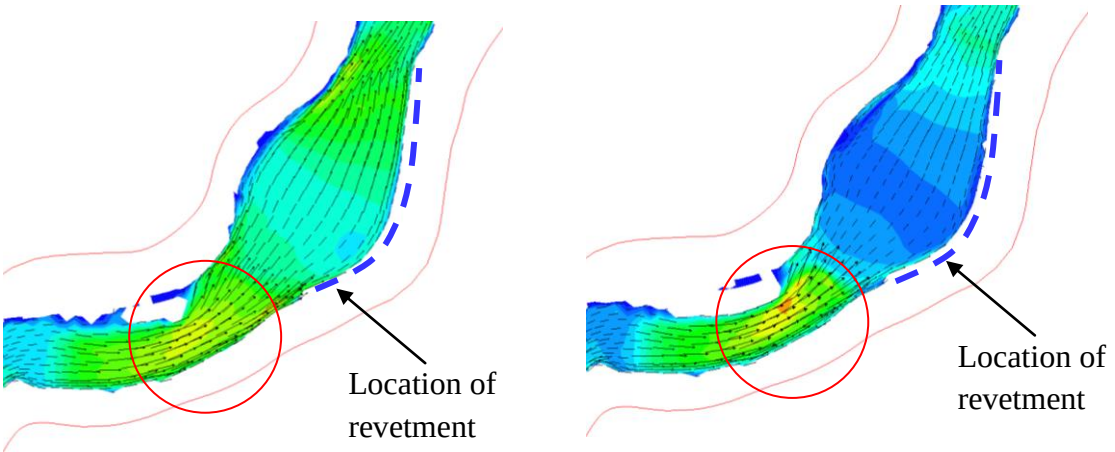

(a) (b)

Figure 4.32 Horizontal distribution of velocity vector in Case 2e and Case 2h

Figure 4.31 shows the horizontal distribution of velocity vector in Case 1e and Case 1h. The excessive dredging increases the flow velocity at the upstream of the dredging area (indicated by red circle). This condition also occurs in Case 2e and Case 2h. It means that the dredging method should consider the level of the dredging area.

4.5.3. Cost Analysis

To discuss the effectiveness of the countermeasure method, the cost analyses are also developed in this study. In Indonesia, the BOW (*Burgelijke van Openbare*

Werken) analysis is a common method for predicting the cost of the project work. The method requires the volume of work, the type of work and the unit price of work.

Dredging Work

In this work, the volume of mid-channel bar is needed. Table 4.5 and Figure 4.33 show the relationship between elevation and volume of mid-channel bar in Sesayap River at Malinau reach. The dredging method in this work is designed to remove the material of mid-channel bar until +21.00 m. This level is the same as the average level of the river (see Figure 4.12). The volume of mid-channel bar until this elevation is around 143.000 m^3. Table 4.6 to Table 4.9 shows the calculation of the cost in dredging work. The estimated cost for dredging mid-channel bar until elevation +21.00 is around 230 million rupiah.

Table 4.5 Relationship between elevation and volume of mid-channel bar in Sesayap River at Malinau reach

Elevasi (m)	Volume (m^3)
20	390000
20.5	250000
21	143000
21.5	50000
22	10000
22.5	5000

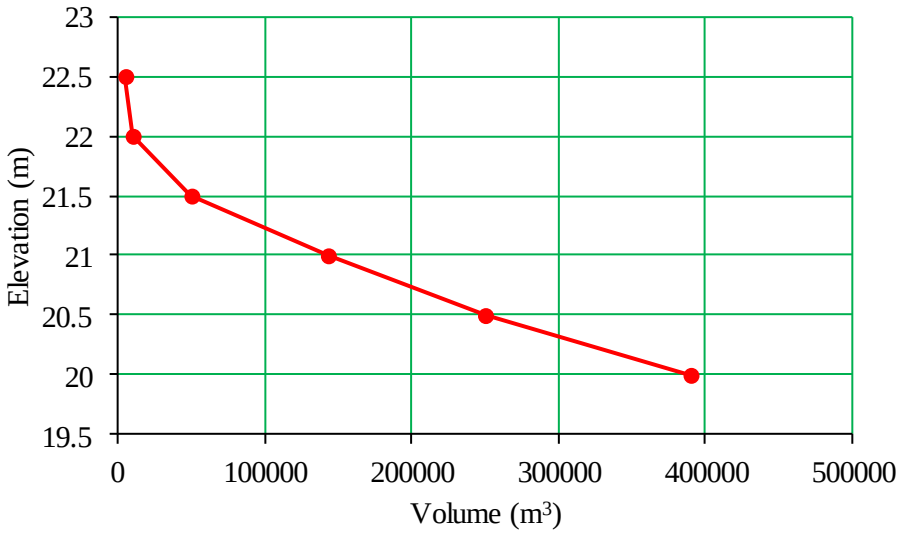

Figure 4.33 Relationship between elevation and volume of mid-channel bar in Sesayap River at Malinau reach

Table 4.6 The calculation of total cost index in measurement work

No	Work description	Unit	Index	Unit cost	Cost index
1	Engineer	day	1	Rp 50,000.00	Rp 50,000.00
2	Worker	day	1	Rp 30,000.00	Rp 30,000.00
4	GPS Sounding	day	1	Rp 15,000.00	Rp 15,000.00
				Total cost index	Rp 95,000.00

Table 4.7 The calculation of total cost index in dredging work

No	Work description	Unit	Index	Unit cost	Cost index
1	Engineer	day	2	Rp 50,000.00	Rp 100,000.00
2	Supervisor	day	2	Rp 40,000.00	Rp 80,000.00
3	Worker	day	1.5	Rp 30,000.00	Rp 45,000.00
4	Excavator driver	day	1	Rp 40,000.00	Rp 40,000.00
5	Excavator technician	day	1	Rp 35,000.00	Rp 35,000.00
				Total cost index	Rp 300,000.00

Table 4.8 The calculation of total cost index in the movement of mid-channel bar material to designed place

No	Work description	Unit	Index	Unit cost	Cost index
1	Ship driver	day	1	Rp 40,000.00	Rp 40,000.00
2	Ship technician	hour	1	Rp 298,269.60	Rp 298,269.60
3	Excavator	hour	1	Rp 298,269.60	Rp 298,269.60
4	Crane	hour	1	Rp 132,000.00	Rp 132,000.00
5	Dump truck	hour	1	Rp 135,000.00	Rp 135,000.00
				Total cost index	Rp 903,539.20

Table 4.9 The estimated cost in dredging work

No.	Type of work	Unit price	Unit	Volume	Unit		Cost (Rupiah)
1	Measurement of area	95000	Rp/m^2	600000	m^2	Rp	57,000,000,000.00
2	Dredging the mid-channel bar	300000	Rp/m^3	143000	m^3	Rp	42,900,000,000.00
3	Removal of the dredged mateial	903539	Rp/m^3	143000	m^3	Rp	129,206,105,600.00
				Total price		Rp	229,106,105,600.00

Revetment Work

The revetment structure is shown in Figure 4.13. This structure consists of two main elements structure. First structure is the toe protection which is made of the rock as the main material. This structure is used for protecting the erosion near the bank toe.

Second structure is the bank protection structure which the pre-cast concrete block as the main structure. The depth of the revetment under the bed is designed at elevation +18.00 m. This number is calculated by considering the deepest of the bed degradation. And then add by 1 m as a safety number. Total length of revetment is 988 m. Table 4.10 to Table 4.15 shows the calculation of the cost in revetment work. The estimated cost for revetment work is around 3.9 billion rupiah.

Table 4.10 The calculation of total cost index cleaning area work

No	Work description	Unit	Index	Unit cost		Cost index	
1	Supervisor	day	0.05	Rp	35,000.00	Rp	1,750.00
2	Worker	day	0.05	Rp	25,000.00	Rp	1,250.00
				Total cost index		Rp	3,000.00

Table 4.11 The calculation of total cost index in measurement work of the cross section of riverbank

No	Work description	Unit	Index	Unit cost		Cost index	
1	Engineer	day	1	Rp	50,000.00	Rp	50,000.00
2	Worker	day	2	Rp	30,000.00	Rp	60,000.00
3	Theodolith	day	1	Rp	100,000.00	Rp	100,000.00
4	Waterpass	day	1	Rp	100,000.00	Rp	100,000.00
				Total cost index		Rp	310,000.00

Table 4.12 The calculation of total cost index in excavation of revetment foundation

No	Work description	Unit	Index	Unit cost		Cost index	
1	Supervisor	day	0.0251	Rp	40,000.00	Rp	1,004.00
2	Worker	day	0.005	Rp	35,000.00	Rp	175.00
3	Excavator driver	day	0.0036	Rp	35,000.00	Rp	126.00
4	Excavator technician	day	0.0018	Rp	30,000.00	Rp	54.00
5	Excavator	hour	0.026	Rp	298,269.60	Rp	7,755.01
				Total cost index		Rp	9,114.01

Table 4.13 The calculation of total cost index in pre-cast concrete work

No	Work description	Unit	Index	Unit cost	Cost index
1	Engineer	day	1.714	Rp 50,000.00	Rp 85,700.00
2	Worker	day	0.141	Rp 25,000.00	Rp 3,525.00
3	Concrete ready mix	m3	1	Rp 380,000.00	Rp 380,000.00
4	Concrete vibrator	hour	0.587	Rp 37,800.00	Rp 22,188.60
5	Truck water	hour	0.036	Rp 105,000.00	Rp 3,780.00
				Total cost index	Rp 495,193.60

Table 4.14 The calculation of total cost index in installing work of the pre-cast concrete and rock

No	Work description	Unit	Index	Unit cost	Cost index
1	Supervisor	day	1	Rp 40,000.00	Rp 40,000.00
2	Worker	day	1.5	Rp 35,000.00	Rp 52,500.00
3	Excavator driver	day	0.029	Rp 40,000.00	Rp 1,160.00
4	Excavator technician	day	0.043	Rp 35,000.00	Rp 1,505.00
5	Excavator	hour	0.026	Rp 298,269.60	Rp 7,755.01
6	Crane	hour	0.075	Rp 132,000.00	Rp 9,900.00
				Total cost index	Rp 112,820.01

Table 4.15 The estimated cost of revetment work

No.	Type of work	Unit price	Unit	Volume	Unit		Cost (Rupiah)
1	Cleanning area	3000	Rp/m^2	2964	m^2	Rp	8,890,629.55
2	Measurement of the cross section of riverbank	310000	Rp/day	30	day	Rp	9,300,000.00
3	Excavation of foundation	9114	Rp/m^3	6302	m^3	Rp	57,436,488.50
4	Concrete block	495194	Rp/m^3	6302	m^3	Rp	3,120,710,067.20
5	Installing the concrete block	112820	Rp/m^3	6302	m^3	Rp	710,991,700.50
				Total cost		Rp	3,907,328,885.75

It is considered that the durable time of the concrete is about 50 years. Hence, the revetment must be reconstructed every 50 years. From the field observation, the slowest formation period of the bars at Malinau reach is about 5 years. Hence, the dredging of the bars must be performed every 5 years. For 50 years, the dredging cost is 2.3 billion rupiah. As a result, the dredging of mid-channel bar requires a low cost and the revetment requires high cost. Of course, the durable time of the concrete and the formation periode of bars change the results. The choice of the bank protection work

will be varies. Here, we can say that the direct bank protection like levee is not the best way all time and the dredging method can be the first choice for countermeasure the bank erosion problem in Sesayap River at Malinau reach, if we consider the bed deformation process.

4.6. Summary

Field surveys and analyses have been conducted to study the bank erosion processes in Sesayap River at Malinau reach. The river reach of Sesayap River at Malinau is the meeting place of the river flow from upstream with the tides of the sea. The mid-channel bar formation in the river. The mid-channel bar is formed in the river and causes large erosion along near the bank toe. Thus, the bank erosion occurs intensively in this location. The prevention of excessive erosion of the bank toe is the basic method to prevent bank erosion. The erosion near the bank toe is caused by formation of the mid-channel bar, so the treatment of the bar height is one of the solutions to prevent river bank erosion in this river reach.

The horizontal two-dimensional bed deformation analysis and the bank line retreat of the Sesayap River at Malinau reach are performed. The lateral erosion of the bank line in Case 1a (the bank composed cohesive and non-cohesive material) and Case 3a (the bank composed of non-cohesive material only) is about 12m and 32m, respectively. The cohesive characteristics and the high surface slope of the upper layer suppress the erosion rate. This result indicates that the cohesive characteristics of the material in banks must be considered, when the bank erosion process is reproduced by mathematical models.

Two main methods are applied to counteract of bank erosion problem this river reach. First, the dredging method to reduce a volume of mid-channel bar is applied. This method is addressed to increase the capacity of river flow. Second, the installing a general construction of riverbank protection is applied. The revetment is chosen as riverbank protection. Furthermore, the advantage of the dredging is discussed. The result of numerical analysis in case of original condition shows that the presence of the mid-channel bar produces high velocity at the downstream bar, especially during low tide. This is the reason why in this location have an intensive activity of bank erosion.

The results of dredging method show that, this method can reduces the erosion at the bed near the bank toe, significantly. As a parameter on triggering bank failure process, reducing of the bed degradation near the bank toe is an important treatment to prevent the bank erosion. The installing a construction such as revetment may protect the bank erosion successfully. However, this method cannot improve the flow pattern and bed deformation near the bank toe. The result of this case shows that the bed degradation still occurs in large value on the bed in front of the construction. This condition will produce instability structure in the future condition. The structure of revetment usually reduces the cross sectional area flow capacity. It may increases the flow velocity at another location. This condition will produce bank erosion problem at another place.

Finally, the dredging of mid-channel bar is the first action to prevent the bank erosion in Sesayap River at Malinau reach. The bank protection using a construction, which installed along the bank, should consider the financial aspect. The construction only prevents the failure process due to the gravitational force, which comes from the bank itself. In fact, the bank is composed of cohesive material, which has a good stability.

References

Ashida, K. and Michiue, M.: Study on hydraulic resistance and bed-load transport rate in alluvial streams, *Proc. of JSCE*, No. 206, pp.59-69, 1972.

Ashworth P.J., Mid-channel bar growth and its relationship to local flow strength and direction, *Earth Surface Processes and Landform*, Vol. 21, pp. 103-123, 1996.

Dapporto, S., Rinaldi, M., Casagli, N., and Vannocci, P.: Mechanisms of riverbank failure along the Arno river, central Italy, *Earth Surf. Process. Landforms*, Vol. 28, pp. 1303–1323, 2003.

Egashira, S. and Ashida, K.: Unified view of the mechanics of debris flow and bed-load, *Advances in Micromechanics of Granular Materials*, (Edited by H.H.Shen et al.) Elsevier, pp. 391-400, 1992.

Engelund, F., Flow and Bed Topography in Channel Bends, *Journal of Hydraulic Div.*, ASCE, Vol. 100, No. HY11, 1974.

Gabel, S.L. and Bridge, J.S.: Flow and sediment dynamics in a low sinuosity, braided river: Calamus River, Nebraska Sandhills, *Sedimentology*, Vol. 39, pp125-142, 1992.

Hooke, J.M.: An analysis of the processes of river bank erosion, *Journal of Hydrology*, Vol. 42, pp. 39-62, 1979.

Hooke J.M., The significance of mid-channel bars in an active meandering river, *Sedimentology*, Vol. 33, Issue 6, pp. 839–850, 1986.

Iwagaki, Y.: Hydrodynamic study on critical shear stress. *Proc. of JSCE*, No. 41, pp. 1-21, 1956.

Jiongxin, X.: Underlying gravel layers in a large sand bed river and their influence on downstream-dam channel adjustment, *Geomorphology*, Vol.17, pp. 351–359, 1996.

Kovacs, A. and Parker, G.: A new vectorial bedload formulation and its application to the time evolution of straight river channels. J. Fluid Mech. Vol. 267, pp. 153-183, 1994.

Liu, B.Y.: Study on Sediment Transport and Bed Evolution in Compound Channels. Thesis presented to Kyoto University, 1991

Nagata, N., Numerical Analysis of the 2-Dimensional Unsteady Flow Using a Generalized Coordinate System, The Lecture Collection on the Computer Use in Hydraulic Engineering, *The Japan Society of Civil Engineers*, pp. 51 – 76, 1999.

Sekine, M., Nishimori, K., Fujio, K. and Katagiri, Y.: On erosion process of cohesive sediment and erosion rate formula, *Annual Journal of Hy. Eng. JSCE*, Vol. 47, pp. 541-546, 2003

Simon A., Curini A., Darby S.E., and Langendoen E.J.: Bank and near-bank processes in an incised channel, *Geomorphology*, Vol. 35, pp. 193-217, 2000.

Shimizu,Y. and Itakura,T., Calculation of Flow and Bed Deformation with a General Non-Orthogonal Coordinate System, *Proc. of XXIV IAHR Congress, Spain*, C-2, pp.41-48, 1991.

Takebayashi, H., Egashira, S. and Okabe, T.: Braided streams formed on beds with non-uniform sediment, *Proc. 3nd IAHR Symposium on River, Coastal and Estuarine Morphodynamics*, pp.787-798, 2003.

Takebayashi, H., River Configuration in Middle-Lower Reach of River Basin, *Journal of Japan Society of Fluid Mechanics*, Vol. 24, pp. 27-36, 2005.

Chapter 5

Numerical Analysis on Erosion Process of Cohesive Sediment Bed by Non-cohesive Sediment Transport in Natural River

5.1. Introduction

The Tonle Sap Lake is located in Cambodia. The hydraulic system of the lake is strongly influenced by Mekong River. The Tonle Sap Lake is connected to the Mekong River by the 100 km long Tonle Sap River. The Tonle Sap River and the Mekong River join at the Chaktomuk near Phnom Penh. The river immediately branches into two arms after the confluence of them, the larger main Mekong River and the smaller Bassac River (see Figure 5.1).

The Tonle Sap Lake and the Mekong River have a unique hydraulic system. During October to May (dry season), the Tonle Sap Lake is a water supplier to the downstream area of the Mekong River. The water flows through the Tonle Sap River from the Tonle Sap Lake. On the other hand, from June to September (flood season), the water discharge of Mekong River becomes so great that causes the water of Tonle Sap River reverses its flow, flowing up to fill with the Tonle Sap Lake. In this season, the lake behaves as an effective flood detention basin.

The flow characteristics of Mekong River, Tonle Sap River and Bassac River are explained using Google aerial image here. Figure 5.2 and Figure 5.3 show the aerial images taken on February 3rd 2003 (dry season) and July 7th 2005 (flood season), respectively. The similarity and difference of the water color explains the source of water. Thus, the flow directions can be estimated. In Figure 5.2, the water color in Bassac River and along the right side in the downstream reach of Mekong River is the same as the color in Tonle Sap River. It means that the flow direction in Tonle Sap River is from the north to the south (from Tonle Sap Lake to Mekong River). In Figure

5.3, the water color in Bassac River and Tonle Sap River is the same as the color in Mekong River. It means that the water comes from Mekong River.

Figure 5.1 Hydraulic system among of Mekong River, Tonle Sap River and Bassac River. (source: http://www.wordtravels.com)

Figure 5.2 Aerial image around Chaktomuk, Cambodia during dry season. The image was taken in February 3rd 2003 (source Google Earth)

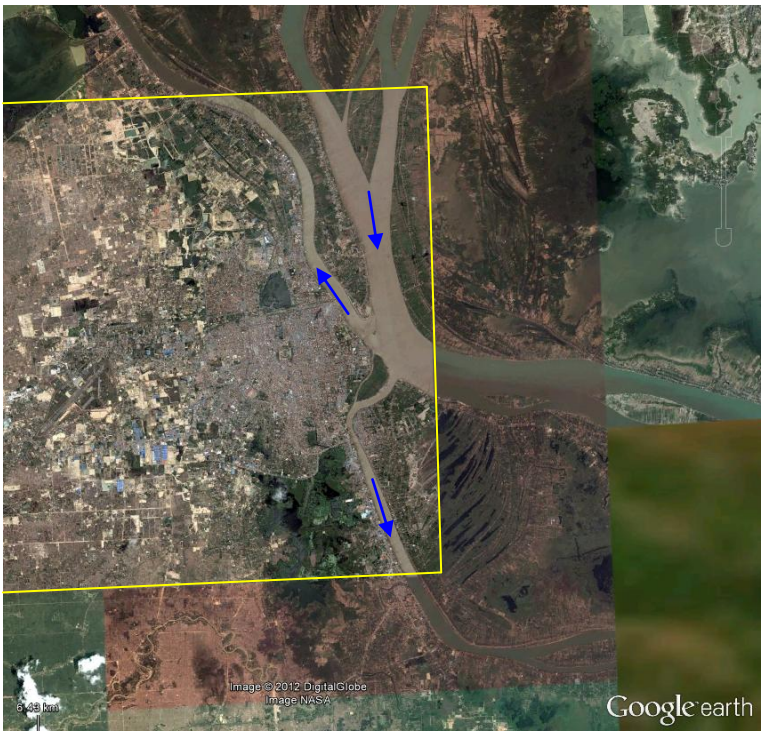

Figure 5.3 Aerial image around Chaktomuk, Cambodia during flood season. The image was taken in July 25th 2005 (source Google Earth)

The mean diameter of the bed material in Tonle Sap River is quite difference from that in Mekong River. The bed material in Tonle Sap River is fine material and in the Mekong River is coarse material. At the beginning of flood season, the bed material in Tonle Sap River is pure cohesive sediment. In this time, the water from Mekong River that contains coarse bed-load transport flows on fine bed material of Tonle Sap River. This fact indicates that the cohesive material can be eroded by both non-cohesive material and water. However, suggested erosion rate equations of cohesive material in the previous studies treats the erosion rate by water only (Parchure *et al.*, 1985; Sekine and Iizuka, 2000; and Aberle *et al.*, 2002). As concluded in Chapter 3, the erosion rate of cohesive sediment bed will increase with increase in the bed-load transport rate, when the sediment transport is enough smaller than the equilibrium sediment transport rate. However, the erosion rate will decrease in spite of the increasing of bed-load transport rate after achieving a certain sediment transport rate. According to these results, it is important to consider the presence of bed-load transport to estimate the shear stress on the bed and calculate the erosion rate of cohesive material. The shear stress on bed must be estimated by velocity and the sediment concentration profiles of the mixed flow of both water and sediment.

Takebayashi *et al.* (2010) treats the bed material as the non-uniform sediment and clarify the effect of the sediment size distribution on the bed deformation characteristics and the horizontal distribution characteristics of the sediment size. In the research, the bed material is treated as non-cohesive material. On the other hand, the bed material in Tonle Sap River consists of cohesive material. It is considered that the cohesive characteristic of the bed material affects the horizontal distribution of bed deformation very well.

In this study, the depth integrated two dimensional bed deformation analysis has been performed to understand the seasonal change of the flow pattern, bed deformation characteristics and horizontal distribution characteristics of bed material size in Chaktomuk near Phnom Penh. The bed material is treated as both the cohesive and the non-cohesive sediments and the effect of the horizontal distribution of cohesive material on bed deformation characteristics is discussed. The analysis is performed under 3 characteristic hydraulic conditions; maximum, minimum and zero water discharge in the Tonle Sap River.

5.2. Riverbed Materials

As explained in introduction, the Tonle Sap River and the Mekong River have different characteristics of the bed material size during dry and flood season. So, the bed materials were sampled at two points in a cross-section using a cable operated sediment sampler during both flood and dry seasons. The sampler can take the sediment in 8 cm thickness from the bed surface. Sediment is also sampled from both the left and the right banks. Figure 5.4 shows the sampling cross-sections of bed and bank materials.

Figure 5.5 shows the size distribution of bed material during dry and flood season of Tonle Sap River and Mekong River. The size distribution at point 24R show fine material during the dry season. In this time, the dominant flow comes from Tonle Sap River. It means that the sediment in Tonle Sap River is fine material. However, during the flood season, the dominant flow at point 24R comes from Mekong River and the size of the material is fine. It is clear that the flow from Mekong River contents the coarse sediment. In other words, seasonal change of flow direction in the Tonle Sap River contributes to the seasonal change of the sediment size in Tonle Sap River.

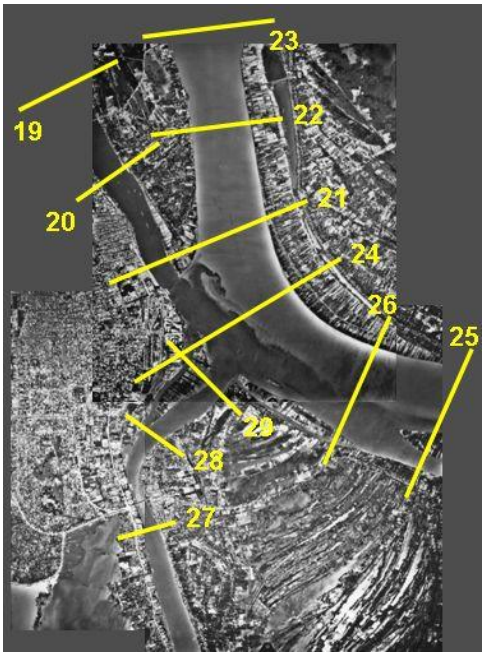

Figure 5.4 Sampled cross-sections of bed and bank materials

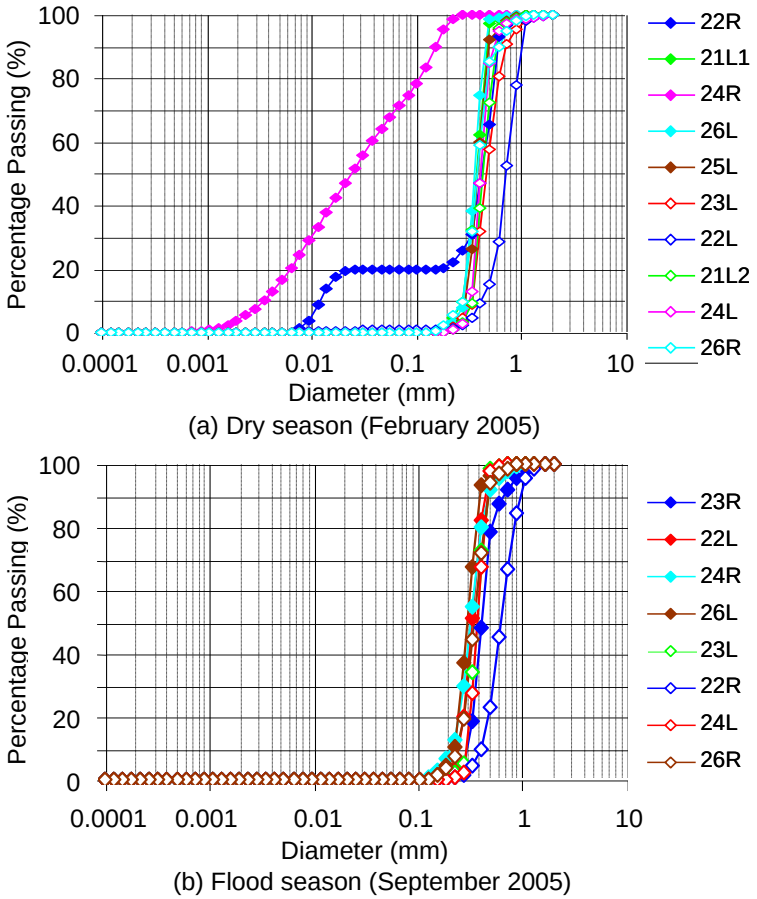

Figure 5.5 Size distribution of bed material in Chaktomuk

5.3. Numerical Analysis and Simulations Cases

Computation of the water flow is performed using the governing equation of the horizontal two dimensional flow averaged with depth (Luu, *et al*., 2004). Equations of the flow in the model are written in Chapter 4. However, the bank erosion is neglected here. Hence, the terms due to the temporal change of numerical grids are neglected. Here the equations on the bed deformation are introduced. Grain size distribution is evaluated using the following mass conservation equation of each sediment size class:

$$\frac{\partial}{\partial t}\left(\frac{c_b E_b f_{bk}}{J}\right)+(1-\lambda)F_{bk}\frac{\partial}{\partial t}\left(\frac{z_b}{J}\right) \tag{5.1}$$

$$+\frac{\partial}{\partial \xi}\left(\frac{q_{b\xi k}}{J}\right)+\frac{\partial}{\partial \eta}\left(\frac{q_{b\eta k}}{J}\right)+\frac{1}{J}w_k\left(c_{sbek}-c_{sbk}\right)=0$$

$$\begin{cases} F_{bk} = f_{d1k},\ \partial z_b/\partial t \le 0 \\ F_{bk} = f_{bk},\ \partial z_b/\partial t \ge 0 \end{cases}$$

$$\frac{\partial}{\partial t}\left(\frac{E_{d1} f_{d1k}}{J}\right) - F_{dk}\frac{\partial}{\partial t}\left(\frac{E_{d1}}{J}\right) = 0 \tag{5.2}$$

$$\begin{cases} F_{dk} = f_{d1k},\ \partial z_b/\partial t \le 0 \\ F_{dk} = f_{bk},\ \partial z_b/\partial t \ge 0 \end{cases}$$

In the formulae above, f_{bk} is the concentration of bed load of size class k in the bed load layer, f_{dmk} is the sediment concentration of size class k in the mth bed layer, c_b is the depth-averaged concentration of bed load. E_b is the bed load layer thickness, $q_{b\xi k}$ and $q_{b\eta k}$ are the bed load of size class k in ξ and η directions, respectively, q_{bxk} and q_{byk} are the bed load of size class k in x and y directions, respectively as follows (Ashida and Michiue, 1972; Liu, 1991 and Kovacsand Parker, 1994).

$$q_{bxk} = q_{bk}\cos\beta_k\ ,\ q_{byk} = q_{bk}\sin\beta_k \tag{5.3}$$

$$q_{bk} = 17\frac{\rho u_{*e}^3}{(\rho_s - \rho)g}\left(1 - \sqrt{K_c}\frac{u_{*ck}}{u_*}\right)\left(1 - K_c\frac{u_{*ck}^2}{u_*^2}\right) f_{bk} r_b \tag{5.4}$$

Therein, ρ_s is the sediment density, u_{*e} is the effective shear velocity, the non-dimensional critical friction velocity of size class k is evaluated as follows (Ashida. and Michiue, 1972).

$$u_{*ck}^2 = u_{*cm}^2\left[\frac{\log_{10}19}{\log_{10}(19 d_k/d_m)}\right]^2\frac{d_k}{d_m} \tag{5.5}$$

$$d_k/d_m \ge 0.4$$

$$u_{*ck}^2 = 0.85 u_{*cm}^2\ d_k/d_m \le 0.4 \tag{5.6}$$

Iwagaki's formula (Iwagaki, 1956) which is formulated for uniform bed material is used for evaluating u_{*cm}. K_c is the correction factor due to the influence of bed inclination on sediment motion.

$$K_c = 1 + \frac{1}{\mu_s}\left[\left(\frac{1}{s} + 1\right)\cos\alpha\tan\theta_x + \sin\alpha\tan\theta_y\right] \tag{5.7}$$

where s is the specific gravity of the sediment in water, α is the angle of deviation of near-bed flow from the x direction. μ_s is the coefficient of static friction. θ_x and θ_y are bed inclinations in x and y directions, respectively. The deviation angle of bed load of size class k to the x direction (β_k), which depends on the flow near bed and inclination of the bed, is calculated by the following relation.

$$\tan\beta_k = \frac{\sin\alpha - \Pi\Theta_y\left(\frac{u_{*ck}^2}{u_*^2}\right)\tan\theta_y}{\cos\alpha - \Pi\Theta_x\left(\frac{u_{*ck}^2}{u_*^2}\right)\tan\theta_x} \tag{5.8}$$

$$\Pi = K_{ld} + 1/\mu_s \tag{5.9}$$

$$\Theta_y = \frac{1}{1+\tan^2\theta_x + \tan^2\theta_y} \tag{5.10}$$

$$\Theta_x = \Theta_y + \frac{\rho}{\rho_s - \rho}\cos^2\theta_x \tag{5.11}$$

where, K_{ld} is the ratio of lift force to drag force. The settling velocity of suspended sediment (w_{fk}) is estimated as follow (Rubey, 1933).

$$w_{fk} = \left(\sqrt{\frac{2}{3} + \frac{36\nu^2}{sgd_k^3}} - \sqrt{\frac{36\nu^2}{sgd_k^3}}\right)\sqrt{sgd_k} \tag{5.12}$$

The equilibrium suspended concentration of k sediment size class at reference level (c_{sbek}) is evaluated as follows (Lane and Kalinske, 1941).

$$c_{sbek} = 5.55\left(\frac{1}{2}\frac{u_*}{w_{fk}}\exp\left(-\frac{w_{fk}}{u_*}\right)\right)^{1.61} f_{bk} r_b \text{ (unit: ppm)} \tag{5.13}$$

When the vertical distribution of concentration of suspended sediment is supposed as exponent distribution, relationship between the depth-averaged suspended concentration (c_{sk}) and the suspended concentration of sediment size class k at reference level (c_{sbk}) is as follows.

$$c_{sk} = \frac{c_{sbk}}{\beta_{sk}}\left(1 - e^{(-\beta_{sk})}\right),\ \beta_{sk} = \frac{w_{fk}h}{D_h} \tag{5.14}$$

where, D_h is the coefficient of dispersion in vertical direction. ν is used as D_h here for simplicity. The depth-averaged suspended concentration of size class k is evaluated the following continuum equation of suspended sediment.

$$
\begin{aligned}
&\frac{\partial}{\partial t}\left(\frac{hc_{sk}}{J}\right)+\frac{\partial}{\partial \xi}\left(\frac{hc_{sk}U}{J}\right)+\frac{\partial}{\partial \eta}\left(\frac{hc_{sk}V}{J}\right)\\
&\quad=\frac{1}{J}w_{fk}\left(c_{sbek}-c_{sbk}\right)\\
&\qquad+\frac{\partial}{\partial \xi}h\left(\frac{1}{J}\left(D_x\left(\frac{\partial \xi}{\partial x}\right)^2+D_y\left(\frac{\partial \xi}{\partial y}\right)^2\right)\frac{\partial c_{sk}}{\partial \xi}\right)\\
&\qquad+\frac{\partial}{\partial \xi}h\left(\frac{1}{J}\left(D_x\frac{\partial \xi}{\partial x}\frac{\partial \eta}{\partial x}+D_y\frac{\partial \xi}{\partial y}\frac{\partial \eta}{\partial y}\right)\frac{\partial c_{sk}}{\partial \eta}\right)\\
&\qquad+\frac{\partial}{\partial \eta}h\left(\frac{1}{J}\left(D_x\frac{\partial \xi}{\partial x}\frac{\partial \eta}{\partial x}+D_y\frac{\partial \xi}{\partial y}\frac{\partial \eta}{\partial y}\right)\frac{\partial c_{sk}}{\partial \xi}\right)\\
&\qquad+\frac{\partial}{\partial \eta}h\left(\frac{1}{J}\left(D_x\left(\frac{\partial \eta}{\partial x}\right)^2+D_y\left(\frac{\partial \eta}{\partial y}\right)^2\right)\frac{\partial c_{sk}}{\partial \eta}\right)
\end{aligned}
\tag{5.15}
$$

where, D_x and D_y are coefficient of dispersion in x and y directions, respectively. (D_x = D_y = ν for simplicity here). Evolution of bed elevation is estimated by means of following formulae.

$$
\begin{aligned}
&\frac{\partial}{\partial t}\left(\frac{c_b E_b}{J}\right)+(1-\lambda)\frac{\partial}{\partial t}\left(\frac{z_b}{J}\right)\\
&\qquad+\frac{\partial}{\partial \xi}\left(\sum_{k=1}^{n}\frac{q_{b\xi k}}{J}\right)+\frac{\partial}{\partial \eta}\left(\sum_{k=1}^{n}\frac{q_{b\eta k}}{J}\right)\\
&\qquad\qquad+\sum_{k=1}^{n}\frac{1}{J}w_k\left(c_{sbek}-c_{sbk}\right)=0
\end{aligned}
\tag{5.16}
$$

$$
E_{sd}\geq E_{be}\frac{c_b}{1-\lambda}
$$

$$
\frac{\partial}{\partial t}\left(\frac{z_b}{J}\right)+\frac{V_e}{J}=0 \quad E_{sd}\leq E_{be}\frac{c_b}{1-\lambda} \tag{5.17}
$$

In them, n represents the number of the size class of sediment. The erosion velocity of cohesive sediment (V_e) is estimated as follows.

$$
V_e=\alpha_c R_{wc}^{2.5}u_*^3\left(1-r_b\right) \tag{5.18}
$$

where, α_c is the coefficient related on kinds of cohesive sediment, R_{wc} is the water content rate. Equation 5.18 is different from equation 4.34 (Sekine *et al.*, 2003). The decrease effect of the erosion rate by the covering the bed by the transported sediment is considered in Equation 5.18. r_b is the function related on thickness of bed load layer as follows.

$$
r_b=1 \qquad E_{sd}\geq E_{be}\frac{c_b}{1-\lambda} \tag{5.19}
$$

$$r_b = \frac{E_b}{E_{be}} \qquad E_{sd} \le E_{be}\frac{c_b}{1-\lambda} \tag{5.20}$$

E_{be} is the equilibrium bed load layer thickness; it is estimated by the following equation (Egashira and Ashida, 1992):

$$\frac{E_{be}}{d_m} = \frac{1}{c_b \cos\theta\left(\tan\phi - \tan\theta\right)}\tau_{*m} \tag{5.21}$$

where d_m is the mean diameter of bed load, ϕ is the angle of repose, and τ_{*m} is the non-dimensional shear stress of mean diameter. E_{sd} is the sediment layer thickness on cohesive sediment bed. E_b is the bed load layer thickness as follows.

$$E_b = E_{be} \qquad E_{sd} \ge E_{be}\frac{c_b}{1-\lambda} \tag{5.22}$$

$$E_b = E_{sd}\frac{1-\lambda}{c_b} \qquad E_{sd} \le E_{be}\frac{c_b}{1-\lambda} \tag{5.23}$$

Equation 5.18 indicates that the erosion rate decreases linearly with increase in the amount of the transported sediment on the bed composed of cohesive material. At the equilibrium transport rate, erosion rate of the cohesive material bed is zero.

Local bed slope was reset to the angle of repose at calculation points where the slope becomes steeper than the angle of repose (Nagase, *et al.*, 1996) and E_{sd} is thicker than E_{be} at the upper erosion area.

5.4. Hydraulic Conditions

Water Discharge

This numerical analysis is performed to discuss the effect of the bed-load transport on the erosion characteristics of cohesive sediment bed in natural rivers. Chaktomuk area in Cambodia was chosen as case study. As explained in the introduction, Tonle Sap River has cohesive sediment bed during the dry season. Water from Mekong River, which contents coarse bed-load transport during flood season, flow on the cohesive sediment bed. To simulate these phenomena, three main upstream discharges are used as follow:

- The discharge in Tonle Sap River and Mekong River are from dry season data,
- The discharge in Tonle Sap River and Mekong River are from intermediate season data,

– The discharge in Tonle Sap River and Mekong River are from flood season data,

Bed Material Size

Figure 5.6 (a) shows the initial bed geometry. Flat bed geometry with the constant longitudinal slope is used as initial bed geometry to clarify the bed deformation characteristics. Figure 5.6 (b) shows the horizontal size distribution of initial bed material. At the upstream boundary of the Mekong River, the coarse bed material which is measured in the Mekong River is used as the initial sediment size. At the upstream boundary of the Tonle Sap River, the fine bed material which is measured in the Tonle Sap River is used as the initial sediment size. In the Bassac River and the downstream of the Mekong River, the average size distribution of bed material between the Mekong's material and the Tonle Sap's material is used as the initial condition.

Simulation Case

Total six cases were simulated in this analysis. The hydraulic and bed material conditions for each case are explained as follow:

- **Case 1**

The upstream water discharge in Tonle Sap River and Mekong River are 8000 m^3/s and 6000 m^3/s, respectively. The discharge in Tonle Sap River is the annual maximum water discharge and can be observed during the dry season.

The bed material in Tonle Sap River is treated as the non-cohesive material for the surface layer and cohesive material for the subsurface layer. The thickness of the surface non-cohesive material layer is distributed linearly from 0 to 0.3 m along the river. The thickness of the surface non-cohesive material layer is 0 at the upstream boundary of the Tonle Sap River and is 0.3 m at the connection between the Tonle Sap River and the confluence. In Mekong River and Bassac River, there is no cohesive material.

- **Case 2**

The upstream water discharge in Tonle Sap River and Mekong River are 0 m^3/s and 20000 m^3/s, respectively. These discharges can be observed between dry season and flood season.

The bed material condition in Tonle Sap River, Mekong River and Bassac River are treated the same as that in Case 1.

- **Case 3**

The upstream water discharge in Tonle Sap River and Mekong River are -8000 m^3/s and 36000 m^3/s, respectively. These discharges are the annual maximum water discharge in Mekong River and can be observed during the flood season. The negative value in Tonle Sap River indicates that the flow is from Mekong River to Tonle Sap Lake.

The bed material condition in Tonle Sap River, Mekong River and Bassac River are treated the same as that in Case 1.

- **Case 4**

The upstream water discharge in Tonle Sap River and Mekong River are treated the same as that in Case 1.

The bed material condition in Tonle Sap River, Mekong River and Bassac River consists of non-cohesive material only. These initial conditions are used to discuss the effect of the horizontal distribution of cohesive material on bed deformation characteristics by comparing the results in Case 1.

- **Case 5**

The upstream water discharge in Tonle Sap River and Mekong River are treated the same as that in Case 2.

The bed material condition in Tonle Sap River, Mekong River and Bassac River are the same as that in Case 4.

- **Case 6**

The upstream water discharge in Tonle Sap River and Mekong River are treated the same as that in Case 3.

The bed material condition in Tonle Sap River, Mekong River and Bassac River are the same as that in Case 4.

The shape of the bank line for all cases is obtained by use of satellite image taken in 1993. Flat bed geometry with 1/100000 longitudinal slope is used as initial bed geometry to clarify the bed deformation characteristics. Table 5.1 shows the summary of hydraulic conditions.

Table 5.1Hydraulic conditions

	Channel geometry	QmekongU (m^3/s)	Qtonle (m^3/s)	Bed material distribution
Case 1	1993	6000	8000	Non-uniform
Case 2	1993	20000	0	Non-uniform
Case 3	1993	36000	-8000	Non-uniform
Case 4	1993	6000	8000	Non-uniform
Case 5	1993	20000	0	Non-uniform
Case 6	1993	36000	-8000	Non-uniform

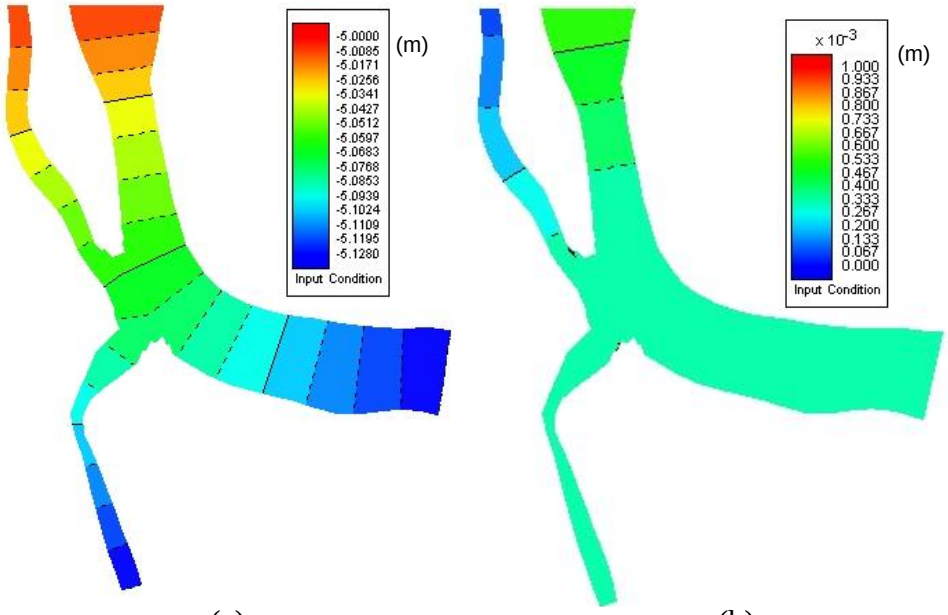

(a) (b)

Figure 5.6 Initial bed geometry and horizontal distribution of initial mean diameter of bed material (Bank line shape: 1993), (a) Bed geometry, (b) Mean diameter of bed material

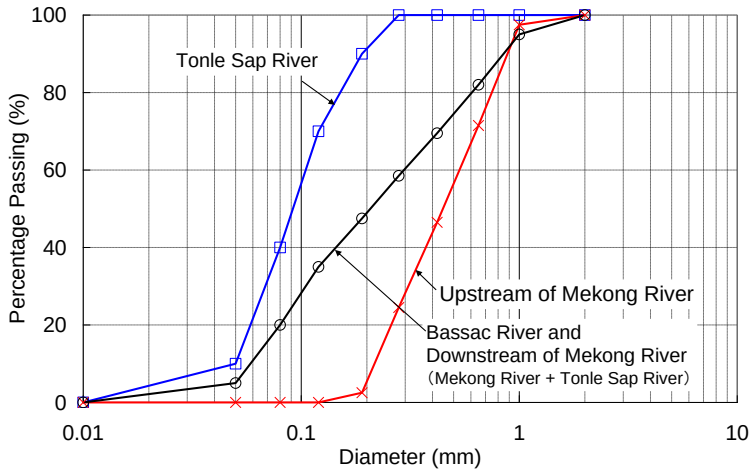

Figure 5.7 Initial size distribution of bed material

Table 5.2 Calculated water discharge in each channel

	$Q_{mekongU}$ (m^3/s)	Q_{tonle} (m^3/s)	$Q_{mekongD}$ (m^3/s)	Q_{bassac} (m^3/s)	Q_{bassac} /$Q_{mekongD}$
Case 1 and Case 4	6000	8000	11133	2867	0.258
Case 2 and Case 5	20000	0	17859	2141	0.120
Case 3 and Case 6	36000	-8000	22687	5313	0.234

5.5. Flow characteristics

Figure 5.8 show the horizontal distributions of the depth averaged water velocity in Cases 1, 2 and 3. Table 2 shows the water discharges of each river. The hydraulic condition in Case 4 is the same as that in Case 1, so the result of the horizontal distributions of the depth averaged water velocity also the same. The result in Case 5 and Case 6 are also the same as Case 2 and Case 3, respectively. During the dry season (Figure 5.8 (a)), water discharge in Tonle Sap River is larger than that in the upstream area of the Mekong River. As shown in Table 5.2, water discharge in the Bassac River is smaller than that in the downstream area of the Mekong River. The percentage rate of the water discharge in the Bassac River to the Mekong River is 25.8%. Hence, the water from the Tonle Sap River diverged to both the Bassac River and the downstream area of the Mekong River during dry season.

When water discharge in the Tonle Sap River is zero (Figure 5.8 (b)), the percentage rate of the water discharge in the Bassac River to the Mekong River is 12.0% and is the minimum value among Cases 1, 2 and 3. Between the entrance of the Bassac River and the Mekong main channel, the very small water velocity area appears because of the zero water discharge in the Tonle Sap River. Hence, the water in the upstream area of the Mekong River is hard to flow into the Bassac River. During the flood season (see Figure 5.8 (c)), the water from the upstream area of the Mekong River flows into the Tonle Sap River. Furthermore, the water from the upstream area of the Mekong River tends to flow into the Bassac River, because the flow direction from the upstream area of the Mekong River is changed almost 90 degree at the entrance of the Bassac River. The percentage rate of the water discharge in the Bassac River to the Mekong River is 23.4% and is slightly smaller than that during the dry season.

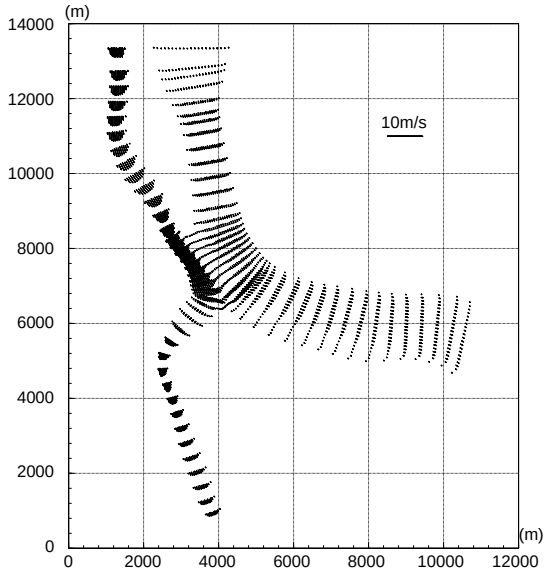

(a) Dry season (Case 1)

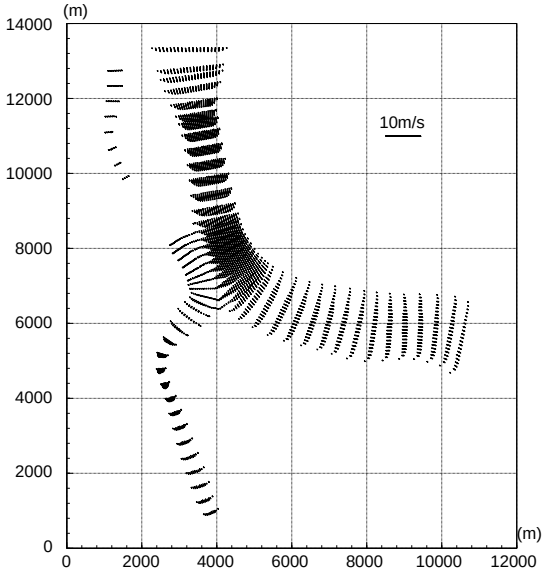

(b) Intermediate (Case 2)

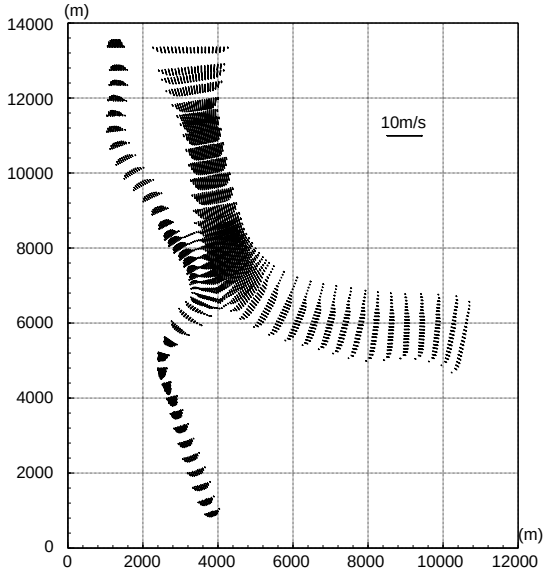

(c) Flood season (Case 3)

Figure 5.8 Depth averaged water velocity

5.6. Bed deformation and Sediment Size Characteristics

Figure 5.9 shows the horizontal distribution of the bed deformation characteristics in Case 1 and Case 4 during dry season. The bed near the confluence in the Tonle Sap

River is eroded well during the dry season (Figure 5.9). Sediment deposited at the entrance of Bassac River. The photo in Figure 5.2 was taken during the dry season. In the photo, the sediment concentration boundary is appeared from the left bank of the Tonle Sap River to the downstream reach of the Mekong River. The photo indicates that the sediment and the water in Tonle Sap River are supplied to the confluence and the Bassac River very well during the dry season. The calculated results show the same tendency. Bed materials at the bed degradation area become coarse and those at the bed aggradation area become fine as shown in Figure 5.10.

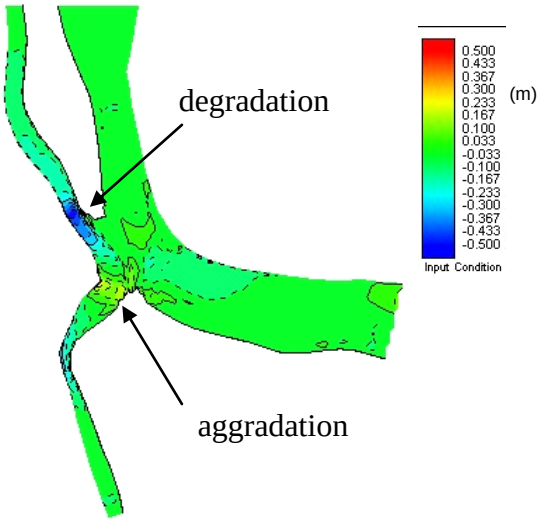

Figure 5.9 Horizontal distribution of bed deformation during dry season in Case 1

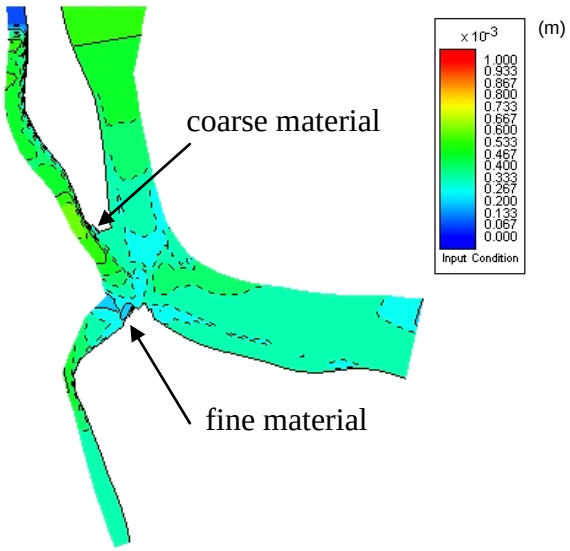

Figure 5.10 Horizontal distribution of mean diameter in Case 1

Figure 5.11 shows the horizontal distribution of the bed deformation characteristics in Case 2 and Case 5 during the intermediate season. When water discharge in the Tonle Sap River is zero (Figure 5.11), the upstream and the downstream areas of the Mekong River and the Bassac River is degradated. Hence, as shown in Figure 5.12, the sediment size becomes coarse at the upstream and the downstream areas of the Mekong River and the Bassac River. Sediment deposits near the bifurcation between the Mekong River and the Bassac River.

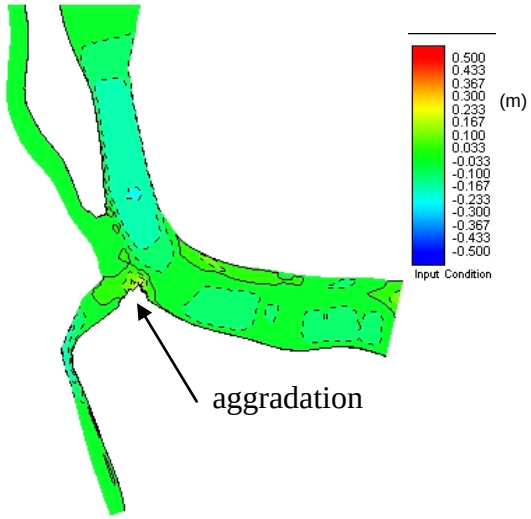

Figure 5.11 Horizontal distribution of bed deformation during intermediate season in Case 2

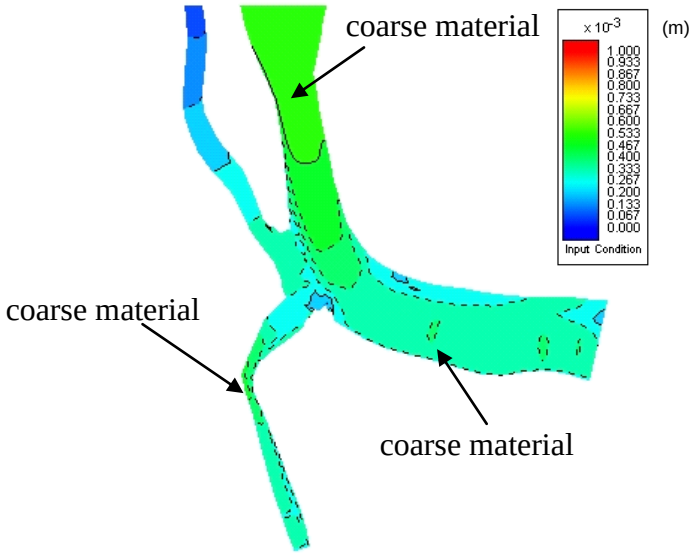

Figure 5.12 Horizontal distribution of mean diameter in Case 2

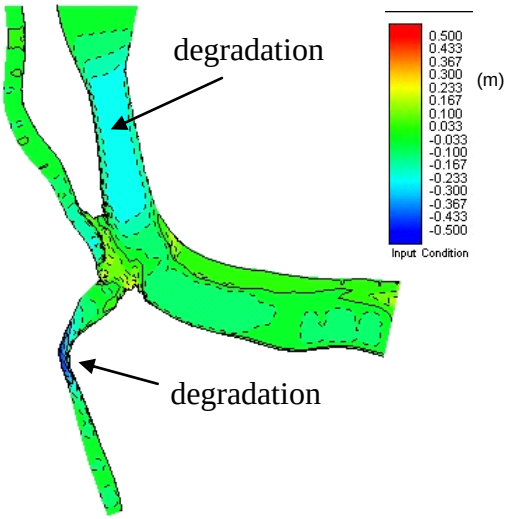

Figure 5.13 Horizontal distribution of bed deformation during flood season Case 3

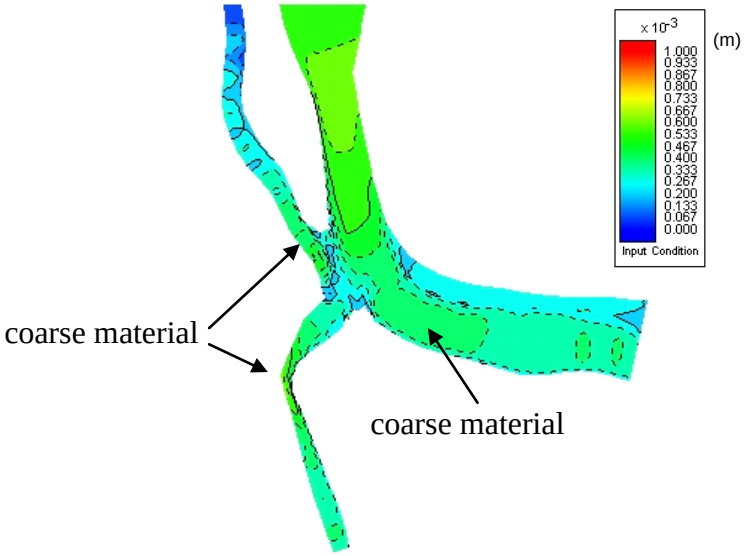

Figure 5.14 Horizontal distribution of mean diameter in Case 3

Figure 5.13 shows the horizontal distribution of the bed deformation characteristics in Case 3 and Case 6 during the flood season. During the flood season (Figure 5.13), both the upstream and the downstream areas of the Mekong River and the Bassac River is degradated. Bed degradation along the outer bank of the Bassac River is especially large. Sediment deposited at the entrance of the Bassac River and the south of peninsula between the Tonle Sap River and the Mekong River. As shown in Figure 5.15, the peninsula between the Tonle Sap River and the Mekong River has been extended to

south year by year. It is considered that the sediment deposition during the flood season cause the extension of the peninsula. As shown in Figure 5.14, the sediment size becomes coarse at both the upstream and downstream areas of the Mekong River and Bassac River. Bed material in the Tonle Sap River also becomes coarse because of the inverse flow from the Mekong River. However, the armoring phenomenon is restricted near the confluence. This result gets agrees with the results of one dimensional bed deformation analysis (Takebayashi, 2006).

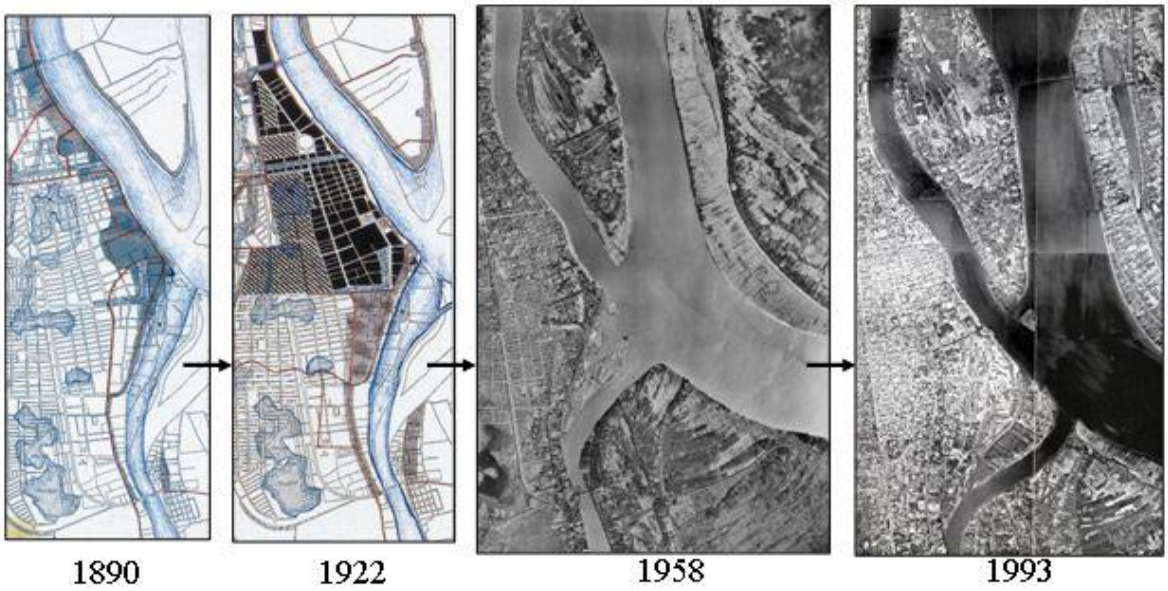

Figure 5.15 Temporal change of channel geometry of Chaktomuk (figs of 1890, 1922 and photo in 1993 is from Ministere de la Culture : Phnom Penh, development urban et patrimoine, photo in 1958 is from Ministry of Industry, Mines and Energy General Department of Mineral Resources, Phnom Penh, Cambodia)

During the flood season, the dominant flow in Tonle Sap River is influenced by flow from Mekong River. The discharge from Mekong River which contains of the non-cohesive bed-load transport flows on the Tonle Sap River. The results from Case 3 (see Figure 5.13) indicates that the cohesive layer at subsurface is not eroded much by flow in Tonle Sap River. The presences of cohesive layer on the bed suppress the erosion in Tonle Sap River. The effect of the cohesiveness of subsurface layer on erosion rate can be seen at upstream reach of the Tonle Sap River. In this area, in Case 3, the river bed

deformation is very small. However, in Case 6 the bed is eroded much. This indicates that the flow condition is enough for eroding the non-cohesive material bed.

Both the surface and the subsurface bed materials are treated as non-cohesive material in Case 4, 5 and 6. Comparing to the results in Case 1, 2 and 3, the difference of the horizontal distribution of the bed deformation is quite large during the dry season (Case 1 and 4). During the dry season (see Figure 5.16) sediment deposited at the entrance of the Bassac River and the downstream area of Mekong River widely, because the coarse material in the Tonle Sap River is transported there very well.

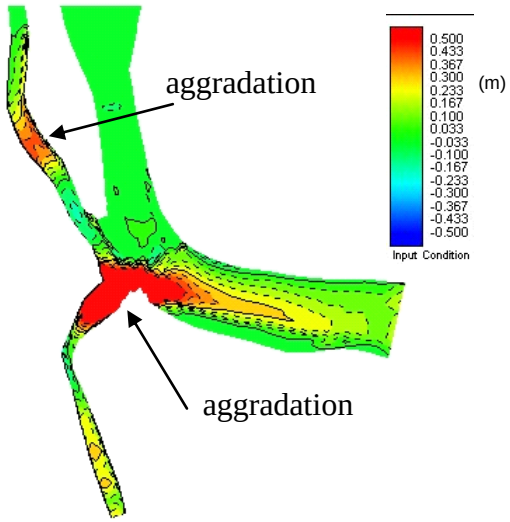

Figure 5.16 Horizontal distribution of bed deformation during dry season in Case 4

When water discharge in the Tonle Sap River is transported equal to zero (Figure 5.17), the difference of the bed deformation characteristics between Case 2 and Case 5 is very small, because the water discharge in the Tonle Sap River is equal to zero and no sediment transport in the Tonle Sap River.

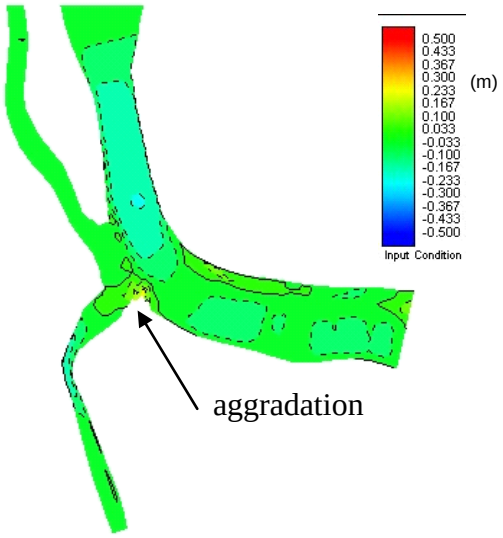

Figure 5.17 Horizontal distribution of bed deformation during dry season in Case 5

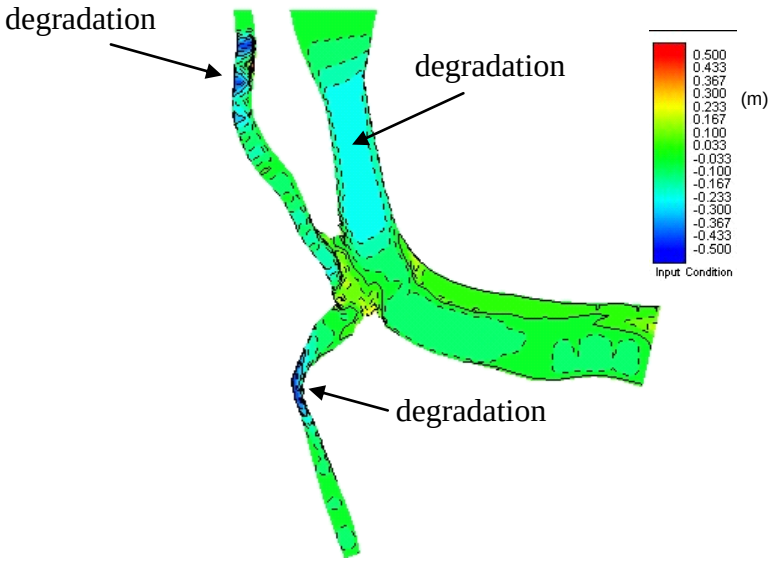

Figure 5.18 Horizontal distribution of bed deformation during dry season in Case 6

During the flood season (Figure 5.18), the difference of bed deformation characteristics between Case 3 and Case 6 is also small except the upstream area of the Tonle Sap River. When the bed material is treated as non-cohesive material, the bed is eroded well in upstream area of the Tonle Sap River. As describe above, cohesive characteristics of the sediment affects the bed deformation characteristics because of the suppression of sediment transport rate and bed degradation. Especially, when rivers

have different sediment size characteristics confluents, difference of the cohesive characteristics of sediment must be considered.

5.7. Summary

The depth integrated two dimensional bed deformation analysis has been performed to understand the effect of cohesive sediment bed deformation characteristics in Tonle Sap River, Cambodia. The obtained results are as follows.

(1) The percentage rate of the water discharge in the Bassac River to the Mekong River is about 25% during both dry and flood seasons. However, when water discharge is equal to zero, the percentage rate of the water discharge in Bassac River to the Mekong River becomes small.

(2) During the dry season, the flow in Tonle Sap River only comes from Tonle Sap Lake. The flow direction is a normal flow (from Tonle Sap Lake to Mekong River). The erosion process occurs especially near the confluence with Mekong River. The Tonle Sap River has non-cohesive material layer on the surface bed. However, the volume of this layer is too small compare the potential bed-load transport under this hydraulics condition. Therefore, all of the non-cohesive material layers transported well to the downstream area and make much erosion on cohesive sediment bed.

(3) During the flood season, sediment deposited at the south of peninsula between the Tonle Sap River and the Mekong River. As shown in Figure 5.15, the peninsula between the Tonle Sap River and the Mekong River has been extended to south year by year. It is considered that the sediment deposition during flood season cause the extension of peninsula.

(4) During the flood season, the bed material in the Tonle Sap River becomes coarse because of the inverse flow from the Mekong River. However, the armoring phenomenon is restricted near the confluence. These results get agrees with the results of one dimensional bed deformation analysis.

(5) Cohesive characteristics of the sediment affect the bed deformation characteristics because of the suppression of sediment transport rate and bed degradation. Especially, when rivers which have different sediment size characteristics

confluents, difference of the cohesive characteristics of the sediment must be considered.

References

Aberle J, Nikora V, McLean S, Doscher C, McEwan I, Green M, Goring D, and Walsh J.: Straight benthic flow-through flume for in situ measurement of cohesive sediment dynamics, *Journal of Hydraulic Engineering*, ASCE, Vol. 129, pp. 63-67, 2003.

Ashida, K. and Michiue, M.: Study on hydraulic resistance and bed-load transport rate in alluvial streams, *Proc. of JSCE*, No. 206, pp.59-69, 1972.

Egashira, S. and Ashida, K. Unified view of the mechanics of debris flow and bed-load, *Advances in Micromechanics of Granular Materials*, (Edited by H.H.Shen et al.) Elsevier, pp. 391-400, 1992.

Hori, H.: The Mekong, Environment and Development, *Kokon-Shoin Publishing Co., Ltd.*, 2000.

Iwagaki, Y.: Hydrodynamic study on critical shear stress. *Proc. of JSCE*, No. 41, pp. 1-21, 1956.

Kovacs, A. and Parker, G.: A new vectorial bed-load formulation and its application to the time evolution of straight river channels. *J. Fluid Mech*. Vol. 267, pp. 153-183, 1994.

Liu, B.Y.: Study on Sediment Transport and Bed Evolution in Compound Channels. *Thesis presented to Kyoto University*, 1991.

Luu X. L., Egashira, S., and Takebayashi, H.: Investigation of Tan Chau Reach in Lower Mekong Usng Field Data and Numerical Simulation, *Annual Journal of Hydraulic Engineering, JSCE*, Vol. 48, No.2, pp. 1057-1062, 2004.

Lane, E.W. and Kalinske, A. A. Engineering calculation of suspended sediment, *Trans. A.G.U*., Vol. 22, 1941.

Nagase, K., Michiue, M. and Hinokidani O.: Simulation of bed elevation around contraction in mountainous river. *Annual Journal of Hy. Eng. JSCE*, Vol. 40, pp. 887-892, 1996.

Olesen, K.W., and Tjerry, S.: Morphological modeling of the Chaktomuk Junction, *River Flow 2002 Balkema*, pp. 879-887, 2002.

Parchure, TM., and Mehta, AJ.: Erosion of Cohesive Sediment Deposits, *ASCE*, Vol. 111, No.10, 1985.

Rubey, W.W.: Settling velocities of gravel, sand and silt particles, *American J. of Science*, Vol. 25, pp. 325-338, 1933.

Sekine, M. and Iizuka N.: (2000) Erosion Rate of Cohesive Sediment, Korea WRA, *ICHE* 4th, 2000.

Sekine, M., Nishimori, K., Fujio, K. and Katagiri, Y.: On erosion process of cohesive sediment and erosion rate formula, *Annual Journal of Hy. Eng. JSCE*, Vol. 47, pp. 541-546, 2003.

Takebayashi, H., Tsukawaki, T., Sim, I., Sambath, T., and Sotham, S.: Characteristics of bed deformation and size distribution of bed material at Chaktomuk in Cambodia, *River Sedimentation*, Vol. 11, CD-ROM version, 2010.

Chapter 6

Conclusions and Recommendations

6.1 Conclusions

Cohesive and non-cohesive material affects the river morphological process due to the different erosion characteristics of them. In river morphological simulations, using non-cohesive material is a common method for modeling bank and bed. However, in natural rivers, cohesive sediment also exists whether on bank or bed. Particularly, riverbanks often contain the cohesive material. Therefore, to study the erosion process of bank or bed which contains cohesive material is important to improve the knowledge of bed deformation characteristics. This research investigates the effect of cohesive material in river morphological processes by using field analysis, experimental test and numerical simulation. The morphological processes are including the deformation processes of the bank and the bed of the channel. The experimental tests are conducted to understand the erosion characteristics. Hence, the results are applied in natural rivers to study their effect. The results of these studies have several important conclusions with respect to the interactions between cohesive material and non-cohesive material.

In Chapter 2, three main cases of the bank erosion experiments were conducted. In the first case, the bank composed of the non-cohesive material is treated. In the second case, the bank is composed of cohesive material in the upper layer and non-cohesive material in the bottom layer. In the last, the bank is composed of cohesive material only. The bed material for all cases is non-cohesive. A fixed mid-channel bar is installed to accelerate the bank erosion. These results show the different behavior on bank erosion processes.

In case that the bank is composed of non-cohesive material, the erosion at bank toe is followed by the mass failure of the upper layer immediately. The shape of bank line in at the final stage is a smooth curve. The erosion at the bank toe under the bank is composed of cohesive material at the upper layer and non-cohesive material at the bottom layer is followed by mass failure of the upper layer. However, the mass failure

occurred later due to the cohesiveness of the bank material. The shape of bank line at the final condition is not a smooth curve. The bank migration tends to form the small radius bend comparing to the case which the bank composed only non-cohesive material. Bank line migration is very small, when the bank is totally composed of cohesive material. The dominant process in this case is the bed degradation.

In case that the bank is composed of non-cohesive material only, the failed bank material enters the channel directly. It becomes another source of the sediment transport in the channel. The surplus of bed-load suppresses the erosion process on the bed. That becomes one of the reasons why the relative bank height in case the bank composed of non-cohesive material is lower than other cases. In case the bank is composed cohesive layer at the upper and non-cohesive at the bottom layer, the failed bank of cohesive material deposits in front of the bank toe for a long time. The failed block also disturbs the flow and local scouring occurs around it. Those phenomena must be considered in a river morphology calculation, because, usually the failed block is assumed to be flashed away by the water flow and does not influence the flow.

In Chapter 3, the erosion characteristics of cohesive sediment bed are studied. This research focus on the effect of bed load transport on erosion process of cohesive sediment bed. The results show that the volume of bed-load transport increases the erosion rate of cohesive sediment when the bed-load transport rate under the small rate conditions. However, after achieving a certain volume, the erosion rate will decrease. This tendency indicates that the relationship between the volume of bed-load transport and erosion rate of cohesive sediment bed is a non-linear function. In fact, the volume or concentrations of the bed-load transport effects on the magnitude of the dynamic shear stress on the bed. The effect of the cohesiveness is strong enough in cases the fine material of the bed-load transport.

In Chapter 4, the field surveys and numerical simulations by using horizontal two-dimensional bed deformation analysis are presented. The researched reach is the Sesayap River in Malinau reach. The results of field observations show that the bank erosion is triggered by the presence of a mid-channel bar. The bar caused a concentration flow along the bank in the downstream area of the bar. Thus, the erosion on the bed occurs in much volume. This will increase the relative bank height and triggers the mass failure. The bank stratification in this reach is cohesive material at the

upper layer and non-cohesive material at the bottom layer. The cohesive characteristics and the high surface slope of the upper layer suppress the erosion rate. This result indicates that the cohesive characteristics of the material in banks must be considered, when the bank erosion process is reproduced by mathematical models. The results show that the dredging of mid-channel bar is an effective method for suppressing the erosion near the bank toe.

In Chapter 5, the bed deformation characteristics of cohesive sediment bed in a natural river are studied. As explained in Chapter 3, the cohesiveness of the bed suppresses the erosion rate by trapping bed-load material. The numerical simulations in a natural river which has such kind phenomenon were performed. The Tonle Sap River in Cambodia was chosen to elucidate the effect of cohesive bed in the river bed deformation process. The results show that the cohesive sediment bed is eroded in much volume if the bed-load transport is under small volume. However, the erosion rate decreases, if the bed-load transport is under large volume.

6.2 Recommendations

Future study is required to improve the knowledge in this study. The following points are recommended to be considered:

(1) In experiments for studying the effect of cohesive material on bank erosion process, using more than two layers of the bank stratifications is needed. Because, many rivers have more than two layer in the bank. Using the flume with wide dimension is better, because, the failed block will disturb the flow. This disturbance will give strong effect in hydraulics condition for narrow channel.

(2) Considering the overhang and protection of the failed block in numerical simulation of channel evolution are an important analysis.

(3) Countermeasures of bank erosion problem must be considering the bed deformations near the bank toe. Improving the bank stability by a river regulation works is not an only method. For example, in Sesayap River at Malinau reach, the dominant factors on triggering the bank erosion is the river bed morphological process. However, most of engineers only consider on the bank stability and ignored the bed morphology to counteract the bank erosion problem.

(4) According to the experiment results, on the effect of bed load transport on cohesive sediment bed, the calculation of the dynamic shear stress on the bed must consider to the presence of bed load transport including the size of sediment transport. The experimental cases with many variety of sediment size are needed.

List of Figures

List of Photos

List of Tables

Curriculum Vitae

Name	Puji Harsanto
Citizenship	Indonesia
Birth/Place	June 7, 1974, Yogyakarta, Indonesia

Ph.D. Student (2009 - 2012)
Department of Civil and Earth Resources Engineering,
Graduate School of Engineering, Kyoto University, Japan

M.Eng. in Hydraulic Engineering (2002-2007)
Department of Civil and Environmental Engineering,
Graduate Studies Program Gadjah Mada University, Yogyakarta, Indonesia

B.E. in Civil Engineering (1992-1998)
Department of Civil Engineering and Environmental Engineering,
Faculty of Engineering, Gadjah Mada University, Yogyakarta, Indonesia

Papers based on the Thesis

Harsanto, P., Takebayashi, H., and Fujita, M.: Study on bank erosion processes with cohesive and non-cohesive material, Proceeding Annual Meeting of Japan Society of Erosion Control Engineering, JSECE Publication, No.66, pp. 288-289, 2012.

Harsanto, P., Toan, N.M.M., Takebayashi, H., and Fujita, M.: Effect of bedload transport on erosion rate of cohesive sediment, Journal of Japan Society of Civil Engineers, Ser. B1 (Hydraulic Engineering), JSCE, Vol. 68, No. 4, pp. I_19 – I_24, 2012.

Harsanto, P., Takebayashi, H., and Fujita, M.: Numerical analysis on countermeasures of bank erosion, Proceeding Int. Symposium on Sediment Disasters under the Influence of Climate Change and Tectonic Activity (2nd), JSECE Publication, No.63, pp. 44-45, 2011.

Harsanto, P., Toan, N.M.M., Takebayashi, H., and Fujita, M.: Erosion characteristics of cohesive sediment by non-cohesive sediment, Annuals of Disas. Prev. Res. Inst., Kyoto Univ., No 54 B, pp. 611-618, 2011.

Takebayashi, H., Fujita, M., and Harsanto, P.: Bank Erosion Model along Banks Composed of both Cohesive and Non-cohesive Material layers, Annuals of Disas. Prev. Res. Inst., Kyoto Univ., No 53 B, pp. 527-536, 2010.

Harsanto, P., Fujita, M., Takebayashi, H., Legono, D., and Fathani, F.: Flow characteristics of Sesayap River, East Kalimantan Province, Indonesia, Proceeding of International Workshop on Multimodal Sediment Disasters Triggered by Heavy Rainfall and Earthquake and the Countermeasures, pp. 175-186, 2010

Takebayashi, H., Fujita, M., and Harsanto, P.: Numerical analysis of bank erosion process along banks composed of both cohesive and non-cohesive layers, Proceeding of International Workshop on Multimodal Sediment Disasters Triggered by Heavy Rainfall and Earthquake and the Countermeasures, pp. 77-86, 2010

Harsanto, P., Takebayashi, H., and Fujita, M.: Effect of cohesive material on bank erosion process in Sesayap River, East Kalimantan Province, Indonesia, Proceeding Annual Meeting of Japan Society of Erosion Control Engineering, JSECE Publication, No.57, pp. 254-255, 2010.